Developing ankle exoskeleton assistance strategies by leveraging the mechanisms involved in human locomotion

Submitted in partial fulfillment of the requirements for

the degree of

Doctor of Philosophy

in

Mechanical Engineering

Rachel W. Jackson

B.S., Mechanical Engineering, Rice University
M.S., Mechanical Engineering, Carnegie Mellon University

Carnegie Mellon University
Pittsburgh, PA

May, 2017

Dissertation Committee

Professor Steven H. Collins, Chair, *Carnegie Mellon University*

Professor Paul S. Steif, *Carnegie Mellon University*

Professor Gelsy Torres-Oviedo, *University of Pittsburgh*

Dr. Alison L. Sheets-Singer, *Nike, Inc.*

Acknowledgements

First and foremost, thank you Steve for embarking on this journey with me. Thank you for teaching me what it takes to conduct high-level, challenging research, for showing me how to ask and tackle the hardest of questions, and for helping me grow into an independent researcher.

Thank you Paul, Gelsy, and Alison for the multitude of interesting discussions related to my research, or about life in general, over the years.

Thank you Josh, Myunghee, and JJ for all the intellectual (and goofy) conversations during those early years in the lab. Thank you Stuart, Katie, Kirby, Vince, Thu, Patrick, Gwen, Rong, Stefan, Ceci, and all the other members of the CMU Experimental Biomechatronics Lab, past and present. You all are amazing and I feel so fortunate to have gotten to know and work with each of you over the past several years.

Thank you Chris Hertz for your endless hard work. Thank you Jim, John, and Ed for fixing all the broken parts I brought to you. Thank you to all the members of the CMU Mechanical Engineering Department; it has truly been a pleasure being part of such a great community.

Thank you Kim, Lili, Kosa, Lauren, Kyle, Katie, Gary, and all the friends I have made during my time at CMU and in Pittsburgh. Thank you Molly, Laura, Emily, Lizzy, Kate, and all my friends that have stuck with me throughout the years. Your friendship means the world to me.

Thank you Evan for your constant love and support. You inspire me every day to be the best I can be.

Thank you Anna for always making light of any situation. You taught me how to get through this PhD (and life) by using obscure movie quotes.

And last, but definitely not least, thank you Mom and Dad. I would not be where I am today without the two of you. Thank you for being there through the highs and the lows, and through everything in between. You are a constant reminder of what is important in life.

The work presented in this thesis was supported by the National Science Foundation under Grant No. IIS-1355716 and Graduate Research Fellowship Grant No. DGE-1252552 and by the Panasonic Corporation under Grant No. A018293.

Abstract

Exoskeletons have the ability to improve locomotor performance for a wide range of individuals: they can improve the economy of normal walking, aid in load carriage for soldiers, assist individuals with walking disabilities, and serve as gait rehabilitation tools. Although it may seem obvious how exoskeletons should be developed to provide a benefit to the user, the complexity of the human neuromuscular system makes developing effective exoskeleton assistance strategies a challenge. Rather than using intuition to guide our attempts at the design and control of ankle exoskeletons, we need to garner a deeper understanding of how ankle exoskeletons affect locomotor coordination and utilize such findings to facilitate effective interaction between the device and the human.

This thesis details an iterative approach towards the development of ankle exoskeleton assistance strategies. We first performed a controlled experiment to observe the human response to specific assistance techniques. We then sought to explain the reasons for the observed responses by estimating muscle-tendon mechanics and energetics at the assisted joint using simulations of a musculoskeletal model. Through experimentation and simulation we found that individuals change and adapt their coordination patterns when walking with ankle exoskeletons, often in unexpected ways. Based on these findings, we developed and tested a novel ankle exoskeleton assistance strategy that adjusts exoskeleton behavior online in response to measured changes in the user. Such individualized, adaptive control approaches seem promising for discovering effective exoskeleton assistance strategies. Eventually we want to apply such strategies to populations with gait disabilities, but only once we have a better understanding of the mechanisms driving gait impairments. To that end, we

designed and are conducting an experiment to investigate the relationship between features of post-stroke gait and energy economy. We expect our experimental findings to aid in the development of more accurate predictive models of human locomotion and to motivate new methods for developing assistive and rehabilitative techniques using robotic exoskeletons.

Contents

List of Tables

List of Figures

Chapter 1

Introduction

1.1 Motivation

Lower-limb exoskeletons have the potential to provide locomotor assistance to people with a wide range of physiological needs. They can provide high intensity, consistent locomotor rehabilitation to post-stroke individuals [5]. They can assist post-stroke individuals and those with other gait impairments, such as cerebral palsy, with everyday mobility [54]. They can help prevent falls and compensate for muscle atrophy caused by aging in the elderly. They can even assist able-bodied individuals by aiding in load carriage for soldiers [84] and improving the economy of normal walking [75].

Effectively controlling exoskeletons to most benefit the user is, however, much more challenging than it may seem. Researchers and designers have been attempting to develop useful assistance strategies for over a century with limited success. Often, it seems obvious how such devices should be designed and controlled to achieve the intended benefit, but the complexity of the human musculoskeletal system and the poorly understood interaction between the device and the user can prove such strategies ineffective. There is still much to learn about the development of exoskeletons for locomotor assistance.

1.2 Ankle Exoskeletons for Assisting Locomotion

Exoskeletons act in parallel with the human body and augment, rather than replace, assumed functionality. Many lower-limb exoskeletons have focused on assisting at the ankle joint due to its importance in powering locomotion and the simplicity of developing devices that can act about this joint. The main difficulty in developing ankle exoskeletons is not in attaching to the human, which is complicated in and of itself, but in determining how such devices should behave and interact with the human during locomotion.

1.2.1 Why the Ankle Joint

The ankle joint is a desirable place to provide assistance during locomotion for several reasons. The ankle joint produces more positive work during the stance phase of gait than both the hip and the knee combined [120]. Additionally, the muscles acting to plantarflex the ankle joint consume about 27% of the metabolic energy used over one gait cycle [113]. Exoskeleton assistance provided at the ankle joint can supplant a portion of the work done by muscles and tendons acting at this joint and improve whole-body metabolic energy cost. Neurological injuries, such as stroke, weaken neural connections to distal muscles, specifically those that act about the ankle joint, and can lead to a reduction in the positive work done by the paretic leg during push-off [85, 14, 3, 99]. Exoskeletons acting about the paretic-leg ankle joint can provide positive work at push-off and compensate for such impaired functionality. Although providing assistance at the ankle joint has the potential to improve locomotor capabilities, the complexity of the muscles and tendons operating about the ankle joint make it challenging to provide effective assistance.

1.2.2 Complexity of the Ankle Joint

Multiple muscles act about the ankle joint in the sagittal plane (Fig. 1.1). The soleus, lateral gastrocnemius, and medial gastrocnemius muscles all act in series with the Achilles tendon and plantarflex the ankle joint. Together, these muscles are referred to as the plantarflexor

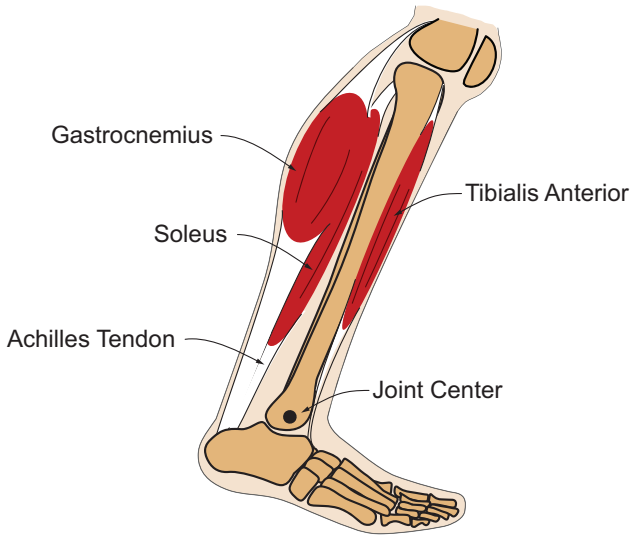

Figure 1.1: Main muscles acting about the ankle joint in the sagittal plane. The soleus and gastrocnemius muscles act in series with the Achilles tendon to plantarflex the ankle joint. The tibialis anterior acts to dorsiflex the ankle joint.

muscles, or Triceps Surae. The tibialis anterior acts antagonistically to the plantarflexor muscles and causes dorsiflexion. Due to the redundancy of the musculoskeletal system, an infinite set of plantarflexor and dorsiflexor muscle force combinations will result in the same ankle joint torque. Therefore, it is not possible to know how much force each muscle is producing about the ankle joint based solely on joint-level torques. Furthermore, tendons, which act in series with muscles, are elements that passively store and return energy as they lengthen and shorten. Due to this elastic energy storage in tendons, positive ankle joint work is not necessarily equivalent to positive work done by muscles.

Muscles are, themselves, complex mechanisms. The force that a muscle can generate is not only dependent on activation, but also on the state of the muscle fiber, specifically fiber length and fiber velocity. Muscles consume metabolic energy to not only do work, but also to produce force at constant length. Furthermore, during normal walking, muscles and tendons exhibit complex interactions that seem finely tuned for efficiency [71, 72, 73, 61]. It is, therefore, difficult to know how to best interact with these mechanisms with external devices to provide a benefit to the user.

1.2.3 Complexity of Assisting Human Locomotion

Placing an exoskeleton in parallel with the biological ankle joint does not only impact the assisted joint, but also impacts whole-body coordination patterns, sometimes in undesirable ways. For instance, users can adopt compensatory strategies that result in overall increases in whole-body metabolic energy consumption. Additionally, user's coordination patterns are not static when walking with ankle exoskeletons; users adapt and change their coordination strategies as they learn how to best interact with such devices [49, 105, 47, 66]. These factors further complicate the issue of developing useful assistance strategies for a wide range of people.

1.2.4 Previous Attempts at Locomotor Assistance Strategies

Simple models, intuition, and our understanding of the biomechanics of human locomotion have guided initial attempts at the design and control of ankle exoskeletons. These attempts have focused primarily on devices that are capable of producing net work, referred to here as active devices, because the biological ankle joint generates net positive work during normal walking. One common control approach for active ankle exoskeletons is time-based assistance [75, 84, 47], in which plantarflexion torque is provided (through e.g. artificial pneumatic muscles [51] or series elastic actuators [84, 121]) at a specific time in the gait cycle. A second common control approach for active ankle exoskeletons is proportional myoelectric control (pEMG) [51, 105, 66], in which exoskeleton torque is provided in proportion to the user's own soleus muscle activity. In the last couple of years, researchers have been able to use such powered devices to reduce metabolic energy consumption below that measured during normal human walking [75, 47, 84].

Providing external work with an exoskeleton will not necessarily benefit the user, especially if the way in which the work is delivered causes undesirable locomotor compensation strategies. Techniques that take into account the complexities of the human musculoskeletal system are most likely to prove effective, even those without any work input. For example, a passive ankle exoskeleton that uses a custom-designed clutch to engage and disengage

springs in parallel with the biological plantarflexor muscles recently reduced metabolic energy consumption below that measured during normal human walking by about 7% [26].

Why certain assistance strategies are more effective than others at providing a benefit to the user is still not well understood. Comparisons between assistance strategies are often confounded by factors other than device behavior, such as device mass, overall device structure, actuation technique, or the co-variation of other potentially influential parameters. Discovering those characteristics that define what makes assistance effective could help the field more rapidly develop novel assistance strategies.

1.3 Scope: Developing Novel Assistance Strategies

To try to overcome the limitations inherent in traditional, intuition-driven approaches, we took an iterative approach to the development of assistance strategies involving observation, explanation, and extension. We conducted controlled biomechanics experiments and performed simulations of a musculoskeletal model to study how humans respond to a variety of assistance techniques. We then used our findings to motivate a novel exoskeleton assistance technique that adjusts device behavior in real time in response to measured changes in the user. We hope to be able to extend the strategies we developed for assisting able-bodied individuals during normal walking to those with walking disabilities or redefine these strategies to serve as gait rehabilitation tools.

1.3.1 Universal Device Emulators

High-performance testbeds, with lightweight and robust end-effectors, enable rapid exploration of the human response to different assistance strategies. Our lab developed a highly versatile testbed with off-board motors and flexible transmissions that actuate custom-made ankle exoskeleton end-effectors (Fig. 1.2). The ankle exoskeletons are lightweight (0.84 kg), have closed-loop torque bandwidth of at least 16.7 Hz, and can provide up to 120 N·m of plantarflexion torque during normal walking. Additional information about the testbed

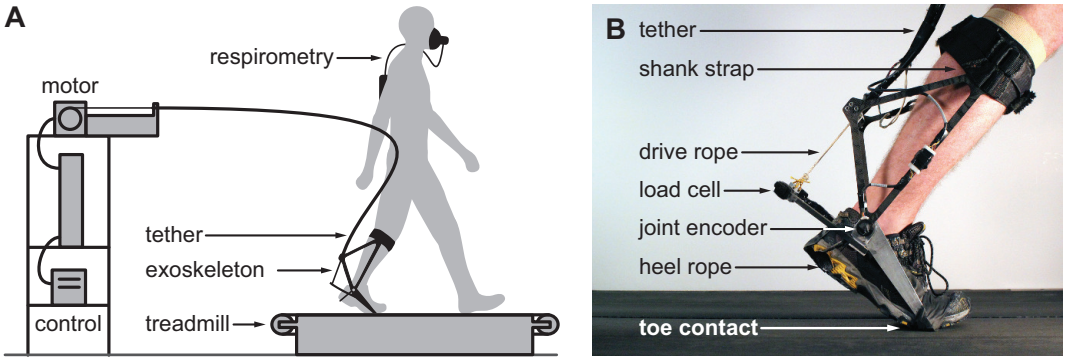

Figure 1.2: Schematic of the (A) universal device emulator and (B) ankle exoskeleton end-effector. *Figure adapted from Zhang (2017).

setup and device design can be found in [19, 121]. We used this emulator to develop various exoskeleton assistance strategies and to conduct all exoskeleton experiments.

1.3.2 Biomechanics Experimentation

To be able to make claims about the effectiveness of different assistance strategies, it is important to conduct controlled experiments that directly compare the impact of each assistance strategy on whole-body locomotor coordination. Biomechanics experiments enable us to measure lower-limb joint kinematics and kinetics, ground reaction forces, lower-limb muscle activity, and whole-body metabolic rate during locomotion. We used such experimental techniques to observe, at a macro-level, how users responded to a wide variety of exoskeleton assistance strategies that were applied via our universal exoskeleton emulator. We analyzed biomechanical outcomes to try to deepen our understanding of how coordination patterns change when walking with different types of exoskeleton assistance. We were, however, limited in our ability to fully explain what we observed because current experimental measurement techniques are not capable of measuring muscle-level mechanics and energetics during locomotion in humans.

1.3.3 Musculoskeletal Modeling

In order to develop meaningful explanations for the observed human response to a variety assistance strategies, it is important to understand how lower-limb muscles and tendons

are impacted by different device behaviors. Musculoskeletal models are effective tools for exploring the mechanics of the muscles and tendons involved in human locomotion. Experimental data, including body-mounted motion capture marker positions, ground reaction forces, and measured electromyography, can be fed into these models to generate estimates of muscle fiber forces, lengths, velocities, and powers [33]. Estimated muscle mechanics can then be fed into muscle-level metabolics models to predict the amount of energy consumed by individual muscles [114]. We used a musculoskeletal modeling approach to estimate how muscle-tendon mechanics and energetics changed with different exoskeleton behaviors. We analyzed these results to understand how exoskeletons can detune muscle-tendon mechanics.

Musculoskeletal models are, however, imperfect. Many assumptions are made when developing these models that affect their validity. Thus, care must be taken when using such models to try to understand muscle-level mechanics. Furthermore, although it is possible to simulate how muscles and tendons change under a known type of exoskeleton assistance, it remains a challenge to use these models to predict the human response to novel device interactions.

1.3.4 Adaptive Assistance Strategies

Control techniques that adjust device behavior online in response to measured changes in the human system may lessen the need for prediction and result in better outcomes. Such strategies can be used to provide individualized assistance to every user, thereby accounting for the inherent variation between people. To that end, we developed and tested a novel assistance strategy that adjusts ankle exoskeleton torque in real time in response to measured changes in the user's muscle activity. Additionally, my colleague developed, and I helped test, a different 'human-in-the-loop' strategy that discovers the ankle exoskeleton assistance strategy that directly minimizes whole-body metabolic energy cost for a given individual [130].

1.3.5 Understanding Gait Impairments in Patient Populations

Strategies developed for assisting able-bodied individuals during normal walking can be extended to those with walking disabilities, however assisting individuals with walking disabilities is very different from assisting their able-bodied counterparts. Understanding the mechanisms driving abnormal gait, before trying to use robotic devices to improve certain gait characteristics, could lead to the development of more effective assistance and rehabilitation strategies. For example, one common target of rehabilitation in post-stroke individuals is gait asymmetry. Clinicians strive to improve symmetry in this patient population to try to improve functional outcomes, yet little work has been done to understand why post-stroke individuals walk with an asymmetric gait. Without understanding what is driving this gait asymmetry, it is difficult to know whether assistive devices should be aimed at reducing asymmetry or if they should be targeting other gait characteristics. Towards this end, we designed and conducted an experiment to deepen our understanding of gait asymmetry in post-stroke individuals.

1.4 Thesis Outline

This thesis presents the approach we have taken for improving the development of ankle exoskeleton assistance strategies. In Chapter 2, I describe a controlled experiment we conducted to compare the independent effects of work and torque assistance provided by a unilateral ankle exoskeleton on human locomotor coordination. In Chapter 3, I detail how we performed simulations of a musculoskeletal model to estimate changes in muscle-tendon mechanics and energetics during walking with different ankle exoskeleton assistance strategies. In Chapter 4, I describe the development and testing of a novel ankle exoskeleton control strategy that uses muscle activity, measured online, to continuously adjust exoskeleton assistance. In Chapter 5, I present an experiment we designed to understand if gait asymmetry in post-stroke individuals is the result of a strategy to minimize metabolic energy economy and what this might mean for the development of robotic

rehabilitation strategies for post-stroke individuals.

Chapter 2

An experimental comparison of the relative benefits of work and torque assistance in ankle exoskeletons [†]

Abstract

Techniques proposed for assisting locomotion with exoskeletons have often included a combination of active work input and passive torque support, but the physiological effects of different assistance techniques remain unclear. We performed an experiment to study the independent effects of net exoskeleton work and average exoskeleton torque on human locomotion. Subjects wore a unilateral ankle exoskeleton and walked on a treadmill at 1.25 $m \cdot s^{-1}$ while net exoskeleton work rate was systematically varied from -0.054 to 0.25 $J \cdot kg^{-1} \cdot s^{-1}$, with constant (0.12 $N \cdot m \cdot kg^{-1}$) average exoskeleton torque, and while average exoskeleton torque was systematically varied from approximately zero to 0.18 $N \cdot m \cdot kg^{-1}$, with approximately zero net exoskeleton work. We measured metabolic rate, center-of-mass mechanics, joint mechanics, and muscle activity. Both techniques reduced effort-related measures at the assisted ankle, but this form of work input reduced metabolic cost (-17%

[†]This work appears as a research article in: Jackson, R.W. and Collins, S. H. (2015). An experimental comparison of the relative benefits of work and torque assistance in ankle exoskeletons. *J. Appl. Physiol.*, 119:541-557.

with maximum net work input) while this form of torque support increased metabolic cost (+13% with maximum average torque). Disparate effects on metabolic rate seem to be due to cascading effects on whole-body coordination, particularly related to assisted ankle muscle dynamics and the effects of trailing ankle behavior on leading leg mechanics during double support. It would be difficult to predict these results using simple walking models without muscles, or musculoskeletal models that assume fixed kinematics or kinetics. Data from this experiment can be used to improve predictive models of human neuromuscular adaptation and guide the design of assistive devices.

Keywords: biomechanics, locomotion, ankle foot orthosis, gait, rehabilitation

2.1 Introduction

Exoskeletons act in parallel with the human body and augment, rather than replace, the assisted joints. Assisting human locomotion with exoskeletons therefore requires consideration of both biological and exoskeleton contributions to assisted joint mechanics. When an exoskeleton is added to a human user, the human must adapt to a novel environment and discover new control strategies, complicating the task of determining useful assistance techniques. Performing human experiments with exoskeletons can help us understand how to best interact with the human user, and may provide insights into fundamental principles governing locomotor coordination and adaptation [44].

Simulations, prior experiments, and intuition can be helpful in deciding what assistance techniques are worth exploring. Simple walking models and related experiments suggest that the trailing leg performs positive work around the step-to-step transition to help redirect the velocity of the body center of mass and compensate for energy lost during leading leg collision [67, 101, 50, 37]. Nearly all of this push-off work is performed at the ankle joint [120, 80], and musculoskeletal simulations suggest that ankle plantarflexor muscles involved in push-off consume about 27% of the metabolic energy of walking [115]. Replacing part of this biological work with external mechanical work, via an exoskeleton acting in parallel with the ankle joint,

may reduce force and work of the plantarflexor muscles and decrease overall metabolic energy consumption. Alternatively, increasing total ankle joint work, by augmenting rather than replacing biological ankle joint work, could reduce metabolic energy consumed elsewhere in the body. Other studies and musculoskeletal models of human walking suggest that there is also a significant metabolic cost associated with generating muscle force to support body weight [53, 52, 96, 113]. Providing exoskeleton torques in parallel with the biological ankle joint, without supplying any net mechanical work, could reduce plantarflexor muscle forces required to support body weight and reduce associated energy consumption.

Although exoskeleton work and torque assistance approaches are well-motivated, they have not been thoroughly tested. Many isolated exoskeleton experiments have been conducted, but comparisons between assistance techniques have often been confounded by factors other than device behavior, such as device mass, differences in study protocols, or co-variation of other possibly influential parameters. Furthermore, complete biomechanical measurements have rarely been obtained. It therefore remains uncertain how different types of assistance impact whole-body coordination. An experiment that uses an exoskeleton to compare the effects of work input and torque support on locomotor mechanics and energetics could help us understand the independent benefits of each assistance technique and could provide insights into the independent costs of performing work and producing force with muscles. Such a study was previously recommended by Sawicki and Ferris [105].

Distinguishing between the relative effectiveness of work and torque assistance is important because these strategies have disparate implications for device design. Providing net positive mechanical work with an exoskeleton requires an actuator system, such as an electric motor and battery, which adds distal mass, potentially offsetting energy reductions [17]. External supporting torques can be achieved with lightweight, elastic mechanisms, such as springs [26], but these unpowered devices cannot deliver net work to the user. In both cases some amount of control can be performed cheaply, for example by embedded microprocessors and small clutches [25, 119], making the amount of net work provided over a cycle the primary distinction between approaches. Some combination of work and torque is likely to be

optimal, but understanding how each independently affects the human user would facilitate a more effective design process.

Using musculoskeletal models to gain insights into fundamental locomotor control and to predict the human response to untested assistance strategies is an appealing alternative to human experiments. These simulations allow for a large number and variety of tests to be run quickly and full-body measurements to be obtained. Generating accurate predictions, however, is a challenging problem due to the complexity and redundancy of the human neuromuscular system. For example, researchers using biomechanics measurements taken after patient adaptation still find it difficult to accurately estimate experimentally-measured *in vivo* knee contact forces [45]. Rich data sets obtained through controlled human experiments, like those mentioned in [45], provide information about the human response to novel interventions and help improve predictive musculoskeletal models.

Our goal was to conduct a controlled experiment comparing the effects of a particular mode of work input and torque support assistance on human mechanics and energetics. Increased exoskeleton work was expected to reduce the metabolic energy cost associated with work input to redirect the body's center-of-mass velocity, appearing as reduced work at the assisted ankle joint and reduced biological contributions to center-of-mass work overall. Increased exoskeleton torque was expected to reduce the metabolic energy cost associated with supporting body weight, appearing as reductions in assisted ankle torque and associated muscle activity. Regardless of the outcomes, we expected the biomechanics and muscle activity data set obtained from this experiment to provide insights into why different assistance strategies are more effective than others, inform future device designs, and provide validation data for predictive models.

2.2 Methods

We conducted an experiment in which we compared the independent effects of one form of exoskeleton work input and torque support on human energetics, mechanics and muscle

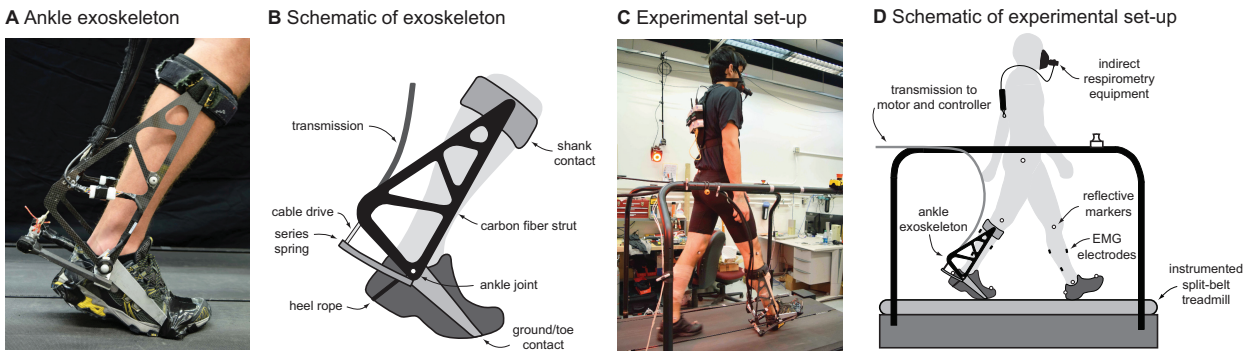

Figure 2.1: Custom-designed ankle exoskeleton and experimental setup. **A.** Photograph of ankle exoskeleton used to apply plantarflexor torques. **B.** Schematic of exoskeleton highlighting key components. **C.** Photograph of experimental setup. **D.** Schematic of experimental setup highlighting key components. Metabolic energy consumption, segment kinematics, ground reaction forces, muscle activity, and exoskeleton mechanics were measured.

activity during walking. We applied a wide range of net work and average torque values using an ankle exoskeleton worn by healthy subjects on one leg as they walked on a treadmill, and compared changes within and across the two assistance techniques.

Ankle Exoskeleton Emulator

Work and torque were applied by a high-performance, tethered ankle exoskeleton. A lightweight instrumented frame (Fig. 2.1A,B), worn on the foot and shank, was connected to an off-board motor via a flexible Bowden cable transmission [21, 121]. The ankle exoskeleton weighed 0.826 kg and was attached to a shoe. Forces were applied to the human at the shank, toe, and heel, resulting in maximum plantarflexor torques of up to 120 N·m [24]. A load cell (LC201 Series, OMEGA Engineering, Inc., Stamford, Connecticut, USA) in series with the transmission at the ankle joint measured torques with a maximum of 1% error after calibration. Fiberglass leaf springs provided series compliance and improved regulation of joint torque [129]. The exoskeleton joint angle was measured with an optical encoder (E8P, US Digital, Vancouver, Washington, USA). The axis of rotation of the exoskeleton was aligned so as to intersect the medial malleolus of the ankle of the human user. A foot switch (McMaster-Carr, Aurora, Ohio, USA) in the heel of the shoe was used to detect heel strike.

Exoskeleton Control

Exoskeleton work and torque were regulated using control of motor position in time with iterative learning. We used a series elastic actuation approach, in which differences between motor position and ankle joint position stretched a series spring, giving rise to torques approximated by:

$$\tau_a \approx k \cdot (\theta_m \cdot R^{-1} - \theta_a) \tag{2.1}$$

where τ_a is the exoskeleton ankle joint torque; k is the series stiffness, which had a maximum value of approximately 130 N·m·rad^{-1} in this study but varied greatly due to friction in the transmission and other nonlinearities in the system; θ_m is the motor angle; θ_a is the exoskeleton ankle joint angle, approximately equal to the human ankle joint angle; and R is the gear ratio between the motor and exoskeleton ankle joint, which was 18.5 in this study. (Note that *measurements* of joint torque were made using a load cell).

We utilized dynamic interactions between the exoskeleton and human to generate desired plantarflexor torque and power over time. We defined a piece-wise linear desired motor position trajectory for each torque and work combination (Fig. 2.2). The first node of this trajectory (θ_1) was reached at 0% stride and was equal to the measured ankle angle at heel strike. The final node (θ_4) was reached at 60% of stride and was approximately equal to the ankle angle at toe-off. The second and third nodes (θ_2 and θ_3) were reached at 36% and 48% of stride, which we estimated would approximately independently affect exoskeleton torque and work, respectively, due to differences in joint velocity at those instants.

The resulting exoskeleton torque and work were measured in real-time on each stride using the load cell and joint encoder. A stride was defined as heel strike to heel strike of the exoskeleton-side leg. Average exoskeleton torque was defined as the integral of measured torque over a stride divided by stride duration. Exoskeleton ankle joint velocity was computed as the discrete derivative of measured exoskeleton ankle angle and low-pass filtered with a cutoff frequency of 50 Hz. Exoskeleton power was calculated by multiplying joint torque by joint velocity. Net exoskeleton work rate was defined as the integral of power

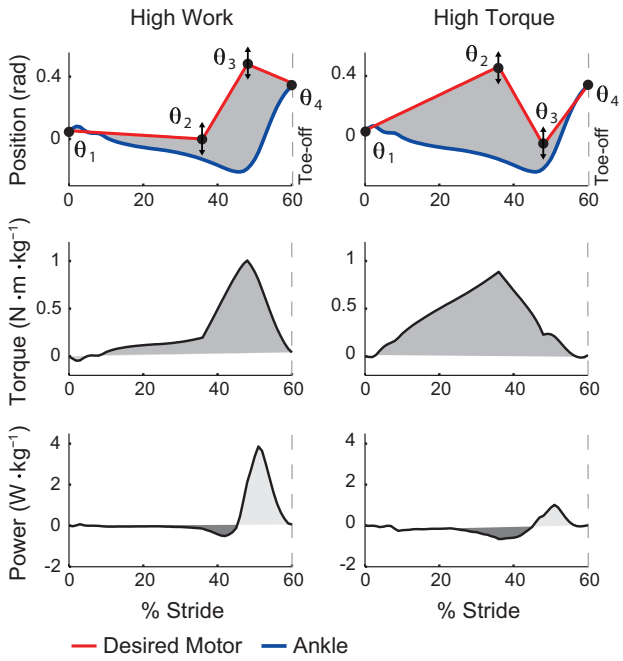

Figure 2.2: Ankle exoskeleton control illustration. *Top row:* Desired motor angle (red) was defined by four nodes in time. Differences between motor angle and ankle angle (blue) stretched a series spring, generating joint torques. The middle two nodes, θ_2 and θ_3, were iteratively updated to maintain desired average torque and net work rate. *Middle row:* Resulting exoskeleton ankle joint torque in time. *Bottom row:* Resulting exoskeleton ankle power in time. *Left column:* An illustration of a motor trajectory that would result in medium average torque and high net work. *Right column:* A trajectory that would result in high average torque and zero net work.

over a stride, divided by stride duration. Negative power phases therefore reduced net work rate. This definition of net work rate is equivalent to average power.

We implemented an iterative learning scheme to maintain desired average exoskeleton torque and work rate, which compensated for changes in human kinematics over time. This approach is conceptually similar to an online version of the controller described in [59]. On each stride, θ_2 and θ_3 were changed in a way expected to reduce errors between desired and measured torque and work on the subsequent stride:

$$\begin{aligned} \theta_2(n+1) &= \theta_2(n) + k_2 \cdot e_{tau}(n) \\ \theta_3(n+1) &= \theta_3(n) + k_3 \cdot e_{wrk}(n) \end{aligned} \tag{2.2}$$

where $\theta_2(n+1)$ and $\theta_3(n+1)$ are the motor positions of the second and third nodes,

respectively, on the $(n+1)^{th}$ stride; $\theta_2(n)$ and $\theta_3(n)$ are the motor positions of the second and third nodes, respectively, on the n^{th} stride; $e_{tau}(n)$ is the error in average torque for the n^{th} stride; $e_{wrk}(n)$ is the error in net work rate for the n^{th} stride; and k_2 and k_3 are iterative learning gains. Changes in node values were made at exoskeleton heel strike, i.e., at the end of the n^{th} stride and the beginning of the $(n+1)^{th}$ stride. Gains were manually tuned during pilot testing to minimize error while maintaining stability, which resulted in values of $k_2 = 3{\cdot}10^{-4}$ rad$\cdot$(N$\cdot$m)$^{-1}$ and $k_3 = 3{\cdot}10^{-4}$ rad$\cdot$(J$\cdot$s^{-1})$^{-1}$.

Experimental Protocol

We independently varied net exoskeleton work rate and average exoskeleton torque in one-dimensional parameter studies referred to here as the Work Study and Torque Study, respectively. In the Work Study, we applied five conditions referred to as Negative Work, Zero Work, Low Work, Medium Work, and High Work, in which desired net exoskeleton work rate ranged from about -50% to 250% of net ankle work rate observed during normal walking and desired average torque was about 25% of the value observed during normal walking [25]. In the Torque Study, we applied four conditions referred to as Zero Torque, Low Torque, Medium Torque, and High Torque, in which desired average exoskeleton torque ranged from about 0% to 40% of the value observed during normal walking and desired net work rate was approximately zero. Parameters in the Zero Work and Medium Torque conditions were identical, so we tested this condition once.

Subjects walked on a treadmill at 1.25 m$\cdot$s^{-1} for 8 minutes while wearing the exoskeleton on one leg for each Study condition (Fig. 2.1C,D). Subjects also completed Quiet Standing and Normal Walking trials in street shoes, which lasted 3 minutes and 6 minutes, respectively. Subjects completed one training day in addition to the collection day. On the training day, subjects were exposed to each condition in a particular order: first in order of increasing average exoskeleton torque, then in order of increasing net exoskeleton work. Subjects were given verbal coaching to “try relaxing your ankle muscles” and “try not to resist the device.” On the collection day, all conditions were presented in random order.

Eight healthy, able-bodied participants (N = 8, 7 men and 1 woman; age = 25.1 ± 5.1 yrs; body mass = 77.5 ± 5.6 kg; leg length = 0.89 ± 0.03 m) were included in the study. All subjects provided written informed consent before completing the protocol, which was approved by the Carnegie Mellon Institutional Review Board. Data from a ninth and tenth subject were excluded as outliers; a large portion of metabolic rate data for these subjects was more than two standard deviations (2 σ) from the study mean and this skewed the average data away from a normal distribution. Two additional recruits were unable to complete all conditions during training, due to difficulty adapting to exoskeleton behavior, and did not progress to the collection day.

Measured Outcomes

Metabolic Rate

Metabolic rate was estimated using indirect calorimetry. Volumetric oxygen consumption and carbon dioxide expulsion rates were measured using wireless, portable metabolics equipment (Oxycon Mobile, CareFusion, San Diego, California, USA). Data from the last three minutes of each trial was averaged and substituted into a widely-used equation [16] to calculate metabolic rate. Net metabolic rate was calculated by subtracting metabolic power during Quiet Standing from the different walking conditions. Change in metabolic rate for the Work Study was calculated by subtracting the metabolic power during the Zero Work condition from metabolic power during the five Work Study conditions. Change in metabolic rate for the Torque Study was calculated by subtracting the metabolic power during the Zero Torque condition from metabolic power during the four Torque Study conditions. Metabolic rate was normalized to body mass.

Center-of-Mass Mechanics

We approximated center-of-mass work rates for the right and left legs using the individual limbs method [38]. Ground reaction forces were sampled at a frequency of 2000 Hz using an instrumented split-belt treadmill (Bertec, Columbus, Ohio, USA). Three-dimensional center-

of-mass acceleration was calculated by summing right and left ground reaction forces and dividing by body mass. Integration of center-of-mass acceleration over a stride resulted in an approximation of center-of-mass velocity in time. Constants of integration were selected such that average center-of-mass velocity equaled that of the treadmill in the fore-aft direction (1.25 $m \cdot s^{-1}$) and zero in the medio-lateral and superior-inferior directions over an average stride. We took the dot product of center-of-mass velocity and the right and left ground reaction force to obtain center-of-mass power in time for the right and left leg, respectively. We calculated work rate during the collision, rebound, preload, and push-off phases of the stance period [38].

Joint Mechanics

We used inverse kinematics and dynamics analyses to approximate joint-level mechanics. Reflective markers were placed on the sacrum, left and right anterior superior iliac spine (ASIS), greater trochanter, medial and lateral epicondyles of the knee, medial and lateral malleoli of the ankle, third metatarsophalangeal joint of the toe, and posterior calcaneus of the heel. Three-dimensional marker positions were recorded using a seven camera motion capture system at a rate of 100 Hz (MX Series, Vicon Motion Systems Ltd, Oxford, UK). We used published anthropometric data [39, 31] to estimate limb masses and rotational inertias. We calculated joint velocities, accelerations, torques, and powers using inverse dynamics analysis [120] of ground reaction forces, joint positions, and estimated segment properties. We calculated joint work rate for features of interest as the integral of joint power over that period of positive or negative work (based on features defined by [120]) divided by the stride period. Exoskeleton-side biological ankle mechanics were calculated by subtracting measured exoskeleton mechanics from total, inverse-dynamics-derived exoskeleton-side ankle mechanics.

Muscle Activity

We measured lower-limb muscle activity using surface electromyography. Wireless electrodes

were placed on the medial and lateral aspects of the soleus, medial and lateral gastrocnemius, tibialis anterior, vastus medialis, biceps femoris, and rectus femoris on both legs and sampled at a frequency of 2000 Hz (Trigno Wireless System, Delsys Inc., Boston, Massachusetts, USA). Each signal was high-pass filtered with a cutoff frequency of 20 Hz, rectified, and low-pass filtered with a cutoff frequency of 6 Hz in post-processing [43]. Erroneous signals for 144 individual muscles on individual trials (about 12% of all electromyographic data) were discarded from the averaged data set. In some cases errors were due to a faulty sensor. In other cases, identified by visual inspection of the measured pattern, errors seem to have been due to poor electrode connectivity. Electromyographic signals for each condition were normalized to average peak activation during Normal Walking. If measured muscle activity for Normal Walking was erroneous, electromyographic signals across conditions were normalized to average peak activation during the Zero Torque condition, in which the exoskeleton did not apply torques. Root-mean-square values of measured electromyography were computed and used to compare muscle activity across conditions.

Normalization and Statistical Analysis

We compared metabolic rate, center-of-mass mechanics, joint mechanics, and muscle activity across conditions. Average trajectories, normalized to percent stride, were generated for each subject. Metabolic rate, center-of-mass mechanics, and joint mechanics were normalized to body mass, while muscle activity measurements were normalized to average peak activation during Normal Walking. Scalar outcomes were obtained by taking the integral of the average trajectory and dividing by average stride time. Some of the resulting measurements have units of watts per kilogram, which we present as $\mathrm{J{\cdot}kg^{-1}{\cdot}s^{-1}}$ so as to distinguish work divided by stride time from instantaneous power. All outcomes were averaged across subjects. Standard deviations represent variations between subjects.

For the Work Study, all pair-wise statistical comparisons were made with respect to the Zero Work condition. For the Torque Study, all pair-wise statistical comparisons were made with respect to the Zero Torque condition. We first performed a repeated-measures

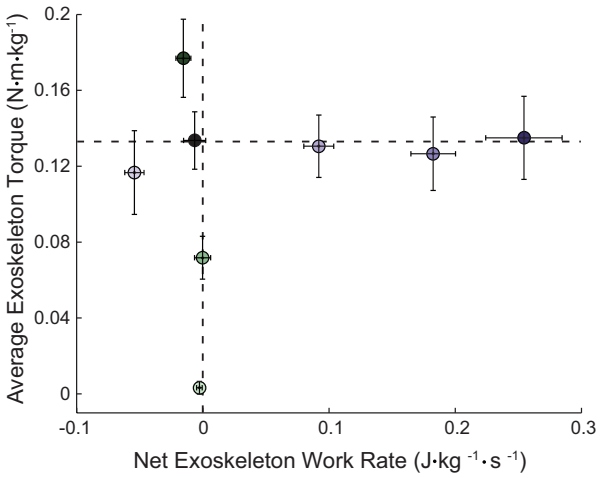

Figure 2.3: Average torque versus net work rate measured for each exoskeleton condition. Work Study is in purple and Torque Study is in green, with darker colors indicating higher values. Dots are mean values and whiskers indicate standard deviations associated with inter-subject variability.

analysis of variance (ANOVA) to test for trend significance in each outcome. On measures that showed significant trends, we performed paired t-tests to compare conditions. We then applied the Holm-Šídák step-down correction for multiple comparisons [48] and used a significance level of $\alpha = 0.05$.

2.3 Results

As applied in this study, increasing net exoskeleton work reduced metabolic energy consumption, while increasing average exoskeleton torque increased metabolic energy consumption. Both assistance techniques decreased effort-related measures at the exoskeleton-side biological ankle. With increasing exoskeleton work, however, total exoskeleton-side ankle work and center-of-mass push-off increased and contralateral-limb collision and rebound decreased, with concomitant decreases in contralateral-limb knee work, torque, and vastus muscle activity. Increasing exoskeleton torque had the opposite effects.

Exoskeleton Work and Torque

The exoskeleton applied a wide range of values of net joint work and average joint torque across conditions (Fig. 2.3). In the Work Study, net exoskeleton work divided by stride

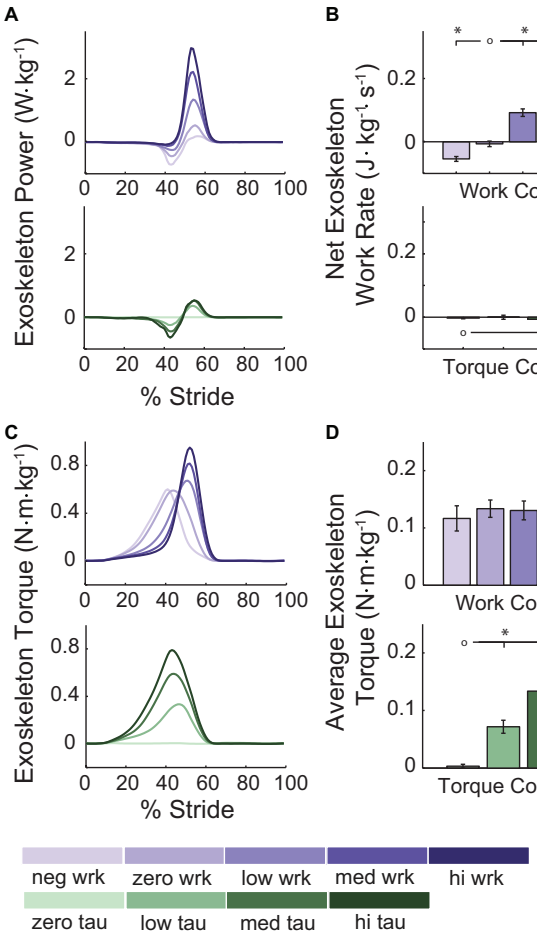

Figure 2.4: Applied exoskeleton net work rate and average torque varied widely across conditions. In the Work Study, exoskeleton power (**A**) and net work rate (**B**) increased across conditions by shifting the exoskeleton torque profile (**C**) but maintaining consistent average torque (**D**). In the Torque Study, net work rate was approximately zero, while average torque increased across conditions. Work Study is in purple and Torque Study is in green, with darker colors indicating higher values. Curves are study-average trajectories. Bars and whiskers are means and standard deviations of subject-wise integrations of corresponding curves. *s indicate statistical significance with respect to the conditions designated by open circles.

time (work rate) increased from the Negative Work condition to the Zero Work condition ($p = 2{\cdot}10^{-7}$) and from the Zero Work condition to the High Work condition ($p = 1{\cdot}10^{-7}$, Fig. 2.4). Across Work Study conditions, average exoskeleton torque was always within 13% of the value in the Zero Work condition. In the Torque Study, average exoskeleton torque increased from the Zero Torque condition to the High Torque condition ($p = 5{\cdot}10^{-8}$). Across Torque Study conditions, there was a trend towards reduced net work rate with increasing average torque (ANOVA, $p = 2{\cdot}10^{-4}$), but the work rate was always within 0.015 ± 0.005 J·kg^{-1}·s^{-1} of zero, or 6% of the maximum value in the Work Study.

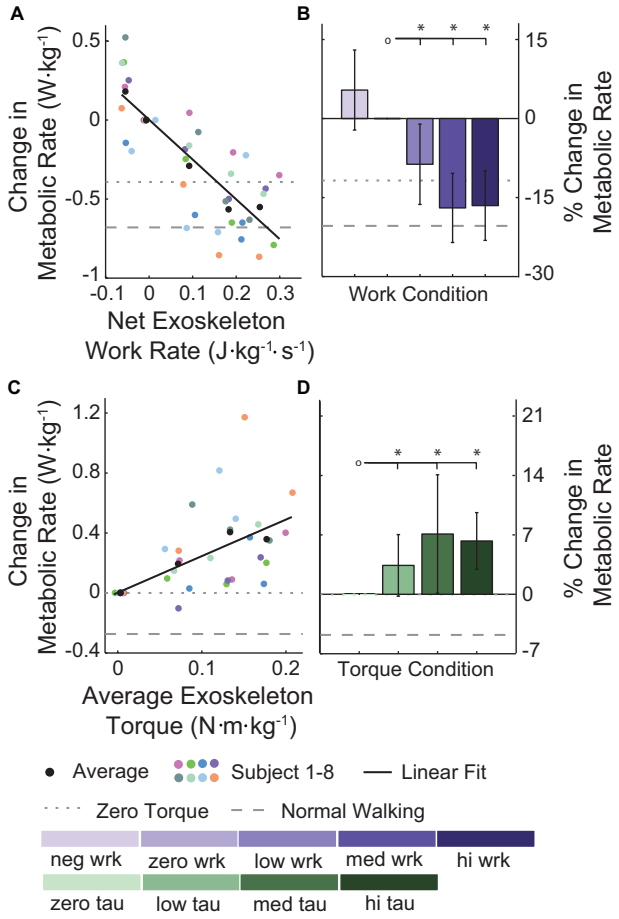

Figure 2.5: Metabolic rate decreased with increasing exoskeleton work input, but increased with increasing exoskeleton torque support. **A**. Change in metabolic rate from the Zero Work condition versus net exoskeleton work rate. Colored dots represent individual subject data, black dots represent average data, and the solid black line is a linear fit. Dotted and dashed gray lines represent average metabolic rate for the Zero Torque and Normal Walking conditions, respectively. **B**. Average change in metabolic rate across Work Study conditions. Darker purple indicates higher work conditions. Error-bars indicate inter-subject variability. **C**. Change in metabolic rate from the Zero Torque condition versus average exoskeleton torque. Dotted and dashed gray lines represent average metabolic rate for the Zero Torque and Normal Walking conditions, respectively. **D**. Average change in metabolic rate across Torque Study conditions. Darker green indicates higher torque conditions. Error-bars indicate inter-subject variability. *s indicate statistical significance with respect to the conditions designated by open circles.

Metabolics

Metabolic energy consumption was reduced with increasing net exoskeleton work rate but increased with increasing average exoskeleton torque. Metabolic rate decreased by 17% from the Zero Work condition to the High Work condition ($p = 2{\cdot}10^{-4}$, Fig. 2.5A,B). Using least-squares linear regression, the best fit line relating the change in metabolic rate, P_{met}, to net exoskeleton work rate, W_{exo}, was found to be $P_{met} \approx -2.52{\cdot}W_{exo}$ ($R^2 = 0.6$, $p = 2{\cdot}10^{-8}$). By

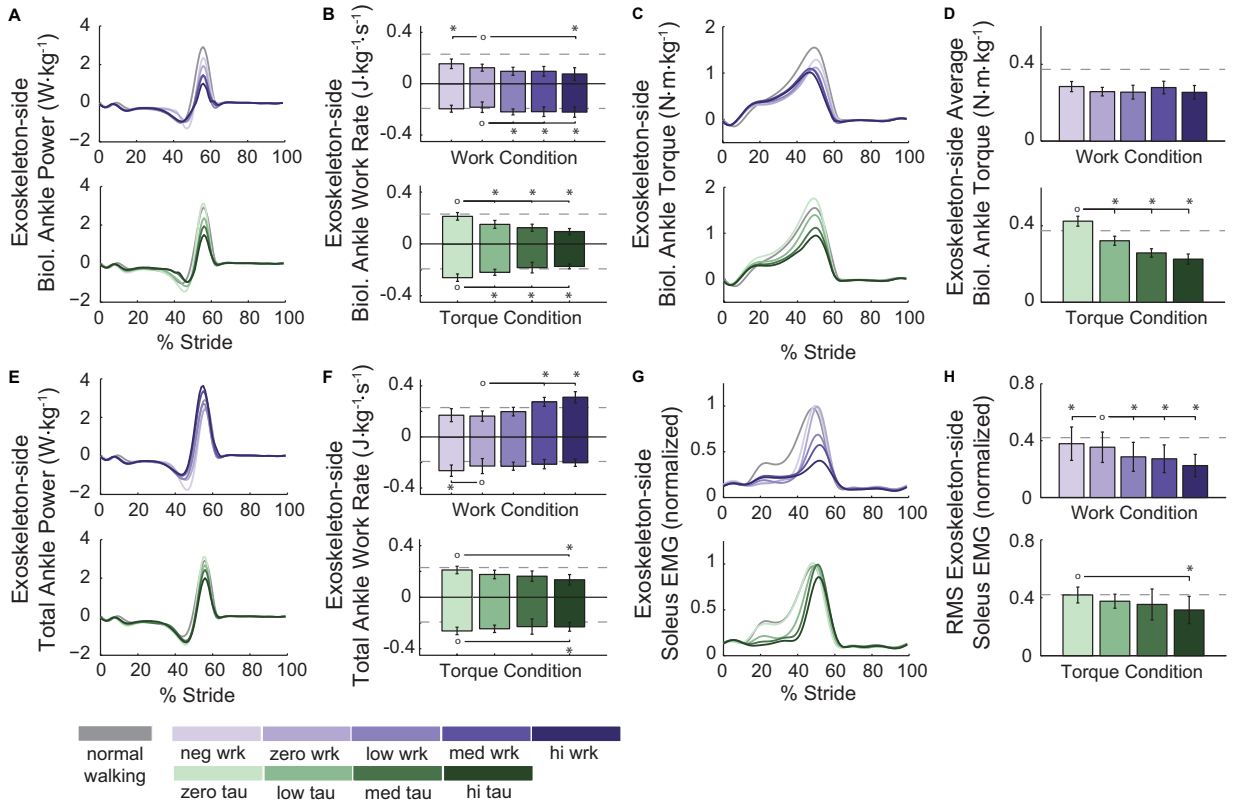

Figure 2.6: Effort-related outcomes improved at the assisted ankle for both the Work Study and the Torque Study, while effects on total ankle work differed. **A**. Biological power. **B**. Biological work rate. **C**. Biological torque. **D**. Average biological torque. **E**. Combined ankle power. **F**. Combined ankle work rate. **G**. Soleus EMG. **H**. Root-mean-square (RMS) soleus EMG. Work Study is in purple, Torque Study is in green, and darker colors indicate higher values. Normal Walking is in gray. Curves are study-average trajectories. Bars and whiskers are means and standard deviations of subject-wise integration of corresponding curves. *s indicate statistical significance with respect to the conditions designated by open circles.

contrast, metabolic rate increased by 13% from the Zero Torque condition to the High Torque condition ($p = 1{\cdot}10^{-3}$, Fig. 2.5C,D). The best fit line relating change in metabolic rate, P_{met}, to average exoskeleton torque, τ_{exo}, was found to be $P_{met} \approx 2.45{\cdot}\tau_{exo}$ ($R^2 = 0.3$, $p = 2{\cdot}10^{-3}$). The large error bars observed in the metabolic data are a result of inter-subject variability.

Exoskeleton-side Ankle Mechanics

Both modes of assistance reduced biological components of work, torque, and plantarflexor muscle activity at the assisted ankle joint. Positive biological ankle work rate decreased by 37% from the Zero Work condition to the High Work condition ($p = 0.02$, Fig. 2.6A,B), while negative biological ankle work rate increased in magnitude by 22% from the Zero Work

condition to the High Work condition ($p = 0.02$). Positive biological work rate decreased by 55% from the Zero Torque condition to the High Torque condition ($p = 1{\cdot}10^{-5}$), while negative biological work rate decreased in magnitude by 35% from the Zero Torque condition to the High Torque condition ($p = 9{\cdot}10^{-5}$). Biological ankle torque was reduced in the Work Study (ANOVA, $p = 0.02$, Fig. 2.6C,D) and was substantially reduced in the Torque Study (ANOVA, $p = 7{\cdot}10^{-14}$). Average biological torque decreased by 45% from the Zero Torque condition to the High Torque condition ($p = 2{\cdot}10^{-7}$). Normalized root-mean-square soleus muscle activity decreased by 37% from the Zero Work condition to the High Work condition ($p = 6{\cdot}10^{-5}$, Fig. 2.6G,H) and decreased by 24% from the Zero Torque condition to the High Torque condition ($p = 2{\cdot}10^{-3}$).

Total exoskeleton-side ankle work increased with increasing exoskeleton work, but decreased with increasing exoskeleton torque. Total positive ankle work rate increased by 94% from the Zero Work condition to the High Work condition ($p = 4{\cdot}10^{-5}$, Fig. 2.6E,F). By contrast, total positive ankle work rate decreased by 33% from the Zero Torque condition to the High Torque condition ($p = 5{\cdot}10^{-3}$).

Center-of-Mass Mechanics

Increasing exoskeleton work increased exoskeleton-side center-of-mass push-off work and decreased contralateral-limb collision and rebound work, while increasing exoskeleton torque led to opposite trends in center-of-mass mechanics (Fig. 2.7). In the Work Study, exoskeleton-side push-off work increased, while contralateral-limb collision and rebound work decreased (ANOVA, $p = 2{\cdot}10^{-13}$, $p = 7{\cdot}10^{-4}$, and $p = 7{\cdot}10^{-5}$, respectively). Assisted-limb push-off work rate increased by 44%, while contralateral-limb rebound work rate decreased by 73% from the Zero Work condition to the High Work condition ($p = 1{\cdot}10^{-6}$ and $p = 6{\cdot}10^{-3}$, respectively). In the Torque Study, exoskeleton-side push-off work decreased, while contralateral-limb collision and rebound work appeared to increase (ANOVA, $p = 4{\cdot}10^{-4}$, $p = 0.06$, and $p = 0.2$, respectively). Assisted-limb push-off work rate decreased by 19% from the Zero Torque condition to the High Torque condition ($p = 6{\cdot}10^{-3}$).

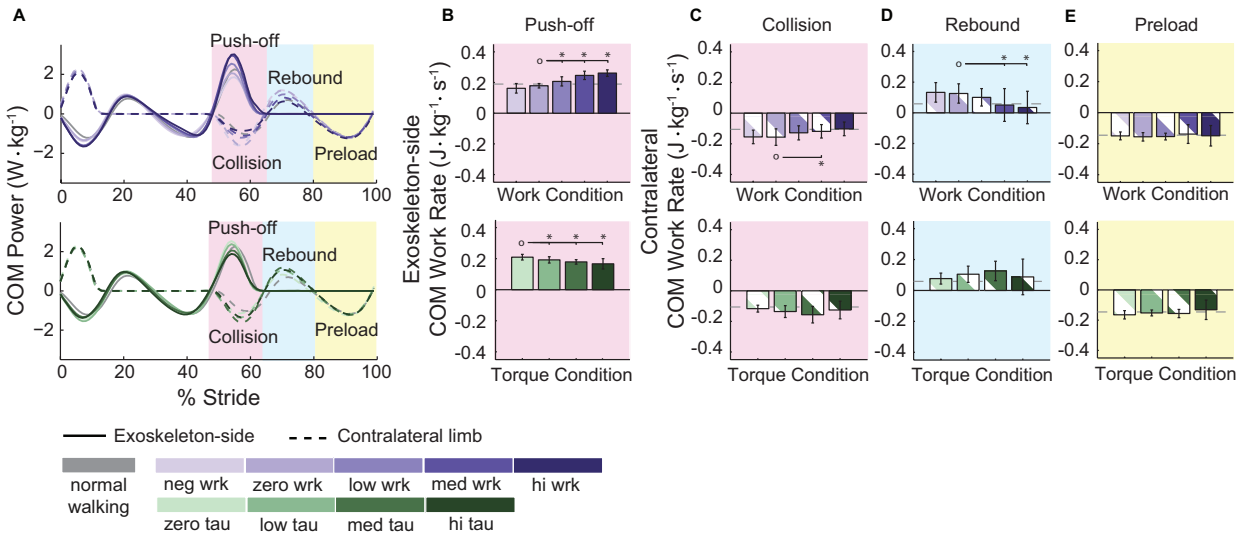

Figure 2.7: In the Work Study, exoskeleton-side center-of-mass push-off work increased and contralateral-limb collision and rebound work decreased, while in the Torque Study opposite trends were observed. **A**. Power. **B**. Exoskeleton-side push-off work rate. **C**. Contralateral-limb collision work rate. **D**. Contralateral-limb rebound work rate. **E**. Contralateral-limb preload work rate. Work rate is defined as the integral of power in the highlighted regions divided by stride time. Work Study is in purple, Torque Study is in green, and darker colors indicate higher values. Normal Walking is in gray. Curves are study-average trajectories, with exoskeleton-side power solid and contralateral-side power dashed. Bars and whiskers are means and standard deviations of subject-wise integration of corresponding curves in the shaded regions, with exoskeleton-side bars solid and contralateral-side bars striped. The pink region corresponds to exoskeleton-side push-off and contralateral-limb collision, the blue region corresponds to contralateral-limb rebound, and the yellow region corresponds to contralateral-limb preload. *s indicate statistical significance with respect to the conditions designated by open circles.

Contralateral-limb push-off work decreased and exoskeleton-side collision work increased across Work Study conditions (ANOVA, $p = 6{\cdot}10^{-5}$ and $p = 6{\cdot}10^{-4}$, respectively, Fig. 2.10), but did not change across Torque Study conditions (ANOVA, $p = 0.5$ and $p = 0.1$, respectively). From the Zero Work condition to the High Work condition, contralateral-limb push-off work rate decreased by 11% and exoskeleton-side collision work rate increased by 31% ($p = 7{\cdot}10^{-4}$ and $p = 0.02$, respectively).

Contralateral Knee Mechanics

Increased net exoskeleton work led to reduced muscle activity and biological components of work and torque at the contralateral knee joint, while increased average exoskeleton torque had the opposite effect (Fig. 2.8). Negative and positive work rates, extension torque, and vastus muscle activity all decreased in magnitude with increasing exoskeleton work

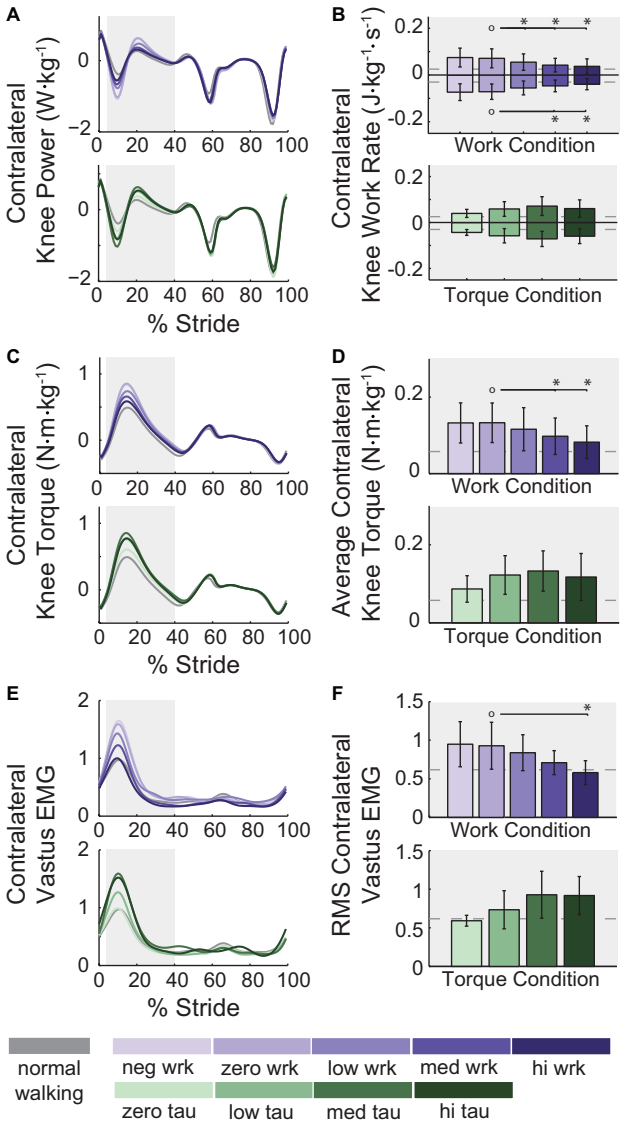

Figure 2.8: Contralateral knee work, torque, and muscle activity decreased in the Work Study, while opposite trends were observed in the Torque Study. **A**. Power. **B**. Work rate. **C**. Extension torque. **D**. Average torque. **E**. Vastus EMG. **F**. RMS vastus EMG. Work rate is defined as the integral of power in the highlighted region divided by stride time. Work Study is in purple, Torque Study is in green, and darker colors indicate higher values. Normal Walking is in gray. Curves are study-average trajectories. Bars and whiskers are means and standard deviations of subject-wise integration of corresponding curves in the shaded region. *s indicate statistical significance with respect to the conditions designated by open circles.

(ANOVA, $p = 2{\cdot}10^{-4}$, $p = 7{\cdot}10^{-7}$, $p = 6{\cdot}10^{-5}$, $p = 0.02$, respectively) and increased with increasing exoskeleton torque (ANOVA, $p = 0.03$, $p = 0.01$, $p = 0.01$, $p = 0.04$, respectively). From the Zero Work condition to the High Work condition, the magnitude of negative and positive contralateral knee work rate decreased by 44% and 48%, respectively ($p = 0.01$ and $p = 2{\cdot}10^{-3}$, respectively). From the Zero Work condition to the High Work condition,

contralateral knee extension torque and vastus muscle activity decreased by 34% and 26%, respectively ($p = 5{\cdot}10^{-3}$ and $p = 0.01$, respectively).

Stride time was 1.16 ± 0.05 s in the Zero Torque condition and remained within 2% of this value across all conditions (ANOVA, $p = 0.2$). Kinematic and kinetic results for all lower limb joints, muscle activity for all measured muscles, and center-of-mass work rates when the contralateral limb is trailing are shown in the appendix. Complete numerical results are presented in Table 2.1 and Table 2.2 in the appendix.

2.4 Discussion

We conducted an experiment in which we explored the independent effects of a particular mode of work input and torque support on metabolic rate, center-of-mass mechanics, joint mechanics, and muscle activity. Metabolic energy consumption decreased with increasing exoskeleton work, but, surprisingly, increased with increasing average exoskeleton torque. Both interventions reduced effort-related measures at the assisted joint, such as biological ankle work, biological ankle torque, and soleus muscle activity. Changes elsewhere in the body, arising from unexpected changes in human coordination, differed between interventions and seemed to best explain the observed trends in metabolic rate.

Metabolic energy consumption decreased with increasing exoskeleton work input. As expected, part of this reduction seems to have been a result of reduced effort at the assisted ankle joint. Net biological ankle joint work became increasingly negative across Work Study conditions, implying increasingly negative muscle work, which is less costly than isometric force production or positive muscle fiber work at the same force [79]. In addition, soleus muscle activity decreased with increasing work input (Fig. 2.6G,H), even though peak biological ankle torque remained relatively constant (Fig. 2.6C). Timing of peak biological ankle torque, however, did seem to be affected. As exoskeleton work increased, biological ankle torque peaked and dropped off earlier in the stance period. This earlier onset of biological ankle torque drop-off may explain reduced soleus muscle activity during the latter

part of stance, i.e. preceding push-off. Musculoskeletal models could be used to explore these ideas further.

Total exoskeleton-side ankle work increased across Work Study conditions. Increases in positive work supplied by the device outweighed reductions in biological work. Increased total ankle work led to an increase in exoskeleton-side center-of-mass push-off work and decreased contralateral-limb collision work and rebound work. These results are consistent with simple walking model predictions of the effect of push-off work on center-of-mass mechanics [67, 101]. Decreased collision and rebound work seem to have been accompanied by changes in contralateral knee mechanics, seen as reduced work, extension torque, and vastus muscle activity around the step-to-step transition. Such changes may account for another substantial portion of the observed reduction in metabolic rate.

Contrary to our expectations, metabolic rate increased with increasing torque support of the described form. Despite large decreases in biological contributions to ankle torque and work, the reduction in energy use at the assisted ankle joint was likely relatively small given the small decreases in plantarflexor muscle activity (Fig. 2.6G,H). These small benefits were apparently outweighed by larger costs elsewhere in the body. The contralateral knee appears to be principally responsible for additional energy use, exhibiting increases in joint torque, joint work, and muscle activity with increasing average ankle exoskeleton torque.

Center-of-mass mechanics during the step-to-step transition may explain the coupling between activities of the trailing ankle and leading knee. Total ankle joint work decreased across Torque Study conditions and led to reduced center-of-mass push-off work. Simple walking models predict that reduced trailing-limb push-off work disproportionately increases collision dissipation and rebound work in the leading leg [67, 101]. Although this result has not always been observed in humans [e.g. 20], in this study increased torque support led to reduced total exoskeleton-side ankle push-off work and increased contralateral knee work during double-support. Alternatively, synergies between ankle plantarflexors and opposite-limb knee extensors, similar to the theorized coupling between stance-leg force and swing-leg afferent presynaptic inhibition [55], could explain how exoskeleton torques applied to the

trailing ankle affected the contralateral knee. This interpretation must be tempered by recent findings suggesting limits in the ability of synergies to accurately capture neuromuscular control strategies [127]. These ideas merit further exploration.

Subjects could have adapted to prevent the observed decrease in exoskeleton-side push-off work and corresponding increase in contralateral knee work in the Torque Study, but they did not. The decrease in biological ankle work is likely due to changes in muscle fascicle dynamics with increasing torque support, and the cost of maintaining consistent biological ankle work may have outweighed the potential benefits. During early and mid-stance, subjects reduced the biological component of ankle plantarflexion torque (Fig. 2.6C,D), perhaps in an effort to maintain consistent total ankle torque [64]. Lower biological ankle torque and soleus muscle activity during the first part of stance suggest that muscle-tendon force and Achilles tendon stretch were reduced leading into late stance. This result is similar to the observed reduction in muscle-tendon force and tendon stretch during hopping with a passive ankle exoskeleton [41]. To provide the usual burst of positive push-off work, the calf muscles would have had to contract with higher velocity than normal, in order to either increase tension to normal levels by quickly stretching the Achilles tendon or increase contraction velocity beyond normal levels for the muscle-tendon unit as a whole. Muscle force per unit activation drops precipitously with increasing contraction velocity, meaning muscle activation would have had to increase substantially to generate normal levels of positive ankle work, incurring a large metabolic cost [114]. This explanation is consistent with the lack of a large reduction in late-stance plantarflexor muscle activity and with the reduced ratio of biological joint torque to activation during the same period (Fig. 2.6C,G). Increased plantarflexor muscle fascicle contraction velocity is also implicated by a greater change in fascicle length during push-off; with high exoskeleton torque, fascicle length at the onset of push-off was likely increased, since tendons stretched less but ankle kinematics were consistent. These ideas merit further examination in a musculoskeletal model.

There are alternate explanations for the observed increase in metabolic rate with increased average exoskeleton torque. One possibility is that subjects did not learn to use the device

effectively due to neurological constraints on patterns of muscle activation [102, 109, 123]. This seems unlikely, because similar issues were not observed in the Work Study, but the idea is worth exploring more deeply in a neuromuscular model. Another explanation is co-activation of the tibialis anterior to counteract exoskeleton torque. While we did observe increased tibialis anterior muscle activity in some conditions (Fig. 2.16), increases did not correlate well with increased metabolic rate.

The increase in metabolic rate with increasing average exoskeleton torque observed in this study would be difficult to predict using models that do not include muscles or models that assume fixed kinematics and kinetics. Simple dynamic walking models, for example, typically do not incorporate muscle dynamics and therefore would likely not have predicted the observed suppression of total ankle push-off work in the Torque Study. More complete skeletal models have been used to predict the effect of similar interventions [116]. These models anticipated reduced torque and power from biological tissues at the assisted joints, consistent with our findings, but assumed fixed kinematics and kinetics and predicted reduced metabolic rate, which are inconsistent with results from this study. Similar difficulties would be encountered using more complete musculoskeletal models under the assumption of fixed kinetics and kinematics [111, 86, 4, 103], since the observed changes in metabolic rate were best explained by changes in whole-body mechanics. Predictive simulations that optimize complete coordination patterns could overcome the above limitations [1, 108, 107]. We expect the data from this study, and others with novel mechanical interventions, will help improve the predictive validity of such models [45].

With the aim of informing improved predictive models, we correlated several outcomes to metabolic rate and found that summed muscle activity fit observations better than joint work or center-of-mass work. It would be beneficial to have mechanical or electrical predictors of metabolic rate, which could be calculated in musculoskeletal models or measured more easily and at a higher frequency than whole-body metabolic rate using respirometry. The sum of all positive and negative mechanical work on the center of mass, multiplied by muscle efficiencies, has been suggested as a determinant of metabolic cost in human walking [37, 68], but poorly

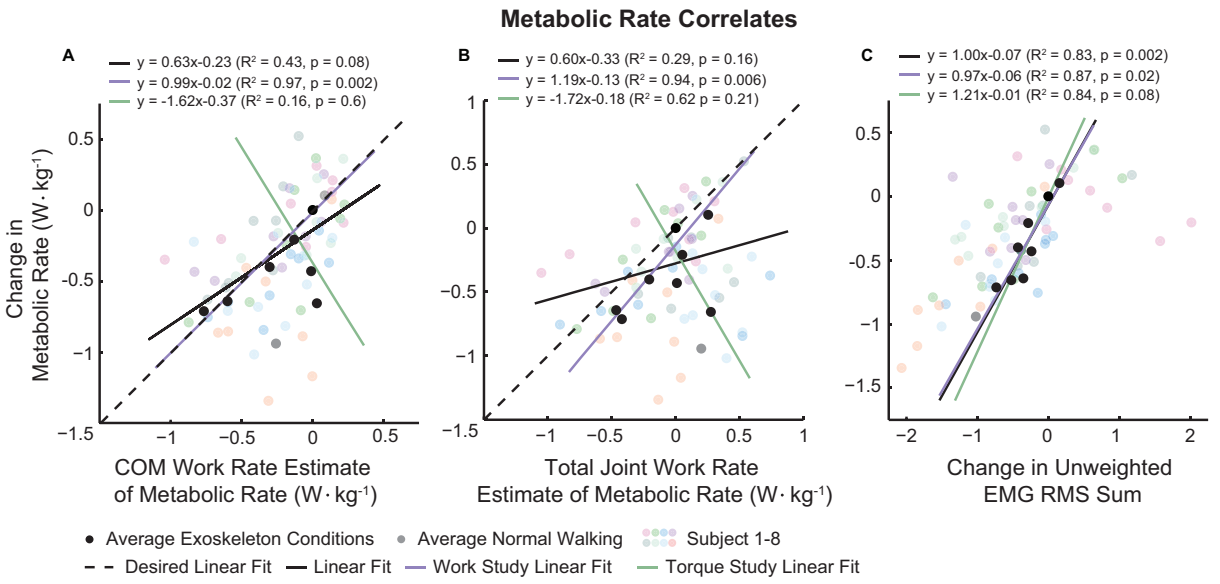

Figure 2.9: Unweighted sum of measured electromyography best correlated with changes in metabolic rate. **A.** Measured metabolic rate versus estimate of metabolic rate based on center-of-mass work. **B.** Measured metabolic rate versus estimated metabolic rate based on total joint work. **C.** Measured metabolic rate versus unweighted sum of the root-mean-square of all measured muscle activity. Black dots represent average data for all conditions. Colored dots represent data for individual subjects. Dashed black line indicates the desired linear fit. Black, purple, and green solid lines are the linear fits to average data for all conditions, average Work Study data, and average Torque Study data, respectively.

fit observations in this study ($R^2 = 0.43$, $p = 0.08$, Fig. 2.9A), particularly across the Torque Study. The weighted sum of all positive and negative joint work has also previously been found to correlate well with metabolic rate [20], but also poorly fit observations in this study ($R^2 = 0.29$, $p = 0.16$, Fig. 2.9B), particularly for the Torque Study. It might be that work-related outcomes naturally tend to be more affected by work-related mechanical interventions or activities. The unweighted sum of all muscle activity measured by electromyography fit trends in both the Work Study and the Torque Study relatively well ($R^2 = 0.83$, $p = 0.002$, Fig. 2.9C), which is consistent with other findings [106, 78]. This signal, or a refined version accounting for muscle volume and maximum voluntary contraction, might be a candidate for online optimization in human locomotion experiments. Given the complexity of the physiological structures involved in human locomotion, however, it seems likely that this measure of muscle activity will not correlate to metabolic rate for some interventions.

Exoskeleton work assistance seems to reduce the energy cost of walking with more

consistency than torque assistance. The finding that augmenting push-off work led to reduced metabolic rate is consistent with several recent studies [105, 56, 24, 75, 20, 84]. Findings for spring-like torque support have been less consistent; metabolic rate has been reduced with some interventions [15, 26], while it was increased here and in other studies [117]. Human-robot interactions, and their cascading dynamical consequences, are complex, and subtle differences between mechanical interventions can lead to substantial differences in the human response [23]. We explored a narrow region of the space of possible torque support patterns, therefore it is likely that more effective spring-like interventions exist. We also may not have provided participants with sufficient training and coaching, although this seems unlikely as these same results were observed in both naïve and experienced participants. Nevertheless, it appears to be easier to obtain benefits from active exoskeletons than passive ones, at least in terms of metabolic energy use. This could mean that active elements should be incorporated into autonomous devices to obtain the greatest reductions in metabolic cost.

Exoskeleton work and torque were decomposed because of their potential relationships to the cost of performing net muscle work and the cost of producing muscle force, respectively. However, any separation of work and torque has inherent limitations due to the dependence of work on torque. Several potential decompositions of torque exist, including timing of torque application, peak torque, and average torque. Systematically changing net work while keeping one decomposition of torque constant across conditions, however, will result in changes in the other measures. For this study, average exoskeleton torque, or the integral of torque over a stride divided by stride time, was chosen as the torque parameter of interest because of its relevance to the cost of muscle force production – researchers have used the integral of muscle force, divided by body weight, as a measure of the metabolic cost of producing force with muscle [53]. The effects of other decompositions of torque on biomechanical outcomes are interesting and should also be explored.

Work and torque were applied unilaterally in this experiment. In the Work Study, exoskeleton-side center-of-mass push-off work increased and contralateral-limb collision and rebound work decreased, while on the subsequent step contralateral-limb push-off work

decreased and assisted-limb collision work increased, indicating an asymmetric gait pattern. Although asymmetric gait patterns are known to increase metabolic cost in some situations [35, 122], it is not known whether a symmetric gait is optimal given an asymmetric morphology. Metabolic energy consumption in the High Work condition was below the value in the Zero Torque condition, in which gait was more symmetric. This supports the idea that a symmetric gait need not be optimal given an asymmetric system.

Two participants had difficulty adapting to the exoskeleton behavior and were excluded as statistical outliers. This may have been due to insufficient training. Additional exposure to the exoskeleton, or coaching on its use, may have allowed participants to better interact with the exoskeleton. Desired exoskeleton torque and work values were normalized to body mass for each participant and enforced via iterative learning compensation. Thus, the applied torque trajectories were likely not optimal for individual participants. Optimizing exoskeleton torque trajectories for each participant could result in faster adaptation to the interaction and more beneficial changes in biomechanical outcomes.

2.5 Conclusions

In this study, we independently varied a particular mode of exoskeleton work input and torque support over a large range and measured metabolic rate, center-of-mass mechanics, joint mechanics, and electromyography to characterize the human physiological response to these two interventions. We found that increasing this mode of exoskeleton work delivery reduced metabolic energy consumption, while increasing this mode of average exoskeleton torque support increased metabolic energy consumption. The observed trends in metabolic rate are best explained by disparate changes in total exoskeleton-side ankle mechanics, arising from interactions with muscle fascicle dynamics, and the cascading effects on whole-body coordination, particularly at the contralateral knee. This result illustrates the difficulty in using very simple models or more complex models that assume fixed kinematics or kinetics to predict the impact of a mechanical intervention on a human. It supports the case for

experimental approaches designed to measure the full biomechanical response of the human to a wide variety of novel assistance strategies. We expect that the empirical data provided by this study will lead to improved predictive models of human coordination and to better designs of assistive devices.

Acknowledgments

This material is based upon work supported by the National Science Foundation under Grant No. IIS-1355716 and Graduate Research Fellowship Grant No. DGE-1252552. The authors thank Anne Alcasid, Roberto Jaime, and Julie Rekant for assistance with data collection and processing, Joshua Caputo and Roberto Quesada for assistance with hardware maintenance, and Hartmut Geyer for use of data collection equipment.

2.6 Appendix A: Tables of Outcomes

Table 2.1: Work Study Outcomes

		Negative Work	Zero Work	Low Work	Medium Work	High Work
	Net Exoskeleton Work Rate ($J \cdot kg^{-1} \cdot s^{-1}$)	-0.054 ± 0.0076*	-0.0065 ± 0.0088	0.092 ± 0.012*	0.18 ± 0.018*	0.25 ± 0.030*
	Average Exoskeleton Torque ($N \cdot m \cdot kg^{-1}$)	0.12 ± 0.022	0.13 ± 0.015	0.13 ± 0.016	0.1 ± 0.019	0.14 ± 0.022
	Change in Metabolic Rate ($W \cdot kg^{-1}$)	0.18 ± 0.25	0.00 ± 0.00	-0.29 ± 0.25*	-0.57 ± 0.22*	-0.55 ± 0.22*
Exoskeleton-Side	**Positive Biol. Ankle Work Rate** ($J \cdot kg^{-1} \cdot s^{-1}$)	0.16 ± 0.037*	0.12 ± 0.027	0.097 ± 0.031	0.097 ± 0.038	0.076 ± 0.049*
	Negative Biol. Ankle Work Rate ($J \cdot kg^{-1} \cdot s^{-1}$)	-0.19 ± 0.027	-0.18 ± 0.041*	-0.22 ± 0.023*	-0.22 ± 0.037*	-0.22 ± 0.040*
	Positive Total Ankle Work Rate ($J \cdot kg^{-1} \cdot s^{-1}$)	0.17 ± 0.051	0.16 ± 0.040	0.20 ± 0.034	0.27 ± 0.035*	0.31 ± 0.043*
	Negative Total Ankle Work Rate ($J \cdot kg^{-1} \cdot s^{-1}$)	-0.26 ± 0.045	-0.23 ± 0.059	-0.23 ± 0.032	-0.21 ± 0.036*	-0.20 ± 0.028*
	Biol. Ankle Torque ($N \cdot m \cdot kg^{-1}$)	0.28 ± 0.026	0.26 ± 0.022	0.26 ± 0.036	0.28 ± 0.033	0.25 ± 0.036
	RMS Soleus EMG (Normalized)	0.38 ± 0.12*	0.35 ± 0.11	0.29 ± 0.10*	0.27 ± 0.097*	0.22 ± 0.079*
	COM Push-Off Work Rate ($J \cdot kg^{-1} \cdot s^{-1}$)	0.16 ± 0.031	0.18 ± 0.014	0.21 ± 0.030*	0.25 ± 0.027*	0.26 ± 0.022*
	COM Collision Work Rate ($J \cdot kg^{-1} \cdot s^{-1}$)	-0.14 ± 0.045	-0.13 ± 0.054	-0.16 ± 0.043	-0.16 ± 0.041*	-0.17 ± 0.060*
Contralateral	**COM Push-Off Work Rate** ($J \cdot kg^{-1} \cdot s^{-1}$)	0.17 ± 0.021	0.18 ± 0.025	0.17 ± 0.024*	0.15 ± 0.016*	0.16 ± 0.019*
	COM Collision Work Rate ($J \cdot kg^{-1} \cdot s^{-1}$)	-0.16 ± 0.044	-0.16 ± 0.054	-0.13 ± 0.046	-0.12 ± 0.044*	-0.10 ± 0.044
	COM Rebound Work Rate ($J \cdot kg^{-1} \cdot s^{-1}$)	0.13 ± 0.064	0.13 ± 0.063	0.10 ± 0.057	0.051 ± 0.11*	0.035 ± 0.11*
	Positive Knee Work Rate ($J \cdot kg^{-1} \cdot s^{-1}$)	0.075 ± 0.040	0.071 ± 0.041	0.055 ± 0.035*	0.042 ± 0.029*	0.037 ± 0.032*
	Negative Knee Work Rate ($J \cdot kg^{-1} \cdot s^{-1}$)	-0.073 ± 0.036	-0.072 ± 0.033	-0.056 ± 0.030*	-0.047 ± 0.025*	-0.040 ± 0.024*
	Knee Extension Torque ($N \cdot m \cdot kg^{-1}$)	0.14 ± 0.048	0.14 ± 0.046	0.12 ± 0.051*	0.11 ± 0.041*	0.093 ± 0.038*
	RMS Vastus EMG (Normalized)	1.24 ± 0.29	1.19 ± 0.26	1.09 ± 0.25*	1.05 ± 0.20*	0.88 ± 0.17*

Values are mean ± SD. *s indicate statistical significance $p < 0.05$.

Table 2.2: Torque Study Outcomes

		Zero Torque	Low Torque	Medium Torque	High Torque
	Net Exoskeleton Work Rate ($J \cdot kg^{-1} \cdot s^{-1}$)	-0.0027 ± 0.0022	-0.0003 ± 0.0064	-0.0065 ± 0.0088	-0.016 ± 0.0059*
	Average Exoskeleton Torque ($N \cdot m \cdot kg^{-1}$)	0.0032 ± 0.0033	0.072 ± 0.011*	0.13 ± 0.015*	0.18 ± 0.021*
	Change in Metabolic Rate ($W \cdot kg^{-1}$)	0.00 ± 0.00	0.19 ± 0.21*	0.41 ± 0.40*	0.36 ± 0.19*
Exoskeleton-Side	**Positive Biol. Ankle Work Rate** ($J \cdot kg^{-1} \cdot s^{-1}$)	0.21 ± 0.029	0.15 ± 0.031*	0.12 ± 0.027*	0.095 ± 0.024*
	Negative Biol. Ankle Work Rate ($J \cdot kg^{-1} \cdot s^{-1}$)	-0.26 ± 0.029	-0.22 ± 0.024*	-0.18 ± 0.041*	-0.17 ± 0.019*
	Positive Total Ankle Work Rate ($J \cdot kg^{-1} \cdot s^{-1}$)	0.21 ± 0.029	0.18 ± 0.033	0.16 ± 0.040	0.14 ± 0.040*
	Negative Total Ankle Work Rate ($J \cdot kg^{-1} \cdot s^{-1}$)	-0.26 ± 0.029	-0.25 ± 0.028	-0.23 ± 0.059	-0.23 ± 0.034*
	Biol. Ankle Torque ($N \cdot m \cdot kg^{-1}$)	0.42 ± 0.026	0.32 ± 0.024*	0.26 ± 0.022*	0.23 ± 0.026*
	RMS Soleus EMG (Normalized)	0.42 ± 0.055	0.38 ± 0.049	0.35 ± 0.11	0.32 ± 0.094*
	COM Push-Off Work Rate ($J \cdot kg^{-1} \cdot s^{-1}$)	0.21 ± 0.018	0.19 ± 0.020*	0.18 ± 0.014*	0.17 ± 0.034*
	COM Collision Work Rate ($J \cdot kg^{-1} \cdot s^{-1}$)	-0.14 ± 0.026	-0.15 ± 0.035	-0.13 ± 0.054	-0.13 ± 0.048
Contralateral	**COM Push-Off Work Rate** ($J \cdot kg^{-1} \cdot s^{-1}$)	0.17 ± 0.019	0.17 ± 0.021	0.18 ± 0.025	0.17 ± 0.019
	COM Collision Work Rate ($J \cdot kg^{-1} \cdot s^{-1}$)	-0.12 ± 0.022	-0.14 ± 0.039	-0.16 ± 0.054	-0.13 ± 0.058
	COM Rebound Work Rate ($J \cdot kg^{-1} \cdot s^{-1}$)	0.077 ± 0.036	0.10 ± 0.053	0.13 ± 0.063	0.088 ± 0.12
	Positive Knee Work Rate ($J \cdot kg^{-1} \cdot s^{-1}$)	0.039 ± 0.018	0.059 ± 0.032	0.071 ± 0.041	0.060 ± 0.038
	Negative Knee Work Rate ($J \cdot kg^{-1} \cdot s^{-1}$)	-0.043 ± 0.013	-0.058 ± 0.031	-0.072 ± 0.033	-0.060 ± 0.032
	Knee Extension Torque ($N \cdot m \cdot kg^{-1}$)	0.098 ± 0.027	0.13 ± 0.047	0.14 ± 0.046	0.13 ± 0.055
	RMS Vastus EMG (Normalized)	0.86 ± 0.071	1.12 ± 0.32	1.19 ± 0.26	1.29 ± 0.39

Values are mean ± SD. *s indicate statistical significance $p < 0.05$.

2.7 Appendix B: Mechanics and Muscle Activity

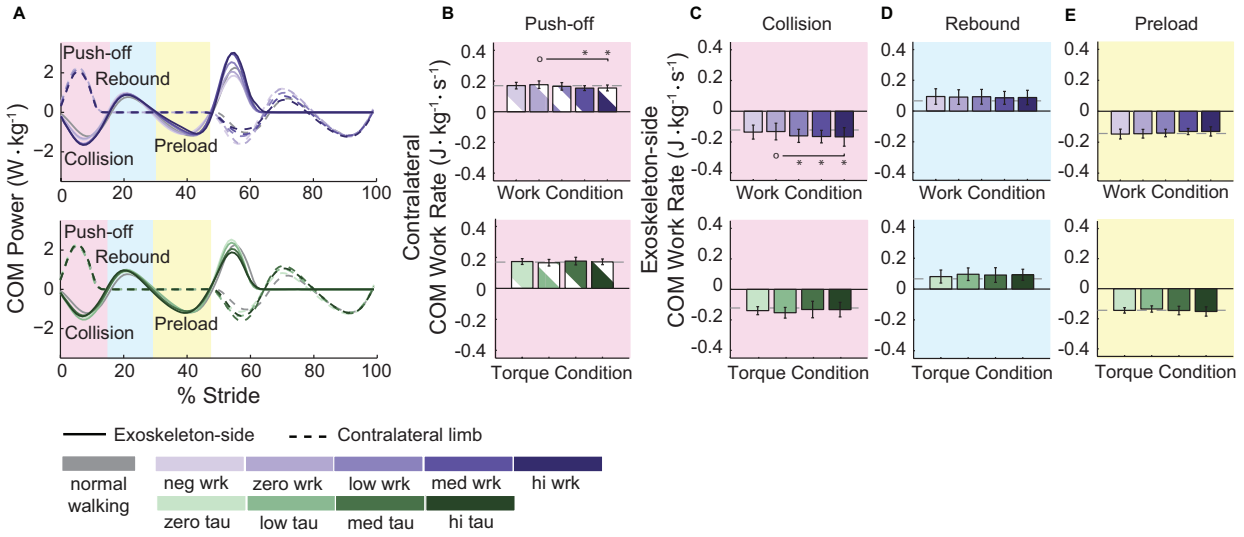

Figure 2.10: In the Work Study, contralateral-limb center-of-mass push-off work decreased and exoskeleton-side collision work increased in magnitude, while in the Torque Study no trends were observed in center-of-mass mechanics when the contralateral limb was trailing. **A**. Power. **B**. Contralateral-limb push-off work rate. **C**. Exoskeleton-side collision work rate. **D**. Exoskeleton-side rebound work rate. **E**. Exoskeleton-side preload work rate. Work rate is defined as the integral of power in the highlighted region divided by stride time. Work Study is in purple, Torque Study is in green, and darker colors indicate higher values. Normal Walking is in gray. Curves are study-average trajectories, with exoskeleton-side power solid and contralateral-side power dashed. Bars and whiskers are means and standard deviations of subject-wise integration of corresponding curves in the shaded regions, with exoskeleton-side bars solid and contralateral-side bars striped. The pink region corresponds to contralateral-limb push-off and exoskeleton-side collision, the blue region corresponds to exoskeleton-side rebound, and the yellow region corresponds to exoskeleton-side preload. *s indicate statistical significance with respect to the conditions designated by open circles.

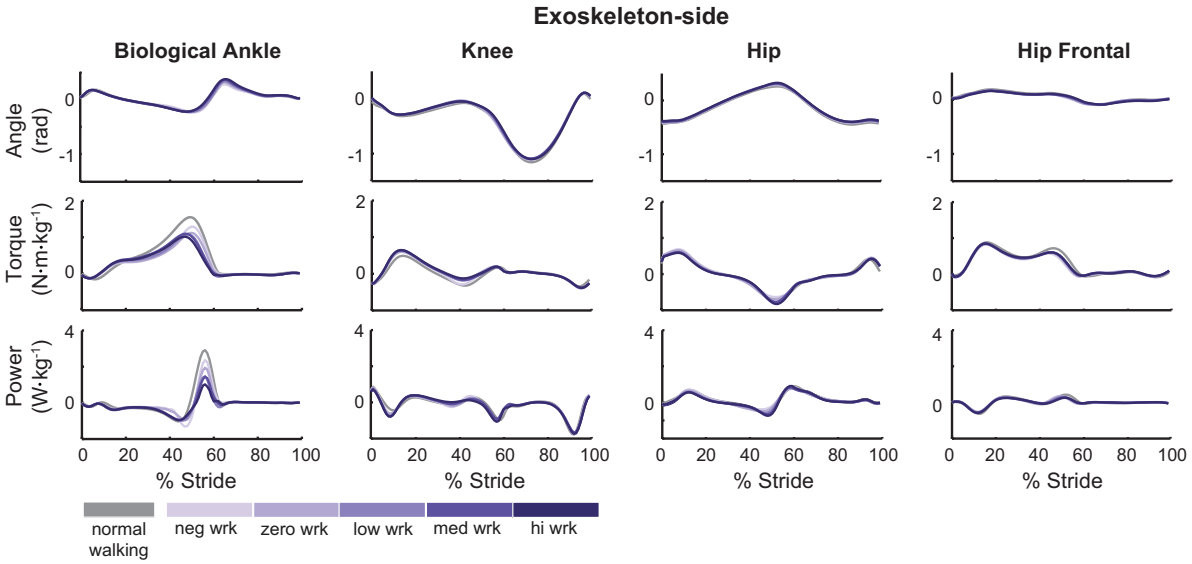

Figure 2.11: Exoskeleton-side joint mechanics across Work Study conditions. The biological component of ankle torque and power decreased with increasing work, while other exoskeleton-side joint mechanics did not appear to change across conditions. Positive values indicate extension and negative values indicate flexion. Purple lines represent average trajectories with darker colors indicating higher work values.

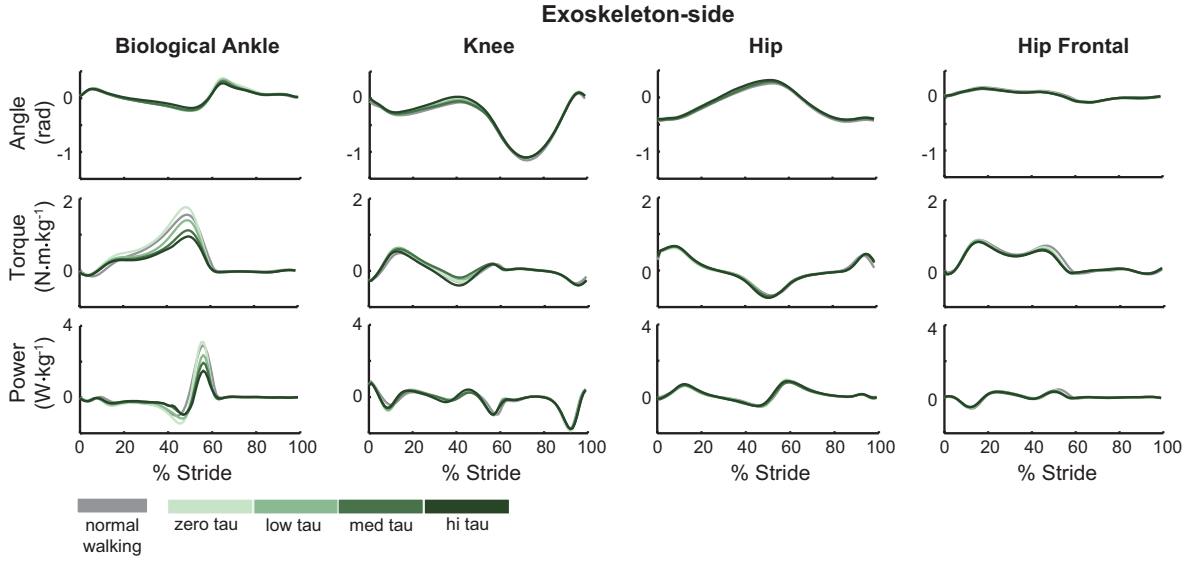

Figure 2.12: Exoskeleton-side joint mechanics across Torque Study conditions. The biological component of ankle torque and power decreased with increasing torque, while other exoskeleton-side joint mechanics did not appear to change across conditions. Positive values indicate extension and negative values indicate flexion. Green lines represent average trajectories with darker colors indicating higher torque values.

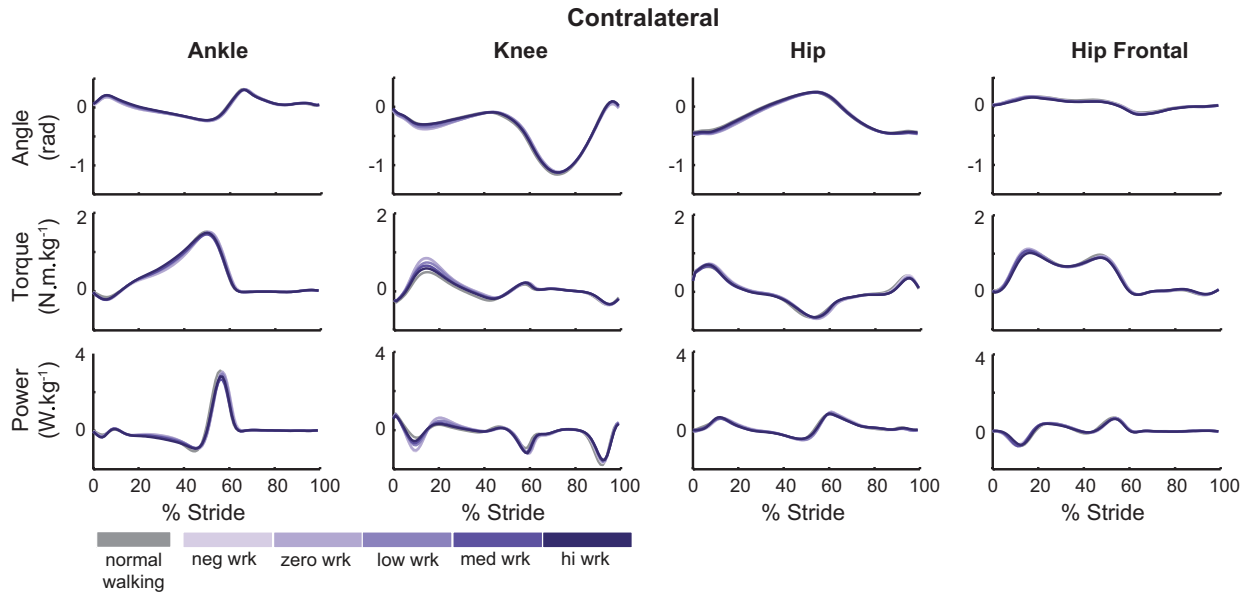

Figure 2.13: Contralateral limb joint mechanics across Work Study conditions. Knee torque and power decreased with increasing work, while other contralateral joint mechanics did not appear to change across conditions. Positive values indicate extension and negative values indicate flexion. Purple lines represent average trajectories with darker colors indicating higher work values.

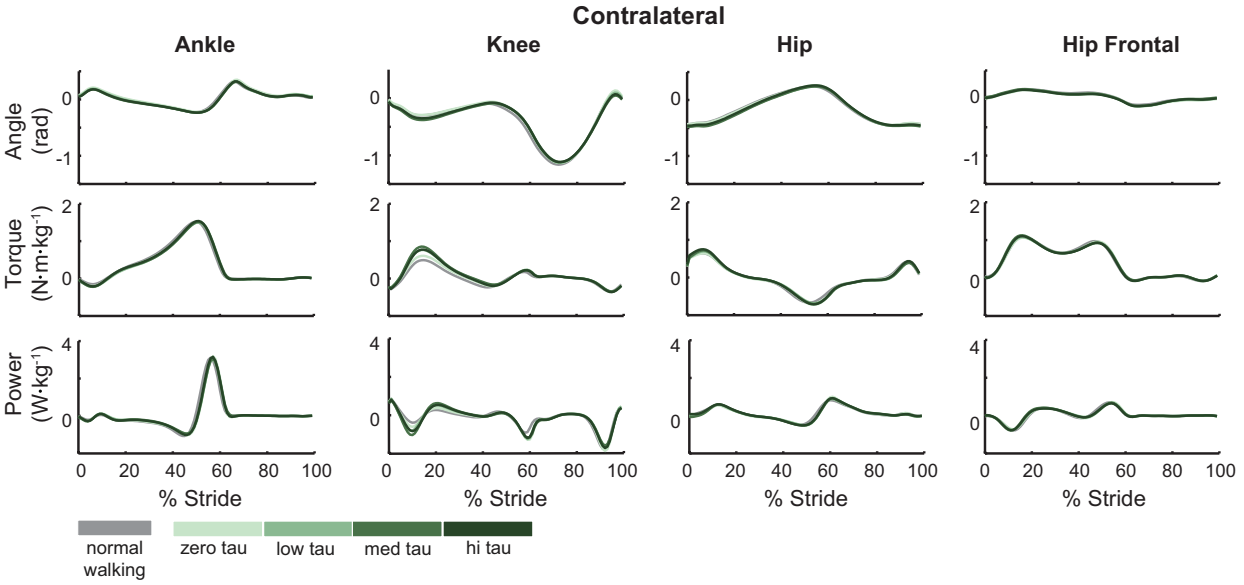

Figure 2.14: Contralateral limb joint mechanics across Torque Study conditions. Knee torque and power increased with increasing torque, while other contralateral joint mechanics did not appear to change across conditions. Positive values indicate extension and negative values indicate flexion. Green lines represent average trajectories with darker colors indicating higher torque values.

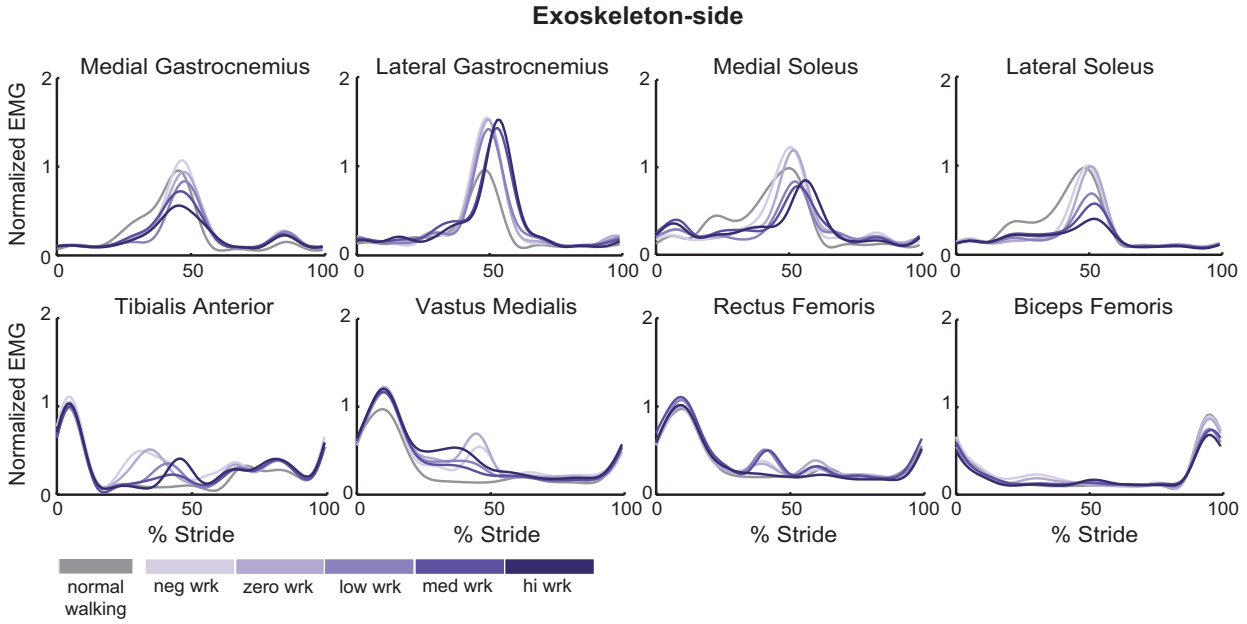

Figure 2.15: Exoskeleton-side electromyography across Work Study conditions. Electromyographic signals were normalized to average peak activation during Normal Walking. Purple lines represent average trajectories with darker colors indicating higher work values.

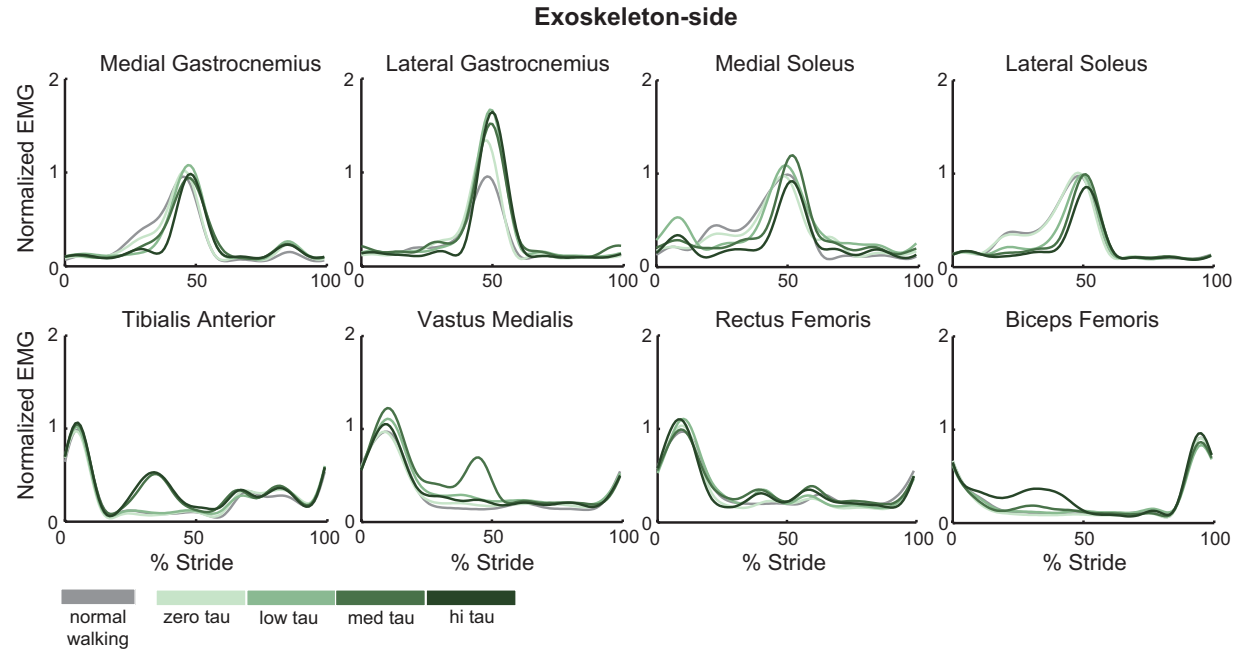

Figure 2.16: Exoskeleton-side electromyography across Torque Study Conditions. Electromyographic signals were normalized to average peak activation during Normal Walking. Green lines represent average trajectories with darker colors indicating higher torque values.

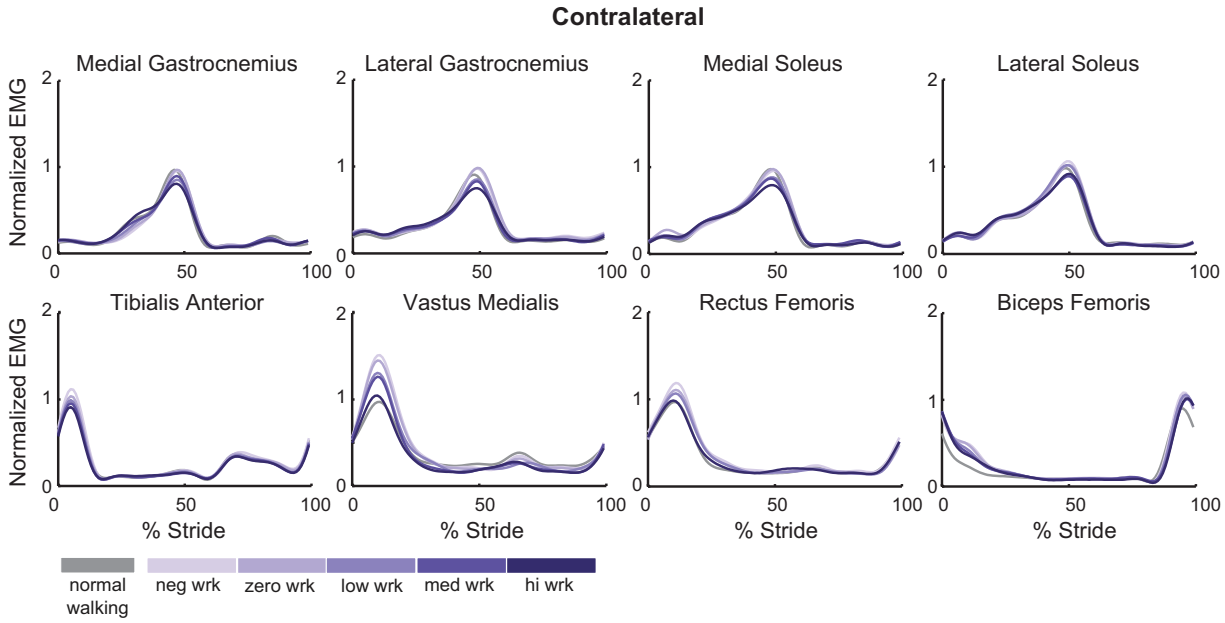

Figure 2.17: Contralateral limb electromyography across Work Study Conditions. Electromyographic signals were normalized to average peak activation during Normal Walking. Purple lines represent average trajectories with darker colors indicating higher work values.

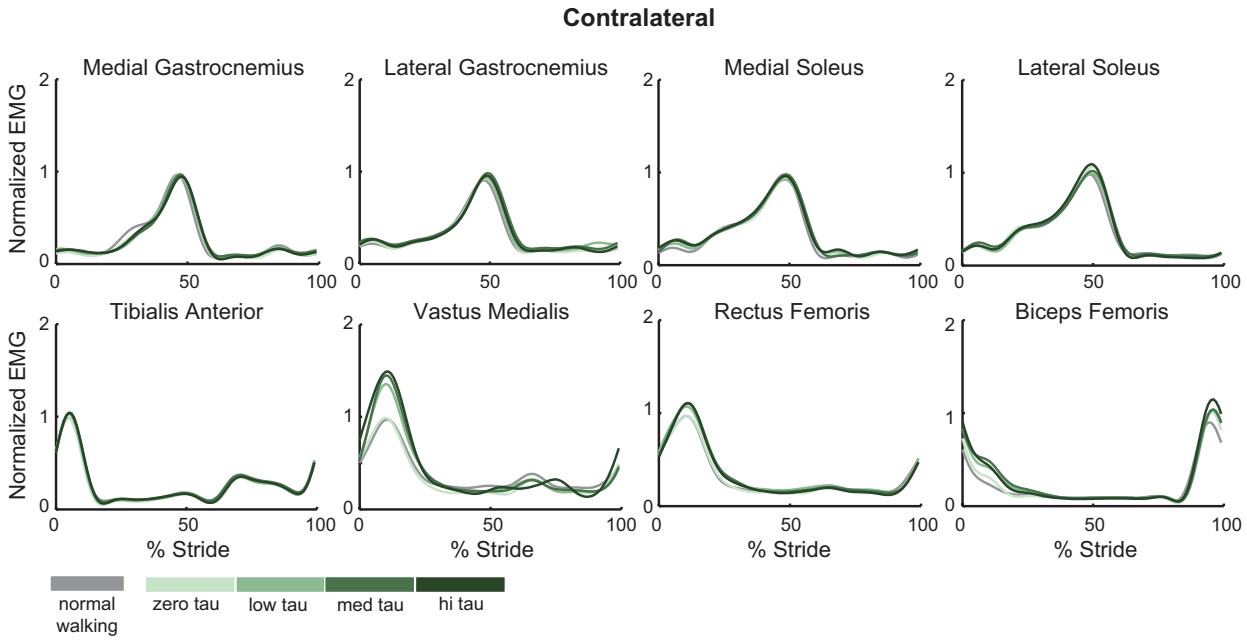

Figure 2.18: Contralateral limb electromyography across Torque Study Conditions. Electromyographic signals were normalized to average peak activation during Normal Walking. Green lines represent average trajectories with darker colors indicating higher torque values.

Chapter 3

Muscle-tendon mechanics explain unexpected effects of exoskeleton assistance on metabolic rate during walking [‡]

Abstract

The goal of this study was to gain insight into how ankle exoskeletons affect the behavior of the plantarflexor muscles during walking. Using data from previous experiments, we performed electromyography-driven simulations of musculoskeletal dynamics to explore how changes in exoskeleton assistance affected plantarflexor muscle-tendon mechanics, particularly for the soleus. We used a model of muscle energy consumption to estimate individual muscle metabolic rate. As average exoskeleton torque was increased, while no net exoskeleton work was provided, a reduction in tendon recoil led to an increase in positive mechanical work performed by the soleus muscle fibers. As net exoskeleton work was

[‡]This work appears as an advance article in: Jackson, R. W., Dembia, C. L., Delp, S. L., and Collins, S. H. (2017). Muscle-tendon mechanics explain unexpected effects of exoskeleton mechanics on metabolic rate during walking. *J. Exp. Biol.* In press.

increased, both soleus muscle fiber force and positive mechanical work decreased. Trends in the sum of the metabolic rates of the simulated muscles correlated well with trends in experimentally-observed whole-body metabolic rate ($R^2 = 0.9$), providing confidence in our model estimates. Our simulation results suggest that different exoskeleton behaviors can alter the functioning of the muscles and tendons acting at the assisted joint. Furthermore, our results support the idea that the series tendon helps reduce positive work done by the muscle fibers by storing and returning energy elastically. We expect the results from this study to promote the use of electromyography-driven simulations to gain insight into the operation of muscle-tendon units and to guide the design and control of assistive devices.

Keywords: biomechanics, series elastic element, ankle foot orthosis, gait, musculoskeletal modeling

3.1 Introduction

The plantarflexor muscle-tendon units seem tuned for near optimal efficiency and power production during unassisted locomotion. During normal walking, the ankle plantarflexor muscles produce force nearly isometrically throughout mid-stance while the Achilles tendon lengthens and stores mechanical energy [46]. This isometric muscle force production is economical because muscles consume relatively little energy to produce force at constant length [12, 13]. At the end of stance, the plantarflexor muscles actively shorten and the Achilles tendon simultaneously recoils [46, 61, 100], generating a significant amount of positive power at push-off [80, 120]. Elastic energy storage and recovery in the Achilles tendon helps reduce plantarflexor muscle work [97, 61]. Furthermore, the stiffness of the Achilles tendon, in conjunction with the resting length of the plantarflexor muscle fibers, has been shown to maximize plantarflexor muscle efficiency during walking and running by allowing the muscle fibers to operate at favorable lengths and velocities during positive fiber work production [110, 97, 95, 72, 73, 70, 8]. Any change to the stiffness of the Achilles tendon can affect the mechanics of the plantarflexor muscle fibers and consequently alter muscle

energy consumption [72]. The architecture of the plantarflexor muscles, the compliance of the Achilles tendon, and the interaction between these mechanisms enables economical operation.

The complexity of these plantarflexor muscle-tendon mechanics poses a challenge for the design of exoskeletons intended to operate in concert with the musculoskeletal system. Previous experiments and simulations of a musculoskeletal model have shown that elastic exoskeletons worn during bilateral hopping significantly reduce plantarflexor muscle force, but not muscle work [42, 41, 40, 98]. Although large reductions were observed in whole-body metabolic rate, estimated metabolic energy consumed by the plantarflexor muscles was not significantly reduced, likely due to unfavorable changes in the operating lengths and velocities of the muscle fibers [40]. Simulations of a simplified, lumped model of the plantarflexor muscle-tendon units acting in parallel with a passive exoskeleton during walking, with fixed joint kinematics, similarly suggest a disruption to the normal operation of the plantarflexor muscle-tendon units [104]. We were curious if similar mechanisms could explain the effect of different types of exoskeleton assistance on locomotor coordination and metabolic rate that we observed in a prior study.

We previously conducted an experiment in which subjects walked in eight conditions with different amounts of net work and average plantarflexion torque provided by an exoskeleton worn on one ankle [62]. We expected that providing net positive exoskeleton work at the ankle joint would replace or augment positive work performed by the plantarflexor muscles and reduce the associated metabolic cost [37, 50]. We expected that providing plantarflexion torque about the ankle joint, without providing any net work, would off-load plantarflexor muscle forces and reduce the metabolic cost associated with force production [52]. Providing increasing amounts of net exoskeleton work decreased metabolic rate as expected. In contrast with our predictions, providing increasing amounts of average exoskeleton torque increased metabolic rate. We thought these surprising results might be explained by changes in the dynamic interactions between muscles and tendons at the assisted joint.

We were unable to explore changes at the muscle-tendon level during assisted walking

using direct measurement in our previous study. Although muscle fiber length changes can be measured using ultrasound imaging, the number of muscles that can be imaged is limited. Furthermore, it is not yet feasible to directly measure individual muscle force and metabolic rate during locomotor tasks in humans. An alternative approach for investigating how plantarflexor muscle-tendon mechanics are affected by different exoskeleton behaviors is to conduct simulations with a musculoskeletal model. Driving a musculoskeletal model with experimentally-measured electromyography and joint kinematics is one promising simulation technique for generating realistic estimates of muscle-tendon mechanics [74, 8, 40, 77]. Simulated muscle-tendon mechanics can be fed into models of muscle energy consumption to obtain estimates of muscle-level energetics [114, 115, 11, 112]. Such estimates could potentially provide an explanation for the observed changes in whole-body energy consumption.

The purpose of this study was to explore how the mechanics and energetics of the plantarflexor muscle-tendon units change when subjected to different perturbations applied by an ankle exoskeleton. We used muscle activity and joint kinematics data to drive simulations of a musculoskeletal model and obtain estimates of muscle-level mechanics and energetics. We focused our musculoskeletal analyses on the soleus because observed changes were most pronounced in this muscle-tendon unit, and it is the muscle-tendon unit most analogous to the exoskeleton. We hypothesized that providing exoskeleton torque without providing any net work detuned the soleus muscle-tendon unit, leading to reduced elastic recoil of the tendon and increased work by the muscle fibers. We hypothesized that providing net positive exoskeleton work, focused at the end of stance, more fully replaced the role of the soleus muscle-tendon unit, thereby reducing energy consumed at the ankle joint and elsewhere. We expected the results from this study to shed light on how exoskeletons should interact with the muscles and tendons to achieve the greatest benefits.

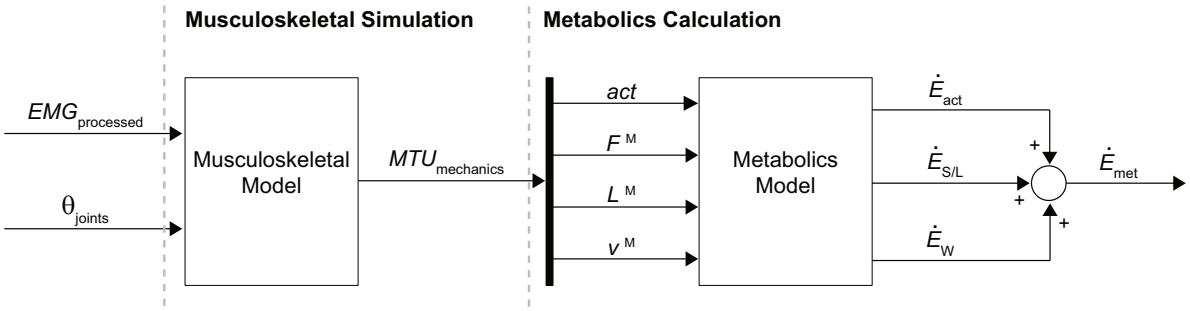

Figure 3.1: **Workflow of the musculoskeletal simulation and metabolics calculation**. Experimentally-collected electromyography ($EMG_{processed}$) and joint angles (θ_{joints}) were fed as inputs into the musculoskeletal model. Processed electromyography was used as muscle excitation and drove the musculoskeletal simulation. Joint angles were used to prescribe lower-body kinematics. The musculoskeletal simulation generated estimates of muscle-tendon unit mechanics ($MTU_{mechanics}$). A subset of muscle-tendon mechanics, namely activation (act), muscle fiber force (F^M), muscle fiber length (L^M), and muscle fiber velocity (v^M), were fed into a metabolics model. This model produced estimates of individual muscle activation/maintenance heat rates ($\dot{E}_{act}$), shortening/lengthening heat rates ($\dot{E}_{S/L}$), and mechanical work rates ($\dot{E}_W$). Summing the heat and work rates together resulted in an estimate of muscle-level metabolic rate ($\dot{E}_{met}$).

3.2 Materials and Methods

We performed electromyography-driven simulations of a musculoskeletal model to explore changes in plantarflexor muscle-tendon mechanics under a variety of systematically chosen ankle exoskeleton perturbations (Fig. 3.1). Electromyography and kinematic data were fed into a musculoskeletal simulation that generated estimates of muscle-level mechanics. The simulated muscle-tendon mechanics were input into a muscle-level metabolics model to obtain estimates of individual muscle metabolic rate. We analyzed these simulations to gain insight into how the ankle plantarflexor muscle-tendon units are impacted during walking with an ankle exoskeleton.

Previous Experiment

We previously conducted an experiment exploring the independent effects of a particular form of ankle exoskeleton torque support and work input on human coordination and metabolic energy consumption during walking [62]. Eight healthy, able-bodied subjects (7 men and 1 woman; age = 25.1 ± 5.1 yrs; body mass = 77.5 ± 5.6 kg; leg length = 0.89 ± 0.03 m) wore a tethered, unilateral ankle exoskeleton, capable of providing up to 120 N·m of plantarflexion

torque [121], while walking on a treadmill at 1.25 $m \cdot s^{-1}$. We ran two separate parameter sweeps. In the first parameter sweep, average exoskeleton torque was increased across conditions while net exoskeleton work was held constant at approximately zero. In the second parameter sweep, net exoskeleton work rate was increased across conditions while average exoskeleton torque was held constant. Metabolic rate, ground reaction forces, motion capture marker positions, and muscle activities were measured across all conditions. Data from these experiments were used to drive the musculoskeletal simulations of the current study.

A small fraction of electromyographic signals could not be properly analyzed due to poor electrode connectivity and a faulty sensor. Raw electromyographic signals were identified as erroneous if they crossed a threshold of 2 mV. An erroneous signal for a specific subject, muscle, and condition led us to exclude that signal across all exoskeleton torque conditions or all exoskeleton work conditions, ensuring that averages were always computed across the same subjects for all conditions in the relevant sweep. Approximately 10% of electromyographic data were thereby excluded from the current study.

Musculoskeletal Model

We drove a generic lower-body musculoskeletal model adapted from a previously published model [9]. The model included the pelvis and both legs, with segments and degrees of freedom as defined in [9]. The bones in this model were created by digitizing bones of an average-height male [9, 34]. We chose this model because it has previously been used to examine muscle fiber dynamics during human walking and running at different speeds [8] and to understand the effects of elastic ankle exoskeletons on the mechanics and energetics of muscles during hopping [40].

Of the original 35 lower-limb muscles in the model, we only included the muscles for which we had electromyographic data: lateral gastrocnemius, medial gastrocnemius, soleus, tibialis anterior, vastus medialis, rectus femoris, and biceps femoris long head. Each muscle was modeled as a Hill-type muscle, with a single fiber contractile element and series tendon.

Table 3.1: Parameters of the Musculoskeletal Model

	Max. Isometric Force, $F_{\max}$ (N)	*Optimal Fiber Length,* L_0 (cm)	*Tendon Slack Length* (cm)	*Tendon Strain at* $F_{\max}$ (%)	*Pennation Angle at* L_0 (rad)
Lateral Gastrocnemius	606	5.9	38.0	10	0.21
Medial Gastrocnemius	1308	5.1	40.3	10	0.17
Soleus	3586	4.4	27.9	10	0.49
Tibialis Anterior	674	6.8	24.1	3.3	0.17
Vastus Medialis	1444	9.7	11.2	3.3	0.10
Rectus Femoris	849	7.6	34.6	3.3	0.24
Biceps Femoris (LH)	705	11.0	32.2	3.3	0.20

Muscle-specific parameters included in the model were optimal fiber length, pennation angle at optimal fiber length, tendon slack length, and maximum isometric force. These parameters were based on measurements of 21 cadavers [118] and the values used for tendon slack length and maximum isometric force were further based on those computed in [9]. The exact muscle-specific parameters of the generic model used in this study are provided in Table 3.1. We used 10% tendon strain at maximum isometric force for the lateral gastrocnemius, medial gastrocnemius and soleus based on results from another study that found these values to result in strains that more closely matched ultrasound measurements [8]. Maximum fiber contraction velocity was set to 10 optimal fiber lengths per second for all muscles [9].

Musculoskeletal Simulation

We performed electromyography-driven simulations of muscle-tendon dynamics during walking with an ankle exoskeleton using the OpenSim musculoskeletal modeling software (v3.1; Delp et al., 2007). Since we were interested in understanding muscle-level mechanics, it was important that individual muscle activation patterns were estimated appropriately. Driving simulations with electromyographic data, rather than estimating muscle excitations by solving a constrained optimization problem, helps to ensure proper estimates of muscle acti-

vations [124, 74, 18, 7]. Prescribing joint kinematics helps to ensure that total muscle-tendon unit length changes are simulated accurately and that experimentally measured motions are obeyed even when muscles are omitted [74, 8, 40]. Muscle-level activations and muscle-tendon unit length changes provide sufficient information to obtain estimates of muscle-tendon mechanics, specifically muscle fiber force, muscle fiber length, muscle fiber velocity, and tendon length [9]. Given measured muscle activity and joint kinematics, we were able to generate estimates of plantarflexor muscle-tendon mechanics. Muscle-tendon mechanics generated using electromyography-driven simulations, with prescribed joint kinematics, have shown reasonable qualitative agreement with ultrasound measurements [40]. Such methods have also been shown to successfully match net joint moments measured via dynamometers [76].

Optimal fiber length and tendon slack length were scaled to each participant's anthropometry using marker data collected from a static trial, such that they maintained the same ratio as in the generic model. For each participant, the same muscle-tendon parameters were used across all experimental conditions. Data from a single averaged stride, for each participant for each condition, was provided as the input to the simulation. Marker data was fed into OpenSim's inverse kinematics tool, which generated joint angles. A processed version of electromyographic data was used as the control, i.e. excitation, signal in OpenSim's forward simulation tool. The raw electromyographic data was high-pass filtered (20 Hz) to remove movement artifact, full-wave rectified, and low-pass filtered (6 Hz) to smooth the signal [43, 32]. It was then normalized to maximum muscle activity measured during normal walking, scaled, and delayed. The process of selecting the scaling and delay factors is discussed in the next subsection.

Electromyography Parameter Optimization

To improve the accuracy of our simulations, we optimized the electromyography scaling and delay factors such that the error between muscle-generated ankle joint mechanics and those derived through inverse dynamics was minimized for each subject across the conditions with increasing average exoskeleton torque. We chose to optimize these parameters because

they had a large impact on muscle-generated ankle joint mechanics. Muscle-generated ankle joint moments were calculated by summing the joint moments, defined as the product of the tendon force and moment arm, of the medial gastrocnemius, lateral gastrocnemius, soleus, and tibialis anterior. Inverse-dynamics-derived ankle joint moments were obtained using OpenSim's inverse dynamics tool, which required joint angles from inverse kinematics, measured ground reaction forces, and exoskeleton torques as inputs. Exoskeleton torques were modeled as equal and opposite external torques applied to the shank and the foot. Both computed ankle joint moments were multiplied by ankle joint velocity to obtain muscle-generated and inverse-dynamics-derived ankle joint powers. Other studies have reported that the combination of the soleus, medial gastrocnemius, and lateral gastrocnemius contribute about 90% of the total ankle plantarflexion moment and the tibialis anterior contributes more than 50% of the total ankle dorsiflexion moment in the model [8], suggesting that these muscles are sufficient for generating realistic ankle joint mechanics. We did not, however, expect a perfect match between the two methods [57].

To obtain the optimal values of the scaling and delay factors for the muscles acting about the ankle joint, we performed gradient descent optimization. In order to address differences across subjects, we used scaling and delay factors that were subject-specific. For a given subject, the same delay was used for all muscles, while a different scaling factor was used for each muscle. Peak muscle activation during walking, relative to maximum voluntary contraction of that muscle, varies significantly across muscles, therefore suggesting the importance of muscle-specific scaling factors [90]. Differences in electromechanical delay across muscles is a more complicated issue [28, 60]. While studies have shown that the delay may be muscle-dependent [27], we were able to achieve sufficiently accurate timing of joint moments and powers without such added complexity. Furthermore, previous studies have used a single electromechanical delay across muscles and subjects and obtained reasonable results [74, 8].

In total, there were five optimization parameters for each subject: the delay, the medial gastrocnemius scaling factor, the lateral gastrocnemius scaling factor, the soleus scaling

Table 3.2: Optimized Electromyography Scaling Factors and Delays

Subject	*Delay* (ms)	*M. Gastrocnemius Scaling Factor*	*L. Gastrocnemius Scaling Factor*	*Soleus Scaling Factor*	*Tibialis Anterior Scaling Factor*
1	0	0.10	0.45	0.95	0.31
2	0	0.23	0.37	0.94	0.55
3	0	0.26	0.26	0.90	0.44
4	0	0.26	0.26	0.90	0.44
5	5.8	0.12	0.10	0.86	0.46
6	0	0.31	0.30	0.95	0.44
7	0	0.29	0.42	0.95	0.39
8	7.8	0.12	0.10	0.95	0.49

factor, and the tibialis anterior scaling factor. The root-mean-square errors between the muscle-generated ankle joint moments and powers and the inverse-dynamics-derived ankle joint moments and powers were used to quantify the quality of fit. The norm of the root-mean-square errors across the five increasing average exoskeleton torque conditions was chosen as the objective function. The optimized parameters for each subject are provided in Table 3.2. Because our simulations only include three muscles that cross the knee and hip joints, muscle-generated knee and hip joint mechanics should not be expected to match inverse-dynamics-derived knee and hip joint mechanics [8]. We, therefore, did not optimize the scaling factors for these three muscles but estimated them as the percent of the maximum voluntary contraction produced during normal walking observed in other experiments [90].

Optimization Testing

The optimized parameters produced reasonable ankle joint moments and powers (Fig. 3.2). The average root-mean-square error (RMSE), over subjects and conditions, between muscle-generated and inverse-dynamics-derived ankle joint moments was 0.13 $\mathrm{N{\cdot}m{\cdot}kg^{-1}}$, which was 11% of the average peak of the inverse-dynamics-derived ankle joint moment (1.2 $\mathrm{N{\cdot}m{\cdot}kg^{-1}}$). The average RMSE between muscle-generated and inverse-dynamics-derived ankle joint powers was 0.19 $\mathrm{W{\cdot}kg^{-1}}$, which was 9% of the average peak of the inverse-dynamics-derived

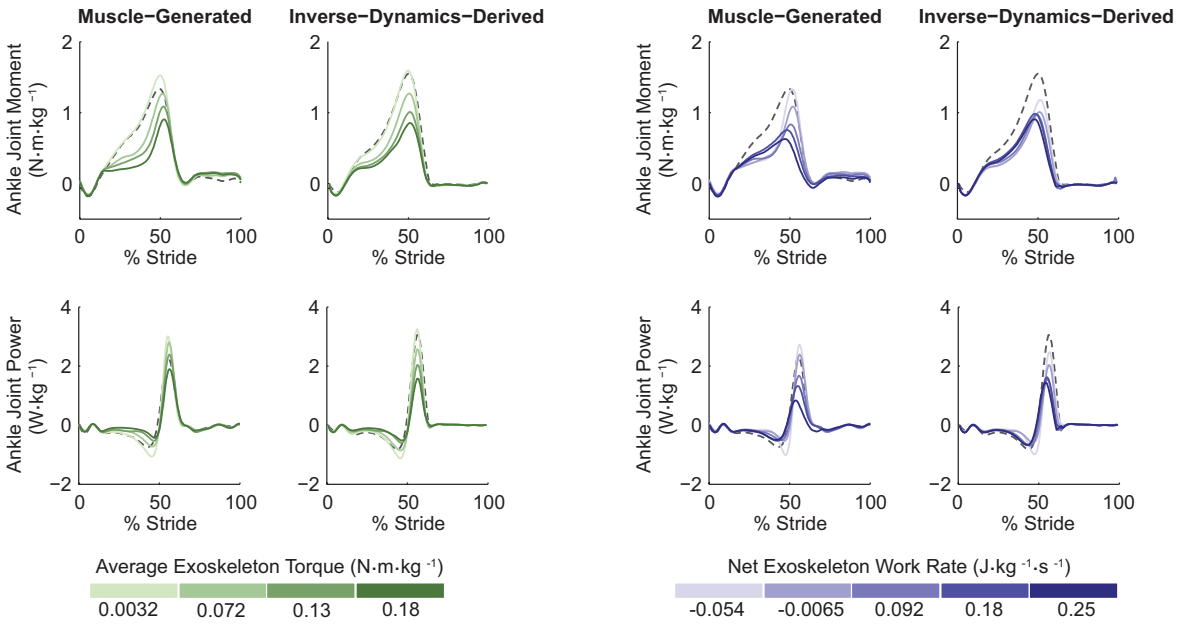

Figure 3.2: **Comparison of simulated muscle-generated and inverse-dynamics-derived ankle joint mechanics**. *Top row:* Simulated muscle-generated ankle joint moments compared to inverse-dynamics-derived ankle joint moments. *Bottom row:* Simulated muscle-generated ankle joint powers compared to inverse-dynamics-derived ankle joint powers. Simulated muscle-generated joint moments and powers were calculated by summing the individual contributions of the exoskeleton-side lateral gastrocnemius, medial gastrocnemius, soleus, and tibialis anterior. Each line is the subject mean ($N = 8$) for a given condition. Conditions with increasing average exoskeleton torque are shown in green. Conditions with increasing net exoskeleton work rate are shown in purple. Darker colors indicate higher values. Normal walking, without an exoskeleton, is shown by the gray dashed line. All values were normalized to body mass. For reference, exoskeleton torque trajectories for each of the different conditions can be found in Figure 4 of [62].

ankle joint power (2.2 W·kg^{-1}). Muscle-generated ankle joint moments were found to be within two standard deviations of inverse-dynamics-derived ankle joint moments, on average, which has been considered acceptable by other researchers [57]. The error in the timing of peak subject-averaged joint moments and powers had a maximum value of 1.6% of the gait cycle across all conditions. We were most interested in trends in ankle joint moments and powers with increasing average exoskeleton torque and net exoskeleton work, so an exact match in the absolute values of muscle-generated and inverse-dynamics-derived ankle joint mechanics was not necessary.

Metabolics Model

We used the results of the electromyography-driven simulations to estimate the energy consumed by each muscle using a modified version of Umberger's muscle metabolics model [114, 113, 112]. The metabolics model contains three different heat rates: the activation/maintenance heat rate, the fiber shortening/lengthening heat rate, and the fiber mechanical work rate. These heat rates depend in part on the muscle's excitation, activation, fiber length, fiber velocity, and fiber force. We explored the effect of each heat rate on the total metabolic rate for the muscles under consideration. Additionally, we summed the metabolic rates for each of the muscles simulated in our study and investigated how well estimated trends in individual and summed muscle metabolic rates explained changes in whole-body metabolic rate.

A lack of comparative experimental data makes it difficult to validate metabolics models. Other studies have validated their metabolics estimates by comparing simulated whole-body metabolic rate, defined as the sum of the individually simulated muscle metabolic rates, and indirect calorimetry [114, 77]. Since our study only includes a subset of potentially costly muscles, we did not expect the sum of metabolic rates of these muscles to accurately represent absolute changes in whole-body metabolic rate. Furthermore, we were most interested in trends across the different experimental conditions, as opposed to absolute differences. For these reasons, we limit our validation to the percent change in the sum of the individually simulated muscle metabolic rates.

The version of Umberger's metabolics model that is implemented in OpenSim is configurable, and we chose to use the original version of Umberger's metabolics model [114] with two modifications introduced by Uchida et al. (2016), as these modifications provided more accurate estimates compared to indirect calorimetry in similar studies. The first modification was the addition of a model of orderly fiber recruitment. Umberger's model assumes that the ratio of slow- to fast-twitch fibers that are recruited is equal to the ratio of slow- to fast-twitch fibers comprising the muscle. In the modified model, the ratio of slow- to fast-twitch fibers that are recruited instead varies with excitation so that fast-twitch fibers

are increasingly used as excitation increases [11]. The second modification was that the total metabolic rate at any time could not be negative (theoretically, total metabolic rate could be negative if the fiber mechanical work rate were negative and exceeded the total heat rate in magnitude). This change was consistent with the argument that eccentric work cannot cause a net synthesis of ATP [81].

Normalization and Statistical Analysis

We compared changes in trajectories of muscle fiber forces, muscle fiber lengths, muscle fiber velocities, muscle fiber powers, and tendon lengths across all experimental conditions. Average values of outcomes of interest were computed by integrating stride-averaged trajectories over the period of interest and dividing by average stride time of the corresponding trial. Instantaneous values of outcomes of interest were computed by taking the values of the stride-averaged trajectories at the defined times for each subject for each condition. Timing of these values varied across conditions; this was taken into account when calculations were performed. Muscle fiber force was normalized to maximum isometric force as defined in the model, tendon length was normalized to tendon slack length, muscle fiber length was normalized to optimal muscle fiber length, and fiber velocity was normalized to the maximum shortening velocity. Muscle fiber power was calculated as the product of muscle fiber force and muscle fiber velocity at each instant in time. Muscle fiber power and work, as well as all measures of metabolic rate, were normalized to body mass. All outcomes were averaged across subjects. Correlations between estimated percent changes in muscle-level metabolic rate and measured percent changes in whole-body metabolic rate were performed on both subject-specific data and data averaged across all subjects. Percent changes that were calculated on data averaged across subjects are referred to in the text as average percent changes. Standard deviations represent inter-subject variability.

We first performed a linear mixed-model ANOVA (random effect = subject; fixed effect = average torque or net work) to test for trend significance across experimental conditions in the different measured outcomes. We applied the Jarque-Bera test of normality to

ensure samples being compared were normally distributed. For measures that showed trend significance and were normally distributed, we performed paired t-tests to compare two conditions. For measures that showed trend significance but were not normally distributed, we used the Wilcoxon Signed Rank Test to compare two conditions. Across those experimental conditions for which average exoskeleton torque was systematically altered, pair-wise statistical comparisons were made with respect to the condition that provided zero average exoskeleton torque. Across those experimental conditions for which net exoskeleton work rate was systematically altered, pair-wise statistical comparisons were made with respect to the condition that provided zero net exoskeleton work with a controlled non-zero amount of average exoskeleton torque. After performing pair-wise comparisons, we applied the Holm-Šídák step-down correction for multiple comparisons [48] and used a significance level of $\alpha = 0.05$. The data used to produce our results are publicly available in Dryad.

Sensitivity Analysis

To test the sensitivity of simulated muscle mechanics to model parameters, we conducted a sensitivity analysis. We varied soleus activation and deactivation time constants by ± 10% relative to the initial value, maximum fiber contraction velocity by ± 20% relative to the initial value, maximum isometric force by ± 10% relative to the initial value, tendon slack length by ± 5% relative to the initial value, and tendon strain at maximum isometric muscle force by an absolute ± 1%. Varying these model parameters as described produced human-like values of muscle mechanics and did not significantly affect trends observed in the outcomes of interest (Figs. 3.8-3.13). The figures presented in the supplementary materials on the sensitivity analysis are representative of the changes observed in muscle mechanics and metabolic rates when the reported model parameters were varied.

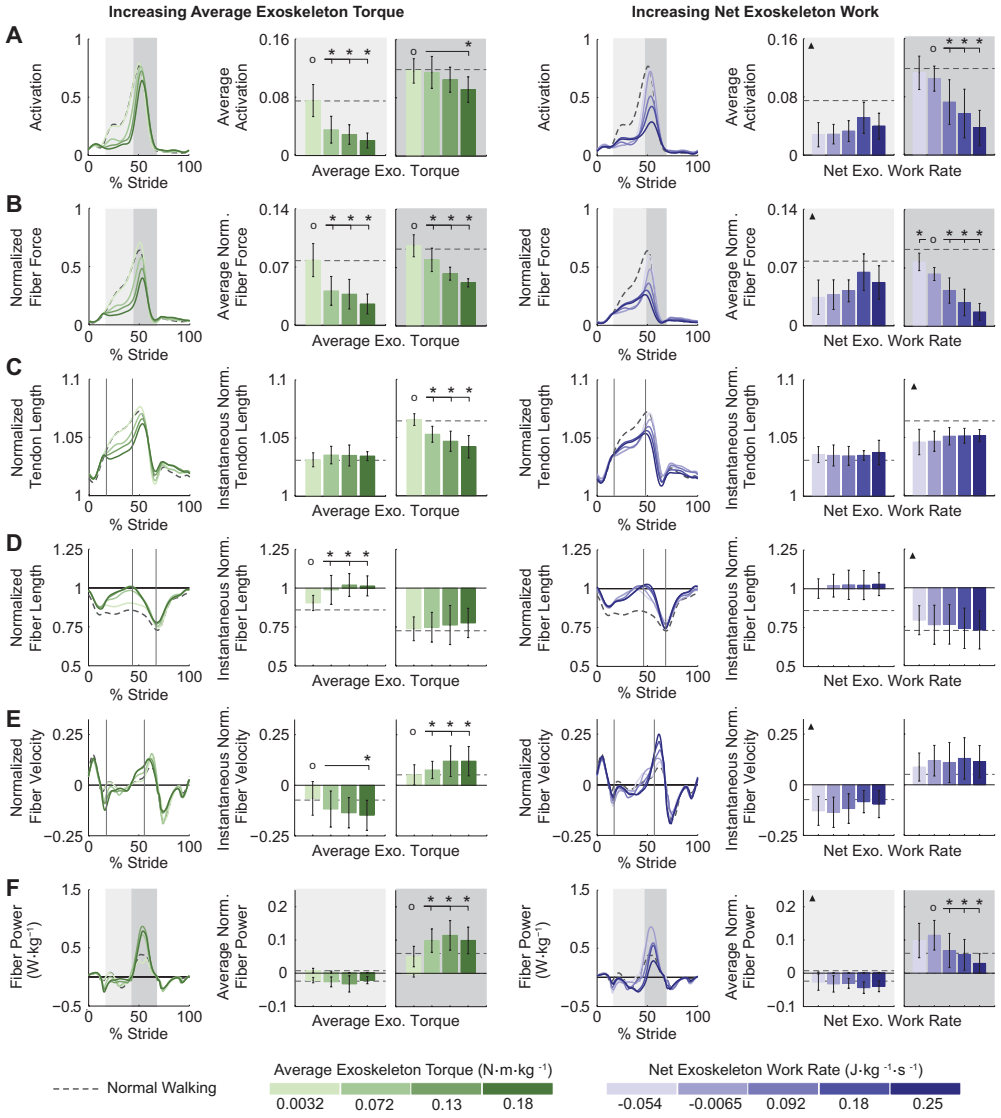

Figure 3.3: **Soleus muscle-tendon mechanics under different ankle exoskeleton perturbations.** (A) Soleus activation. (B) Soleus muscle fiber force normalized to maximum isometric force. (C) Tendon length normalized to tendon slack length. (D) Soleus muscle fiber length normalized to optimal fiber length. (E) Soleus muscle fiber velocity normalized to maximum fiber shortening velocity. (F) Soleus muscle fiber power normalized to body mass. Each curve is a subject-average ($N = 8$) trajectory. Bars and whiskers are subject means and standard deviations. Shaded bar plots represent the average of the corresponding trajectories over the shaded region. Unshaded bar plots represent instantaneous values of corresponding trajectories. Conditions with increasing average exoskeleton torque are shown in green. Conditions with increasing net exoskeleton work rate are shown in purple. Darker colors indicate higher values. Normal walking is shown by gray dashed lines. *s indicate statistical significance ($P < 0.05$) with respect to the conditions designated by open circles. Triangles indicate ANOVA significance.

3.3 Results

Perturbing the biological ankle joint with an active exoskeleton altered plantarflexor muscle-tendon mechanics and energetics as well as whole-body coordination patterns. Applying exoskeleton torques in parallel with the biological ankle muscles, without providing any net work, reduced soleus activation and force, but increased muscle fiber excursion, contraction velocity, and consequently, positive muscle fiber work. Increased positive muscle fiber work offset the observed decrease in activation heat rate of the exoskeleton-side soleus. Providing net work with an ankle exoskeleton reduced soleus activation and force during push-off, without significantly altering muscle fiber excursion and velocity, leading to an overall decrease in metabolic rate. Trends in estimated individual and combined muscle metabolic rates correlated well with experimentally observed trends in whole-body metabolic rate.

Effects of Increasing Average Exoskeleton Torque on Locomotor Coordination

Exoskeleton-Side Soleus Muscle-Tendon Mechanics

As exoskeleton average torque was independently increased, the mechanics of the soleus muscle-tendon unit at the assisted ankle joint were disrupted. Average exoskeleton-side soleus muscle activation decreased by 69% during mid-stance and by 21% during late stance across exoskeleton torque conditions ($P = 8 \cdot 10^{-3}$ and $P = 0.02$, respectively, Fig. 3.3A). Average exoskeleton-side soleus muscle fiber force decreased by 65% during mid-stance and by 45% during late stance across exoskeleton torque conditions ($P = 8 \cdot 10^{-3}$ and $P = 2 \cdot 10^{-5}$, respectively, Fig. 3.3B). Change in tendon length, from the instant the soleus muscle fiber started lengthening to the instant it transitioned from lengthening to shortening, decreased by 74% across exoskeleton torque conditions ($P = 1 \cdot 10^{-3}$, Fig. 3.3C). Soleus muscle fiber length, at the instant the soleus muscle transitioned from lengthening to shortening, increased by 12% and muscle fiber contraction velocity, at the instant of peak muscle fiber power, increased by 155% across exoskeleton torque conditions ($P = 1 \cdot 10^{-3}$ and $P = 0.02$, respectively, Fig. 3.3D,E). Positive muscle fiber work during late stance increased by 232%

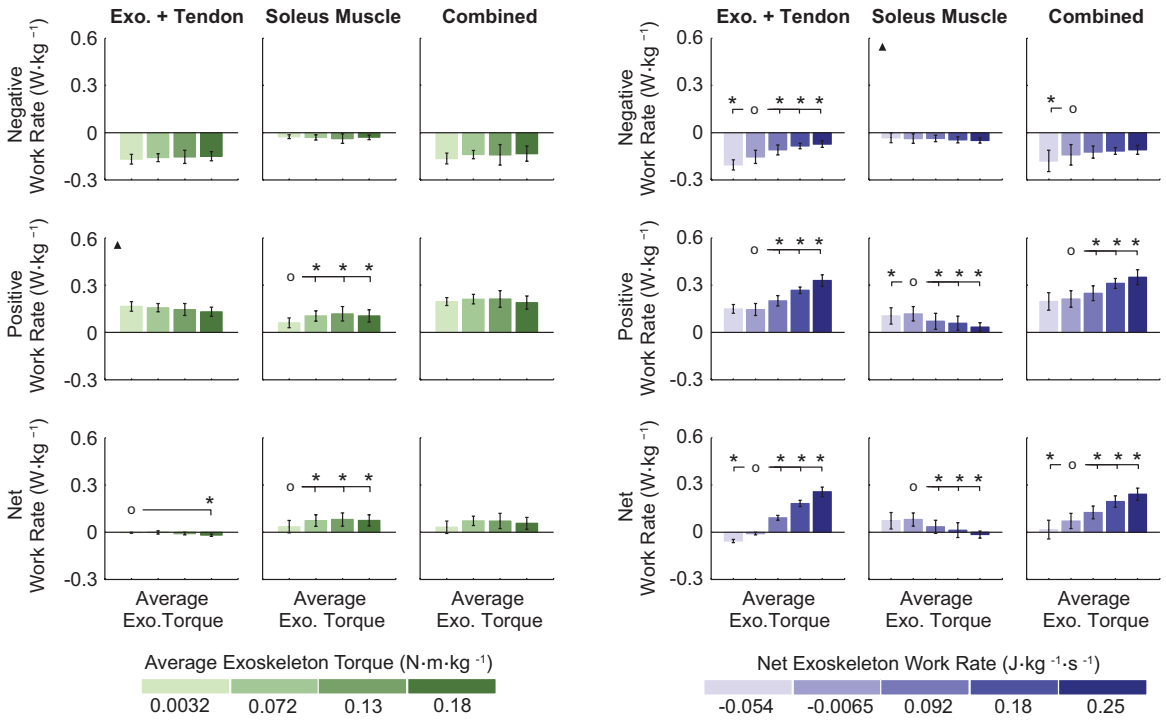

Figure 3.4: **Negative, positive, and net work rates of the soleus muscle and the combined passive elastic elements.** *From left to right:* Work rates of the exoskeleton plus tendon; work rates of the soleus muscle; work rates of the combined exoskeleton, tendon, and soleus muscle. The top row shows negative work rates for the different elements, the middle row shows the positive work rates for the different elements, and the bottom row shows the net work rates for the different elements. Conditions with increasing average exoskeleton torque are shown in green. Conditions with increasing net exoskeleton work rate are shown in purple. Darker colors indicate higher values. Bars and whiskers are subject means and standard deviations ($N = 8$). *s indicate statistical significance ($P < 0.05$) with respect to the conditions designated by open circles. Triangles indicate ANOVA significance.

across exoskeleton torque conditions ($P = 0.01$, Fig. 3.3F). Similar trends were observed in the medial and lateral gastrocnemii for a majority of these outcomes, but to a lesser extent (Figs. 3.6 & 3.7).

Exoskeleton-Side Soleus and Elastic Element Work Rates

The positive work rate of the exoskeleton plus tendon decreased with increasing average exoskeleton torque (ANOVA, $P = 2 \cdot 10^{-3}$) while the positive work rate of the soleus muscle increased by 142% across exoskeleton torque conditions ($P = 0.02$). The positive work rate of the combined exoskeleton, tendon, and soleus muscle remained relatively unchanged as exoskeleton torque was increased (ANOVA, $P = 0.9$).

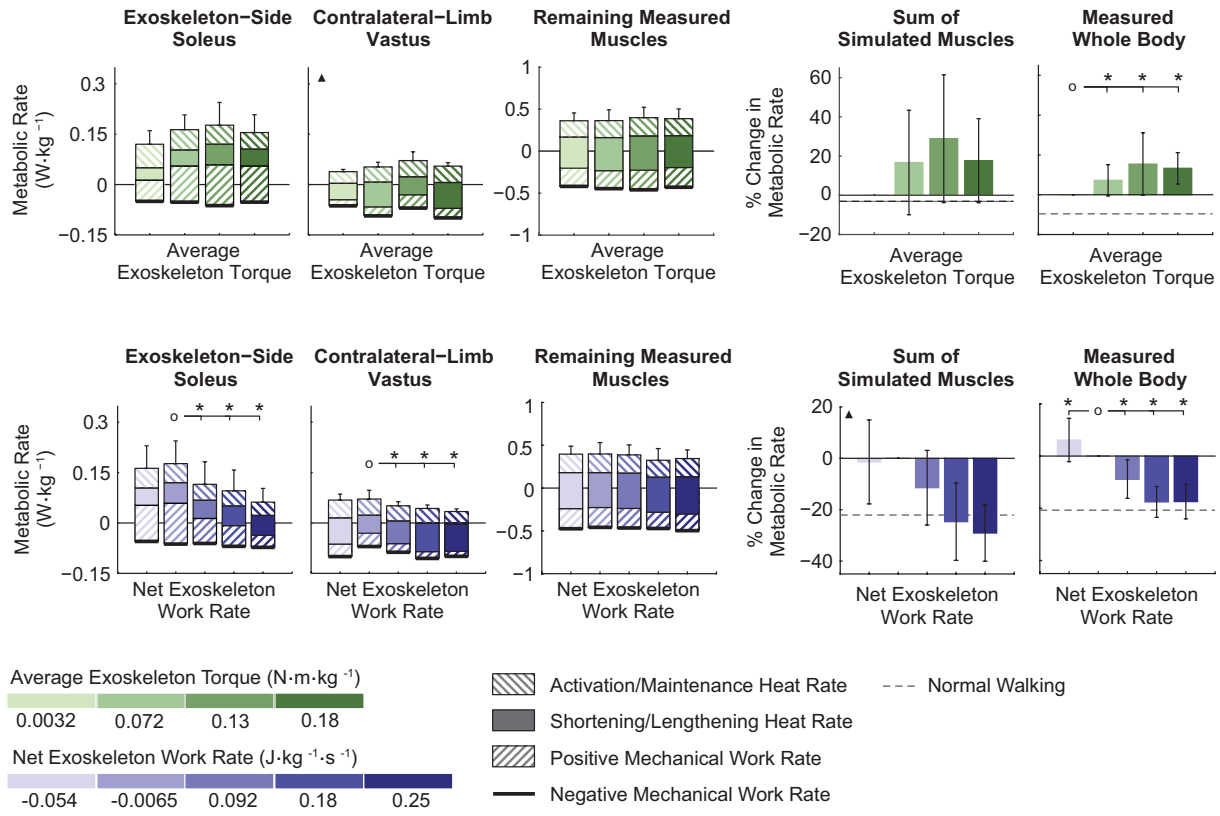

Figure 3.5: **Metabolic rate from simulated muscles and whole-body measurements**. *From left to right:* Estimated exoskeleton-side soleus metabolic rate; estimated contralateral-limb vastus metabolic rate; estimated metabolic rate of the sum of the remaining muscles with electromyographic data; estimated percent change in the sum of the simulated muscle metabolic rates; and measured percent change in whole-body metabolic rate. The top and bottom rows show changes in estimated and measured metabolic rate with increasing average exoskeleton torque (green) and increasing net exoskeleton work rate (purple), respectively. Darker colors indicate higher values. Normal walking is shown by a gray dashed line. Bars and whiskers are subject means and standard deviations. Bar shadings represent different muscle heat and work rates. The solid black line at the base of each bar shows the average negative mechanical work rate. Starting at the value of average negative mechanical work rate (below zero), the average positive mechanical work rate, shortening/lengthening heat rate, and activation/maintenance heat rate are stacked on top of each other. The ordinate value of the top of the bars indicates the total metabolic rate for that specific muscle, or sum of muscles, for a given condition. Data from $N = 8$ subjects, except for the top and bottom plots of the contralateral-limb vastus metabolic rate, for which $N = 5$ and $N = 6$, respectively. *s indicate statistical significance ($P < 0.05$) with respect to the conditions designated by open circles. Triangles indicate ANOVA significance.

Exoskeleton-Side Soleus Metabolic Rate

The trend in estimated metabolic rate of the exoskeleton-side soleus as average exoskeleton torque was increased appeared to be similar to the trend in measured whole-body metabolic rate (Fig. 3.5). Average activation/maintenance heat rate decreased by 28% across exoskele-

ton torque conditions ($P = 2 \cdot 10^{-3}$). Average shortening/lengthening heat rate appeared to increase with increasing average exoskeleton torque, however the trend was not significant (ANOVA, $P = 0.1$). Positive mechanical work rate increased by 144% from the condition with no exoskeleton torque to the condition with the second-highest exoskeleton torque ($P = 8 \cdot 10^{-3}$). Correlating the estimated percent change in soleus metabolic rate, $\dot{E}_{\text{soleus}}$, with the experimentally observed percent change in whole-body metabolic rate, $\dot{E}_{\text{measured}}$, the best fit line was found to be $\dot{E}_{\text{measured}} \approx 0.1 \cdot \dot{E}_{\text{soleus}} + 5.0$ ($R^2 = 0.3$, $P = 2 \cdot 10^{-3}$). Correlating the average estimated percent change in soleus metabolic rate, $\dot{E}_{\text{soleus,avg}}$, with the average experimentally observed percent change in whole-body metabolic rate, $\dot{E}_{\text{measured,avg}}$, the best fit line was found to be $\dot{E}_{\text{measured,avg}} \approx 0.2 \cdot \dot{E}_{\text{soleus,avg}} + 0.1$ ($R^2 = 0.8$, $P = 0.1$).

Contralateral-Limb Vastus Metabolic Rate

Estimated metabolic rate of the contralateral-limb vastus increased with increasing average exoskeleton torque (ANOVA, $P = 0.02$, Fig. 3.5) and matched trends in measured whole-body metabolic rate. Correlating the estimated percent change in contralateral-limb vastus metabolic rate, $\dot{E}_{\text{vastus}}$, with the experimentally observed percent change in whole-body metabolic rate, $\dot{E}_{\text{measured}}$, the best fit line was found to be $\dot{E}_{\text{measured}} \approx 0.2 \cdot \dot{E}_{\text{vastus}} + 1.2$ ($R^2 = 0.8$, $P = 2 \cdot 10^{-8}$). Correlating the average estimated percent change in contralateral-limb vastus metabolic rate, $\dot{E}_{\text{vastus,avg}}$, with the average experimentally observed percent change in whole-body metabolic rate, $\dot{E}_{\text{measured,avg}}$, the best fit line was found to be $\dot{E}_{\text{measured,avg}} \approx 0.2 \cdot \dot{E}_{\text{vastus,avg}} + 1.0$ ($R^2 = 0.9$, $P = 0.05$).

Sum of the Metabolic Rates of Simulated Muscles

The trend in the sum of the metabolic rates of simulated muscles with increasing average exoskeleton torque was similar to the trend observed in measured whole-body metabolic rate (Fig. 3.5). Correlating the estimated percent change in the sum of the metabolic rates of the simulated muscles $\dot{E}_{\text{estimated}}$, with the experimentally observed percent change in whole-body metabolic rate, $\dot{E}_{\text{measured}}$, the best fit line was found to be $\dot{E}_{\text{measured}} \approx 0.4 \cdot \dot{E}_{\text{estimated}} + 3.4$

($R^2 = 0.6$, $P = 7 \cdot 10^{-8}$). Correlating the average estimated percent change in the sum of the metabolic rates of the simulated muscles, $\dot{E}_{\text{estimated,avg}}$, with the average experimentally observed percent change in whole-body metabolic rate, $\dot{E}_{\text{measured,avg}}$, the best fit line was found to be $\dot{E}_{\text{measured,avg}} \approx 0.7 \cdot \dot{E}_{\text{estimated,avg}} - 3.4$ ($R^2 = 0.9$, $P = 0.02$).

Effects of Increasing Net Exoskeleton Work on Locomotor Coordination

Exoskeleton-Side Soleus Muscle-Tendon Mechanics

Effort-related measures of the assisted soleus decreased with increasing net exoskeleton work. Average exoskeleton-side soleus muscle activation and fiber force during mid-stance increased as net exoskeleton work was increased (ANOVA, $P = 8 \cdot 10^{-3}$ and $P = 3 \cdot 10^{-3}$, respectively, Fig. 3.3A,B). Average exoskeleton-side soleus muscle activation and fiber force during late stance decreased by 66% and 73%, respectively, across exoskeleton work conditions ($P = 5 \cdot 10^{-6}$ and $P = 2 \cdot 10^{-6}$, respectively). Change in tendon length, from the instant the soleus muscle started lengthening to the instant it transitioned from lengthening to shortening, remained relatively unchanged as net exoskeleton work was increased (ANOVA, $P = 0.2$, Fig. 3.3C). Soleus muscle fiber length, at the instant the soleus muscle transitioned from lengthening to shortening, and fiber contraction velocity at the instant of peak muscle fiber power, remained relatively constant across exoskeleton work conditions (ANOVA, $P = 0.06$ and $P = 0.06$, respectively, Fig. 3.3D,E). Muscle fiber work during late stance decreased by 77% across exoskeleton work conditions ($P = 8 \cdot 10^{-3}$, Fig. 3.3E). Similar trends were observed in the medial and lateral gastrocnemii for a majority of these outcomes, but to a lesser extent (Figs. 3.6 & 3.7).

Exoskeleton-Side Soleus and Elastic Element Work Rates

The positive work rate of the ankle exoskeleton plus the tendon increased by 137%, while the positive work rate of the soleus muscle decreased by 73% across exoskeleton work conditions ($P = 1 \cdot 10^{-5}$ and $P = 2 \cdot 10^{-4}$, respectively, Fig. 3.4A). The positive work rate of the combined system increased by 72% across exoskeleton work conditions ($P = 1 \cdot 10^{-4}$).

Exoskeleton-Side Soleus Metabolic Rate

Estimated metabolic rate of the exoskeleton-side soleus decreased with increasing net exoskeleton work (Fig. 3.5). Average activation/maintenance heat rate and positive mechanical work rate decreased by 30% and 72%, respectively, across exoskeleton work conditions ($P = 5 \cdot 10^{-4}$ and $P = 8 \cdot 10^{-3}$, respectively). Average shortening/lengthening heat rate remained relatively unchanged, while negative mechanical work rate decreased as net exoskeleton work was increased (ANOVA, $P = 0.3$ and $P = 1 \cdot 10^{-3}$, respectively). Total estimated soleus metabolic rate decreased by 66% across exoskeleton work conditions ($P = 8 \cdot 10^{-3}$). Correlating the estimated percent change in soleus metabolic rate, $\dot{E}_{\text{soleus}}$, with the experimentally observed percent change in whole-body metabolic rate, $\dot{E}_{\text{measured}}$, the best fit line was found to be $\dot{E}_{\text{measured}} \approx 0.2 \cdot \dot{E}_{\text{soleus}} + 0.1$ ($R^2 = 0.4$, $P = 8 \cdot 10^{-6}$). Correlating the average estimated percent change in soleus metabolic rate, $\dot{E}_{\text{soleus,avg}}$, with the average experimentally observed percent change in whole-body metabolic rate, $\dot{E}_{\text{measured,avg}}$, the best fit line was found to be $\dot{E}_{\text{measured,avg}} \approx 0.4 \cdot \dot{E}_{\text{soleus,avg}} + 3.6$ ($R^2 = 0.8$, $P = 0.03$).

Contralateral-Limb Vastus Metabolic Rate

Estimated total metabolic rate of the contralateral-limb vastus decreased with increasing net exoskeleton work (ANOVA, $P = 9 \cdot 10^{-8}$, Fig. 3.5). Correlating the estimated percent change in contralateral-limb vastus metabolic rate, $\dot{E}_{\text{vastus}}$, with the experimentally observed percent change in whole-body metabolic rate, $\dot{E}_{\text{measured}}$, the best fit line was found to be $\dot{E}_{\text{measured}} \approx 0.3 \cdot \dot{E}_{\text{vastus}} - 1.7$ ($R^2 = 0.5$, $P = 2 \cdot 10^{-4}$). Correlating the average estimated percent change in contralateral-limb vastus metabolic rate, $\dot{E}_{\text{vastus,avg}}$, with the average experimentally observed percent change in whole-body metabolic rate, $\dot{E}_{\text{measured,avg}}$, the best fit line was found to be $\dot{E}_{\text{measured,avg}} \approx 0.5 \cdot \dot{E}_{\text{vastus,avg}} + 3.5$ ($R^2 = 0.9$, $P = 8 \cdot 10^{-3}$).

Sum of the Metabolic Rates of Simulated Muscles

The sum of the metabolic rates of simulated muscles decreased with increasing net exoskele-

ton work (ANOVA, $P = 3 \cdot 10^{-8}$, Fig. 3.5). Correlating the estimated percent change in the sum of the metabolic rates of the simulated muscles, $\dot{E}_{\text{estimated}}$, with the experimentally observed percent change in whole-body metabolic energy consumption, $\dot{E}_{\text{measured}}$, the best fit line was found to be $\dot{E}_{\text{measured}} \approx 0.5 \cdot \dot{E}_{\text{estimated}} - 1.1$ ($R^2 = 0.5$, $P = 1 \cdot 10^{-7}$). Correlating the average estimated percent change in the sum of the metabolic rates of the simulated muscles, $\dot{E}_{\text{estimated,avg}}$, with the average experimentally observed percent change in whole-body metabolic rate, $\dot{E}_{\text{measured,avg}}$, the best fit line was found to be $\dot{E}_{\text{measured,avg}} \approx 0.8 \cdot \dot{E}_{\text{estimated,avg}} + 2.4$ ($R^2 = 0.9$, $P = 6 \cdot 10^{-3}$).

3.4 Discussion

Providing increasing amounts of average exoskeleton torque, while maintaining zero net exoskeleton work, had both detrimental and beneficial effects on soleus muscle-tendon interactions. Normally, the soleus produces large forces throughout the dorsiflexion phase of stance, allowing the tendon to lengthen substantially and store mechanical energy. In this study, however, the exoskeleton displaced and reduced force in the soleus during early and mid-stance. This caused less stretch in the tendon and greater excursion of the muscle fibers than observed during unassisted walking. The decrease in tendon stretch had the detrimental effect of shifting work from the tendon to the muscle fibers. Reduced tendon stretch meant reduced elastic recoil during push-off, which was not adequately compensated for by the exoskeleton. The muscle fibers, therefore, did more work to maintain normal levels of total ankle positive work, but doing positive work with muscles is costly. The increase in muscle fiber excursion had complicated effects on the muscle's force generating capacity. The muscle fibers operated closer to their optimal length at the time of peak power in late stance, which was beneficial to the muscle's ability to generate force. However, the muscle fibers also had to shorten a greater distance during push-off, thereby significantly increasing shortening velocity. Although the increase in fiber velocity helped increase fiber power, force

generating capacity of muscle drops sharply with increased contraction velocity, thereby explaining the substantial reductions in soleus fiber force during late stance, despite much smaller reductions in activation.

Energy consumed by a muscle can be approximated by a combination of different heat and work rates [58, 82]. As average exoskeleton torque increased, exoskeleton-side soleus activation/maintenance heat rate decreased, due to the forces applied in parallel with the soleus by the exoskeleton (Fig. 3.5). The shortening/lengthening heat rate, however, appeared to increase due to increased lengthening of muscle fibers during mid-stance and increased shortening during push-off. Exoskeleton-side soleus positive mechanical work rate increased with increasing average exoskeleton torque. Summing the activation/maintenance heat rate, shortening/lengthening heat rate, and net mechanical work rate together, soleus metabolic rate did not change significantly across conditions, but seemed to follow a similar trend to experimentally measured whole-body metabolic rate.

Reductions in the elastic recoil in the tendon, as well as increased lengthening and shortening of the soleus muscle fibers, negated the reductions in muscle activation and fiber force afforded by the exoskeleton. The human-robot system proved less efficient than the human system alone. Similar changes in soleus muscle-tendon mechanics were also observed during hopping with passive ankle exoskeletons [40]; plantarflexor muscle fiber force decreased when passive assistance was provided, but fiber shortening velocity increased, resulting in no significant change in positive muscle fiber work. Such trade-offs in the observed changes in plantarflexor muscle-tendon mechanics led the metabolic rate of the plantarflexor muscles to remain relatively constant when hopping with and without assistance, which is comparable to our results for walking. Hopping with passive ankle exoskeleton assistance, however, still led to a reduction in whole-body energy consumption, likely due to off-loading of other muscle forces, particularly about the knee joint [40]. Simulations of a simple, lumped model of the plantarflexor muscle-tendon units during walking with an elastic ankle exoskeleton also showed similar results: increasing exoskeleton stiffness decreased activation and force of the plantarflexor muscle fibers, but increased

muscle fiber length changes and led to no change in work done by the muscle fibers [104]. In contrast with our results, this simulation study showed that plantarflexor muscle metabolic rate decreased with increasing exoskeleton stiffness. This could be a result of differences in the way in which exoskeleton torque was applied in our study compared to Sawicki (2016), a result of different changes elsewhere in the body, or a result of different constraints on joint kinematics. In general, it seems the soleus muscle-tendon unit is sensitive to changes in operation. Slight alterations to the nominal system can have significant effects on coordination, which can be beneficial or detrimental to individual muscle and whole-body metabolic energy consumption, depending on the specific task.

As average exoskeleton torque was increased, changes in contralateral-limb vastus mechanics and energetics were observed, which helps further explain the increase in experimentally measured whole-body metabolic rate. Changes in estimated contralateral-limb vastus metabolic rate correlated well with experimentally observed changes in whole-body metabolic rate. Summing the metabolic rate of each muscle for which we had electromyographic data, we found that trends matched experimentally observed trends in whole-body metabolic rate well (Fig. 3.5).

Joint work is not necessarily a good predictor of muscle work and, consequently, energy consumed by a muscle. Positive exoskeleton-side soleus muscle fiber work increased with increasing average exoskeleton torque, but the biological ankle joint work remained relatively unchanged according to the muscle-generated ankle joint work computations, and actually decreased according to the inverse-dynamics-derived ankle joint work computations.

Changing the amount of net work the exoskeleton provided also impacted exoskeleton-side soleus muscle mechanics and energetics, but in ways that were more expected. With increasing net exoskeleton work, peak exoskeleton-applied torque occurred later in stance, leading to significant changes in muscle-tendon dynamics. Reduced activation, in addition to reduced positive power during late stance, resulted in reduced effort of the soleus (Fig. 3.3A). Soleus muscle fiber force (Fig. 3.3B) and work (Fig. 3.3F) were reduced as net exoskeleton work was increased, thereby compromising the normal capabilities of the

biological ankle. Positive work provided by the exoskeleton more than compensated for the reduced performance of the biological mechanisms, leading to an improved human-robot cooperative system. Metabolic rate of the exoskeleton-side soleus muscle significantly decreased with increasing net exoskeleton work, which accounted for a portion of the reduction in whole-body energy expenditure (Fig. 3.5).

As net exoskeleton work was increased, changes in contralateral-limb vastus mechanics and energetics were observed, helping to further explain reductions in experimentally measured whole-body metabolic rate. Decreases in exoskeleton-side soleus metabolic rate were greater than those observed in the contralateral-limb vastus, but both contributed to reductions in whole-body metabolic rate. Summing the metabolic rate of each muscle for which we had electromyographic data, trends fit experimentally observed reductions in whole-body metabolic rate well (Fig. 3.5).

Tendon stiffness and other muscle-tendon properties seem to be tuned such that the biological ankle joint operates efficiently. The results of this study support the idea that the physiological value of the Achilles tendon stiffness is optimal for muscle efficiency during walking and running [72]. The lengthening and shortening of the Achilles tendon, instead of the muscle fibers, allows for energy to be stored and returned passively throughout stance. Positive work done by elastic elements can reduce the amount of positive work done by muscles.

Usefully interacting with biological muscles and tendons, via an external device, is complicated. Muscle-tendon mechanics are important and should be taken into account when designing devices to assist human motion. Adding an external device to the human body may affect muscle-level mechanics and energetics in unexpected ways. Disrupted muscle-tendon interactions were observed in this study and have similarly been observed in human hopping with ankle exoskeletons [41, 40]. Assistive devices should be designed and controlled to compensate for any compromised performance or functioning of muscles and tendons. Analyses similar to those discussed above can be used to help understand how different exoskeleton behaviors affect muscle-level mechanics, and provide insights into why certain

device behaviors are more effective than others at assisting locomotion. For instance, torque support with a device can be an effective assistance strategy [26], but subtleties of how the external torques are applied and how the device interacts with the human musculoskeletal system greatly impact coordination patterns and overall effectiveness.

The modeling approaches used in this study can be applied to a wide array of human motions. The results suggest that, given a coordination pattern, via measured muscle activity and joint kinematics, it is possible to generate reasonable estimates of individual muscle mechanics and metabolic rate. In the future it may be possible to invert the process. Based on what we know about the mechanics and energetics of individual muscles, we can try to generate a set of desirable coordination patterns. It may even be possible to prescribe exoskeleton behaviors that elicit desirable changes in coordination.

Our modeling and simulation approach required making a number of assumptions and choices that need to be considered when evaluating the generated results. If the parameters used in the model were inaccurate, this could have led to invalid estimates of muscle mechanics and energetics. The parameters we used are, however, comparable to previously published work [6, 9] which are based on cadaver studies [118]. Furthermore, to validate our approach, we compared muscle-generated ankle joint moments and powers to inverse-dynamics-derived ankle joint moments and powers (Fig. 3.2). We optimized parameters to reduce the root-mean-square error between the two and performed an in-depth sensitivity analysis (Figs. 3.8-3.13) the shows the qualitative trends are robust to model parameters.

The soleus, lateral gastrocnemius, and medial gastrocnemius were each modeled with a separate tendon as opposed to one shared tendon. It is unclear which modeling choice is more appropriate for our study, but our fiber and tendon excursions were consistent with experimental ultrasound studies [30, 29, 46, 71, 100]. Moreover, qualitative trends in elastic element negative, positive, and net work (Fig. 4) held for the combination of all plantarflexor tendons. Combined with the results of our sensitivity analysis, we are confident that this modeling choice does not affect our conclusions.

We were limited by the number of muscles we could measure experimentally. In particular,

we did not measure muscle activity from the glutei, or other muscles acting about the hip, which are thought to consume a substantial amount of energy during walking. Nonetheless, the change in the sum of metabolic energy consumption from simulated muscles showed a similar trend to the change in whole-body metabolic energy consumption measured via indirect calorimetry; this independent validation increases our confidence in the primary findings of the study. Including more muscles in future experiments would make these analyses more complete.

Muscle-generated ankle joint mechanics did not perfectly match inverse-dynamics-derived ankle joint mechanics, but most trends were consistent across the two methods. Results from inverse dynamics suggested that total exoskeleton-side positive ankle joint work decreased as average exoskeleton torque increased, while results from the electromyography-driven simulations suggested that total exoskeleton-side positive ankle joint work remained relatively unchanged. This inconsistency could have implications for our understanding of why contralateral-limb knee mechanics and vastus metabolic rate were affected by torque applied at the exoskeleton-side ankle joint. We only optimized across those conditions with increasing average exoskeleton torque, but do not expect a better match would be obtained if we optimized across those conditions with increasing net exoskeleton work as well. There are inherent trade-offs that prevent errors across all conditions from simultaneously improving. These results illustrate the importance of knowing the limitations and assumptions inherent in a model and taking these into consideration when analyzing and interpreting its outputs. To account for these limitations, we conducted sensitivity analyses and minimized inconsistencies between inverse-dynamics-derived and muscle-generated joint mechanics by optimizing those model parameters in which we had the least confidence.

3.5 Conclusions

We simulated plantarflexor muscle-tendon mechanics and individual muscle energetics during walking with an ankle exoskeleton to gain a deeper understanding of how different ex-

oskeleton assistance strategies affect the operation of the plantarflexor muscles and tendons. Providing increasing amounts of average plantarflexion torque with an ankle exoskeleton while providing no net work, disrupted soleus muscle-tendon interactions. Reduced tendon recoil was not sufficiently compensated for by the exoskeleton and this led to an increase in positive work done by the soleus muscle, which is costly. Providing increasing amounts of net exoskeleton work more than compensated for reduced work done by the soleus muscle-tendon unit, leading to a reduction in soleus force, work, and total metabolic rate. Trends in the sum of the metabolic rates of the simulated muscles correlated well with trends in experimentally-observed whole-body metabolic rate, suggesting that the mechanical and metabolic changes observed in the simulated muscles contributed to the measured changes in whole-body metabolic rate.

By performing these analyses we were able to explain experimentally observed changes in coordination patterns and metabolic energy consumption. Models without muscles and tendons would not have been able to capture these effects. Due to the sensitivity of muscle-tendon units to external disturbances, assisting locomotion by placing a device in parallel with muscles is challenging. When designing assistive devices, it is therefore important to consider how muscle-tendon mechanics might change due to interactions with the device and to ensure that the device sufficiently replaces any compromised function of the human musculoskeletal system.

Acknowledgments

This material is based upon work supported by the National Science Foundation under Grant No. IIS-1355716 and Graduate Research Fellowship Grant No. DGE-114747, and by the National Institute of Health under Grant No. NIH-P2CHD065690 and Grant No. NIH-U54EB020405. The authors thank Thomas Uchida for assistance with the OpenSim metabolics model.

3.6 Appendix A: Gastrocnemius Muscle Mechanics

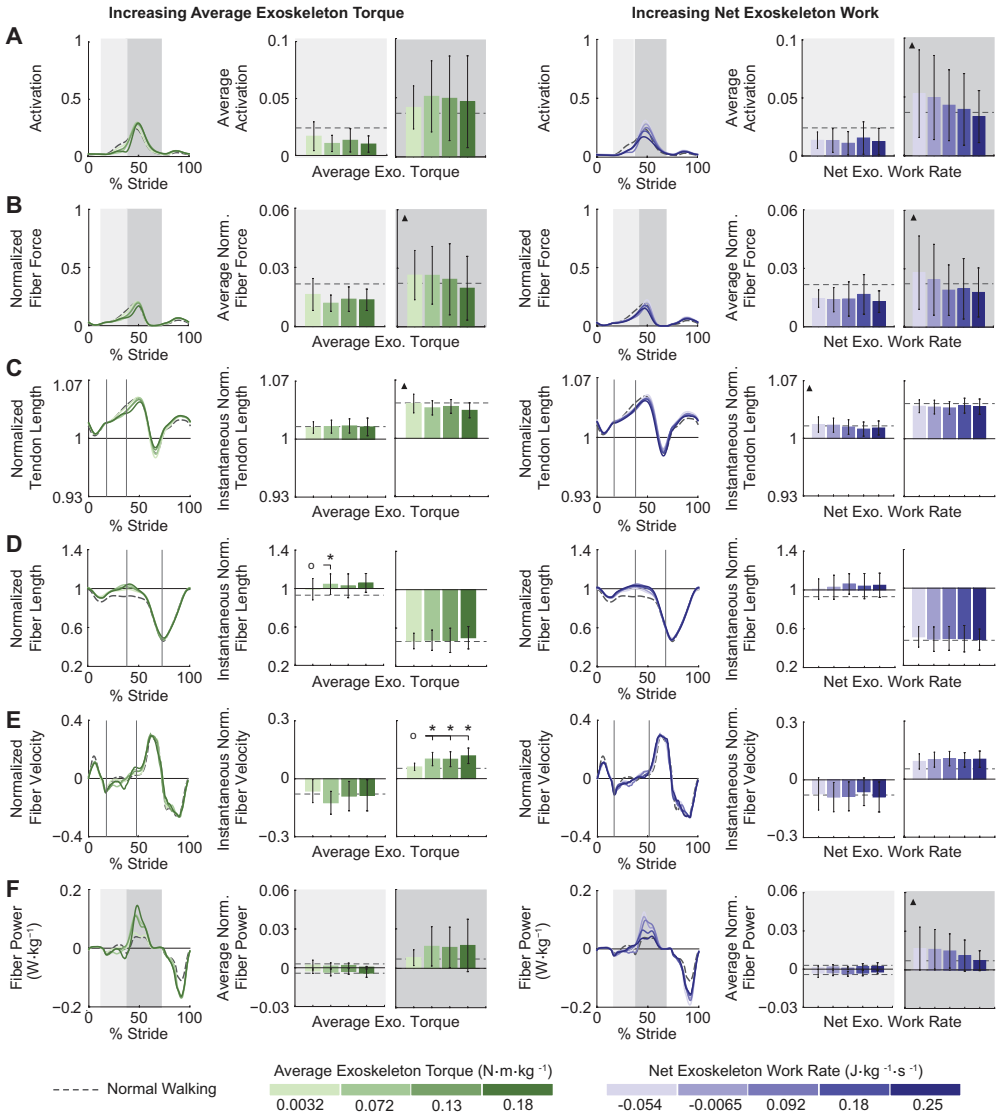

Figure 3.6: Medial gastrocnemius muscle-tendon mechanics under different ankle exoskeleton perturbations. Trends in medial grastrocnemius muscle-tendon mechanics closely matched those of the soleus. (A) Medial gastrocnemius activation. (B) Medial gastrocnemius muscle fiber force normalized to maximum isometric force. (C) Tendon length normalized to tendon slack length. (D) Medial gastrocnemius muscle fiber length normalized to optimal fiber length. (E) Medial gastrocnemius muscle fiber velocity normalized to maximum fiber shortening velocity. (F) Medial gastrocnemius muscle fiber power normalized to body mass. Each curve is a subject-average ($N = 8$) trajectory. Bars and whiskers are subject means and standard deviations. Shaded bar plots represent the average of the corresponding trajectories over the shaded region. Unshaded bar plots represent instantaneous values of corresponding trajectories. Conditions with increasing average exoskeleton torque are shown in green. Conditions with increasing net exoskeleton work rate are shown in purple. Darker colors indicate higher values. Normal walking is shown by gray dashed lines. *s indicate statistical significance ($P < 0.05$) with respect to the conditions designated by open circles. Triangles indicate ANOVA significance.

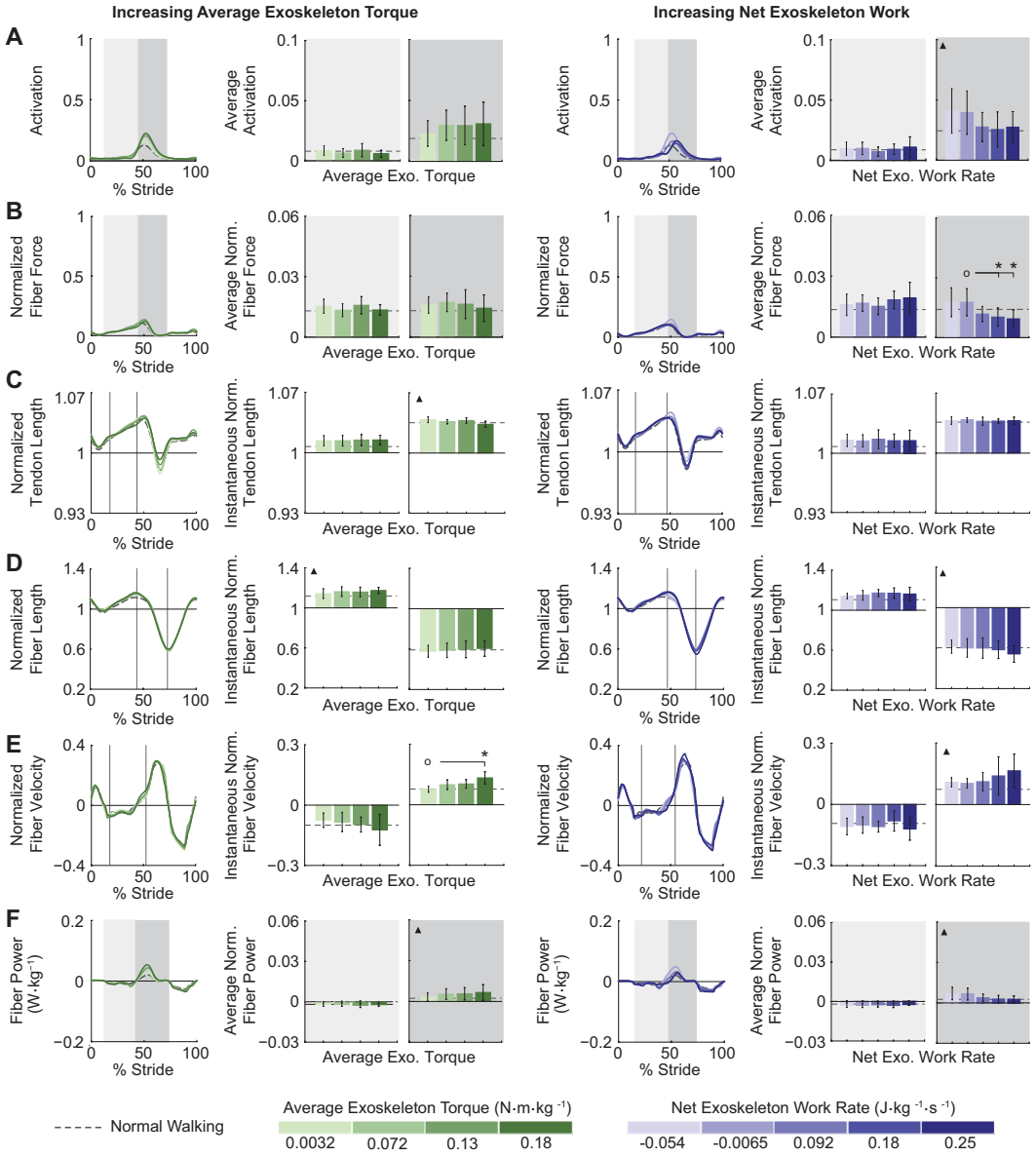

Figure 3.7: Lateral gastrocnemius muscle-tendon mechanics under different ankle exoskeleton perturbations. Trends in lateral grastrocnemius muscle-tendon mechanics closely matched those of the soleus. (A) Lateral gastrocnemius activation. (B) Lateral gastrocnemius muscle fiber force normalized to maximum isometric force. (C) Tendon length normalized to tendon slack length. (D) Lateral gastrocnemius muscle fiber length normalized to optimal fiber length. (E) Lateral gastrocnemius muscle fiber velocity normalized to maximum fiber shortening velocity. (F) Lateral gastrocnemius muscle fiber power normalized to body mass. Each curve is a subject-average ($N = 5$) trajectory. Bars and whiskers are subject means and standard deviations. Shaded bar plots represent the average of the corresponding trajectories over the shaded region. Unshaded bar plots represent instantaneous values of corresponding trajectories. Conditions with increasing average exoskeleton torque are shown in green. Conditions with increasing net exoskeleton work rate are shown in purple. Darker colors indicate higher values. Normal walking is shown by gray dashed lines. *s indicate statistical significance ($P < 0.05$) with respect to the conditions designated by open circles. Triangles indicate ANOVA significance.

3.7 Appendix B: Sensitivity Analyses

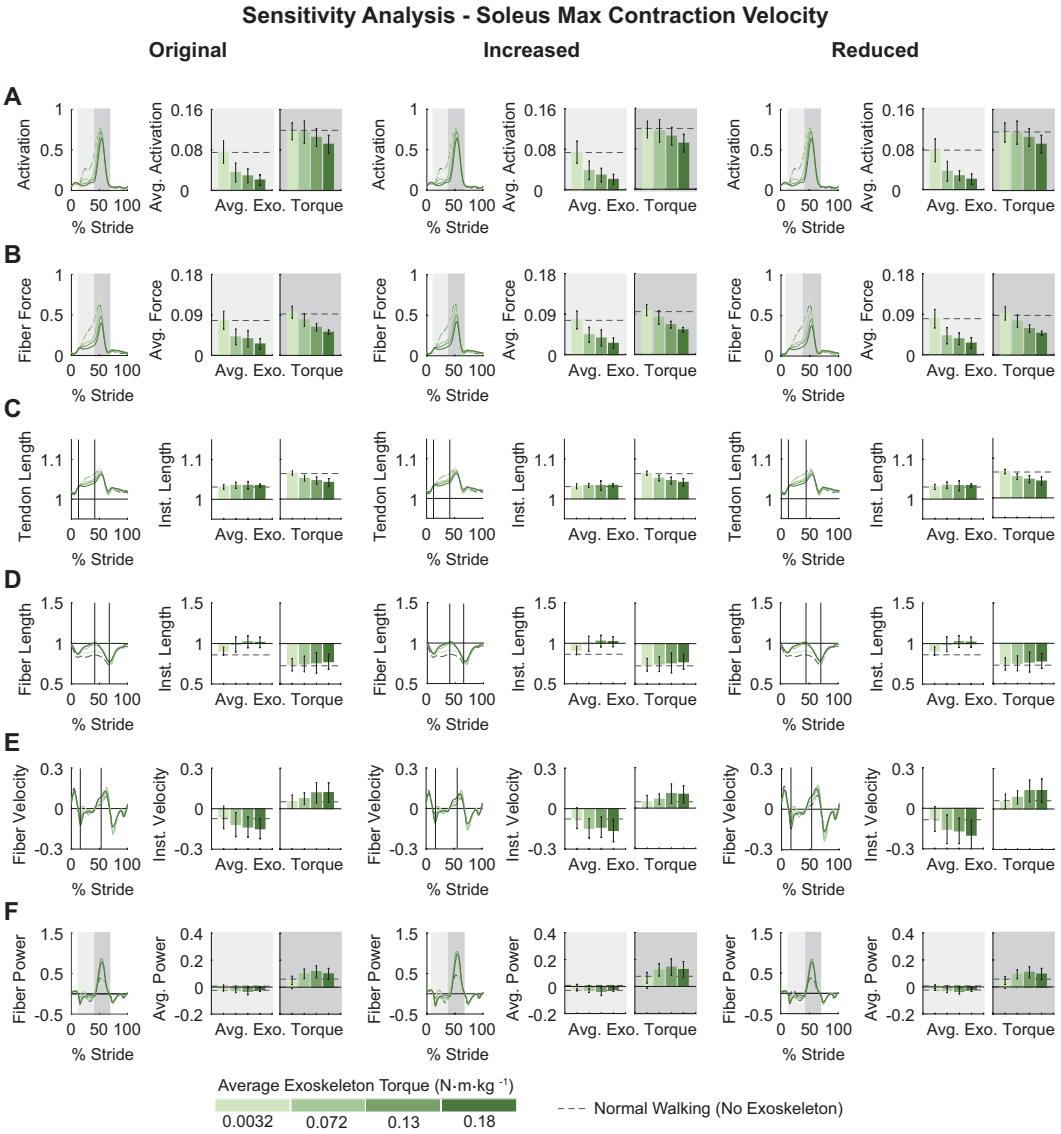

Figure 3.8: Sensitivity Analysis: Exoskeleton-side soleus muscle-tendon mechanics with varying soleus maximum fiber contraction velocities. Trends in muscle mechanics were insensitive to changes in maximum fiber contraction velocity. (A) Soleus activation. (B) Soleus muscle fiber force normalized to maximum isometric force. (C) Tendon length normalized to tendon slack length. (D) Soleus muscle fiber length normalized to optimal fiber length. (E) Soleus muscle fiber velocity normalized to maximum fiber shortening velocity. (F) Soleus muscle fiber power normalized to body weight. Left panel shows results with original maximum contraction velocity, middle panel shows results with 20% increased maximum contraction velocity, right panel shows results with 20% reduced maximum contraction velocity. Each curve is a subject-average ($N = 8$) trajectory. Bars and whiskers are subject means and standard deviations. Shaded bar plots represent subject-wise integration of corresponding trajectories over the shaded region. Unshaded bar plots represent subject-average instantaneous values of corresponding trajectories. Darker colors indicate higher values. Normal walking is shown by gray dashed lines.

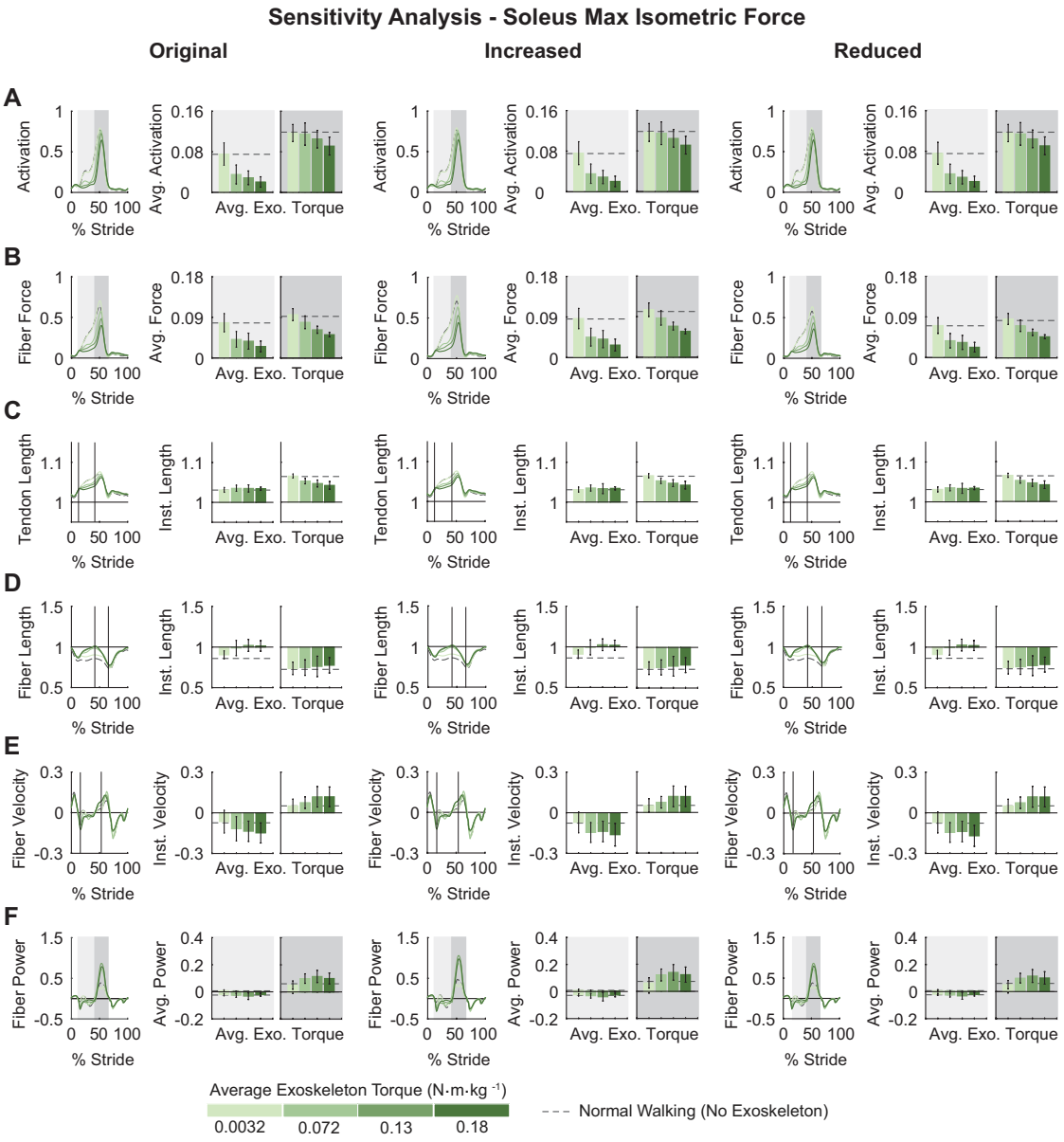

Figure 3.9: Sensitivity Analysis: Exoskeleton-side soleus muscle-tendon mechanics with varying soleus maximum isometric forces. Trends in muscle mechanics were insensitive to changes in maximum isometric force. (A) Soleus activation. (B) Soleus muscle fiber force normalized to maximum isometric force. (C) Tendon length normalized to tendon slack length. (D) Soleus muscle fiber length normalized to optimal fiber length. (E) Soleus muscle fiber velocity normalized to maximum fiber shortening velocity. (F) Soleus muscle fiber power normalized to body weight. Left panel shows results with original maximum isometric force, middle panel shows results with 10% increased maximum isometric force, right panel shows results with 10% reduced maximum isometric force. Each curve is a subject-average ($N = 8$) trajectory. Bars and whiskers are subject means and standard deviations. Shaded bar plots represent subject-wise integration of corresponding trajectories over the shaded region. Unshaded bar plots represent subject-average instantaneous values of corresponding trajectories. Darker colors indicate higher values. Normal walking is shown by gray dashed lines.

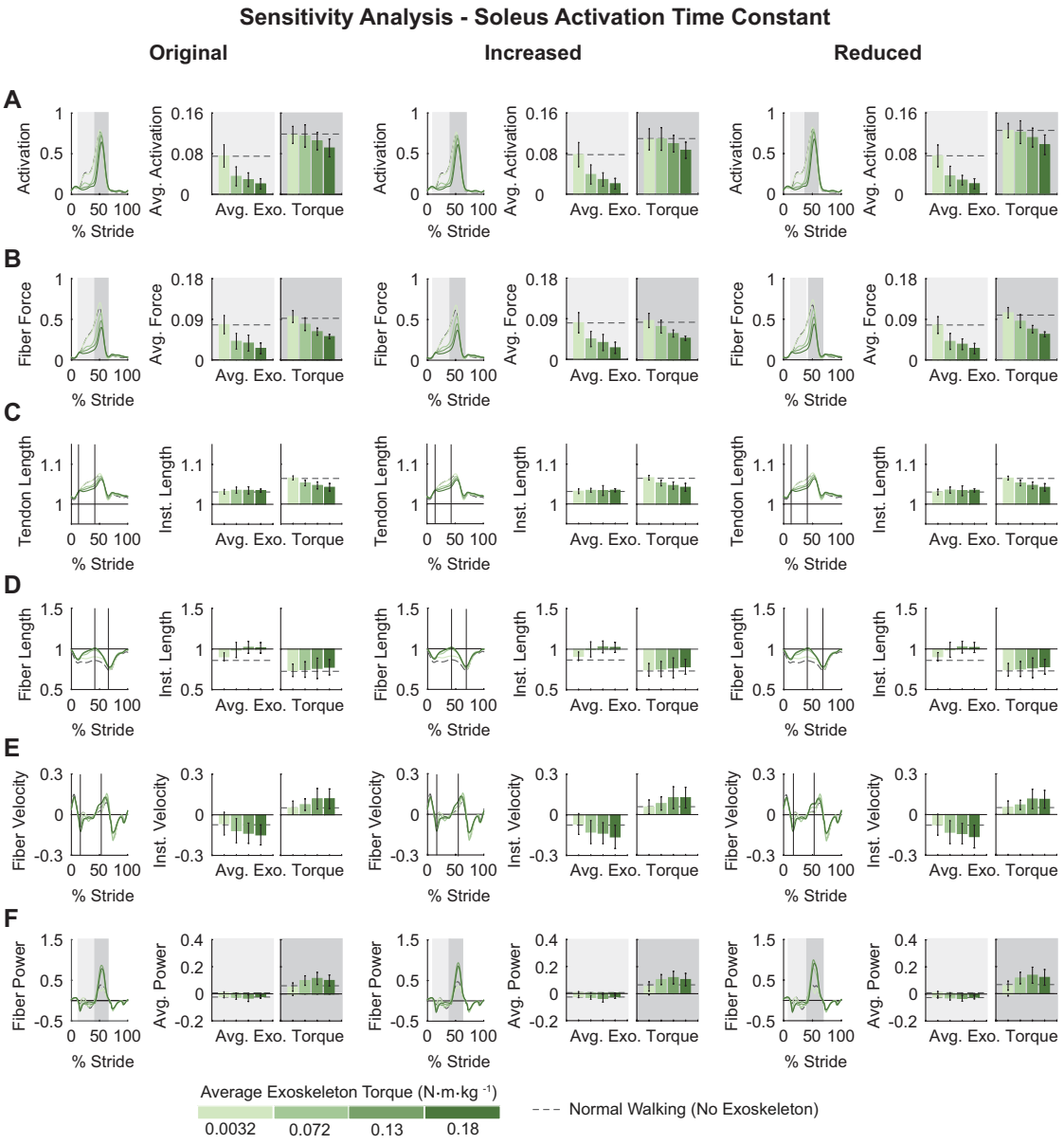

Figure 3.10: Sensitivity Analysis: Exoskeleton-side soleus muscle-tendon mechanics with varying soleus activation time constants. Trends in muscle mechanics were insensitive to changes in activation time constant. (A) Soleus activation. (B) Soleus muscle fiber force normalized to maximum isometric force. (C) Tendon length normalized to tendon slack length. (D) Soleus muscle fiber length normalized to optimal fiber length. (E) Soleus muscle fiber velocity normalized to maximum fiber shortening velocity. (F) Soleus muscle fiber power normalized to body weight. Left panel shows results with original activation time constant, middle panel shows results with 10% increased activation time constant, right panel shows results with 10% reduced activation time constant. Each curve is a subject-average ($N = 8$) trajectory. Bars and whiskers are subject means and standard deviations. Shaded bar plots represent subject-wise integration of corresponding trajectories over the shaded region. Unshaded bar plots represent subject-average instantaneous values of corresponding trajectories. Darker colors indicate higher values. Normal walking is shown by gray dashed lines.

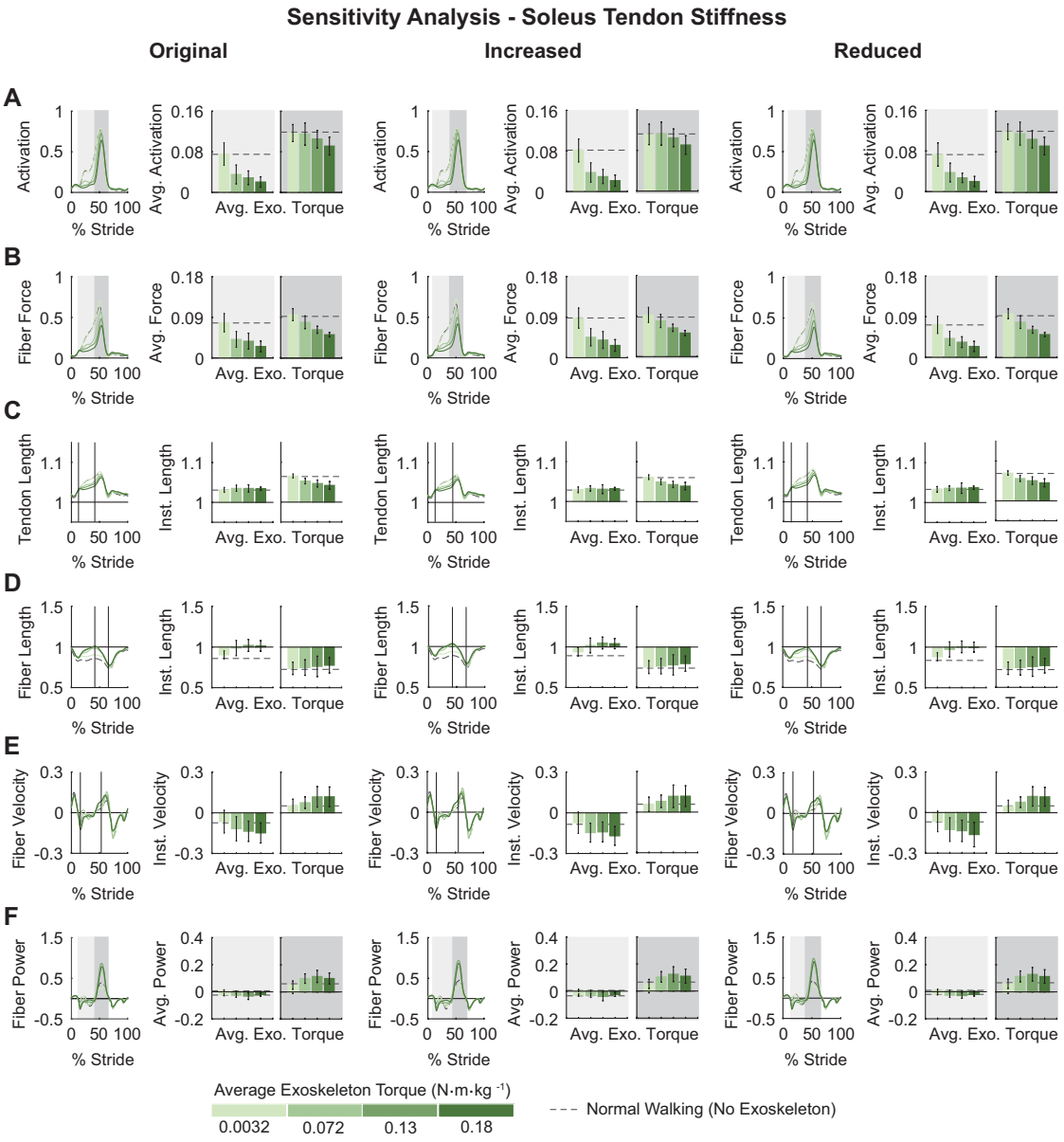

Figure 3.11: Sensitivity Analysis: Exoskeleton-side soleus muscle-tendon mechanics with varying soleus tendon stiffnesses. Trends in muscle mechanics were insensitive to changes in tendon stiffness. (A) Soleus activation. (B) Soleus muscle fiber force normalized to maximum isometric force. (C) Tendon length normalized to tendon slack length. (D) Soleus muscle fiber length normalized to optimal fiber length. (E) Soleus muscle fiber velocity normalized to maximum fiber shortening velocity. (F) Soleus muscle fiber power normalized to body weight. Left panel shows results with original tendon strain at maximum isometric force, middle panel shows results with 1% absolute reduction in tendon strain at maximum isometric force, right panel shows results with 1% absolute increase in tendon strain at maximum isometric force. Each curve is a subject-average ($N = 8$) trajectory. Bars and whiskers are subject means and standard deviations. Shaded bar plots represent subject-wise integration of corresponding trajectories over the shaded region. Unshaded bar plots represent subject-average instantaneous values of corresponding trajectories. Darker colors indicate higher values. Normal walking is shown by gray dashed lines.

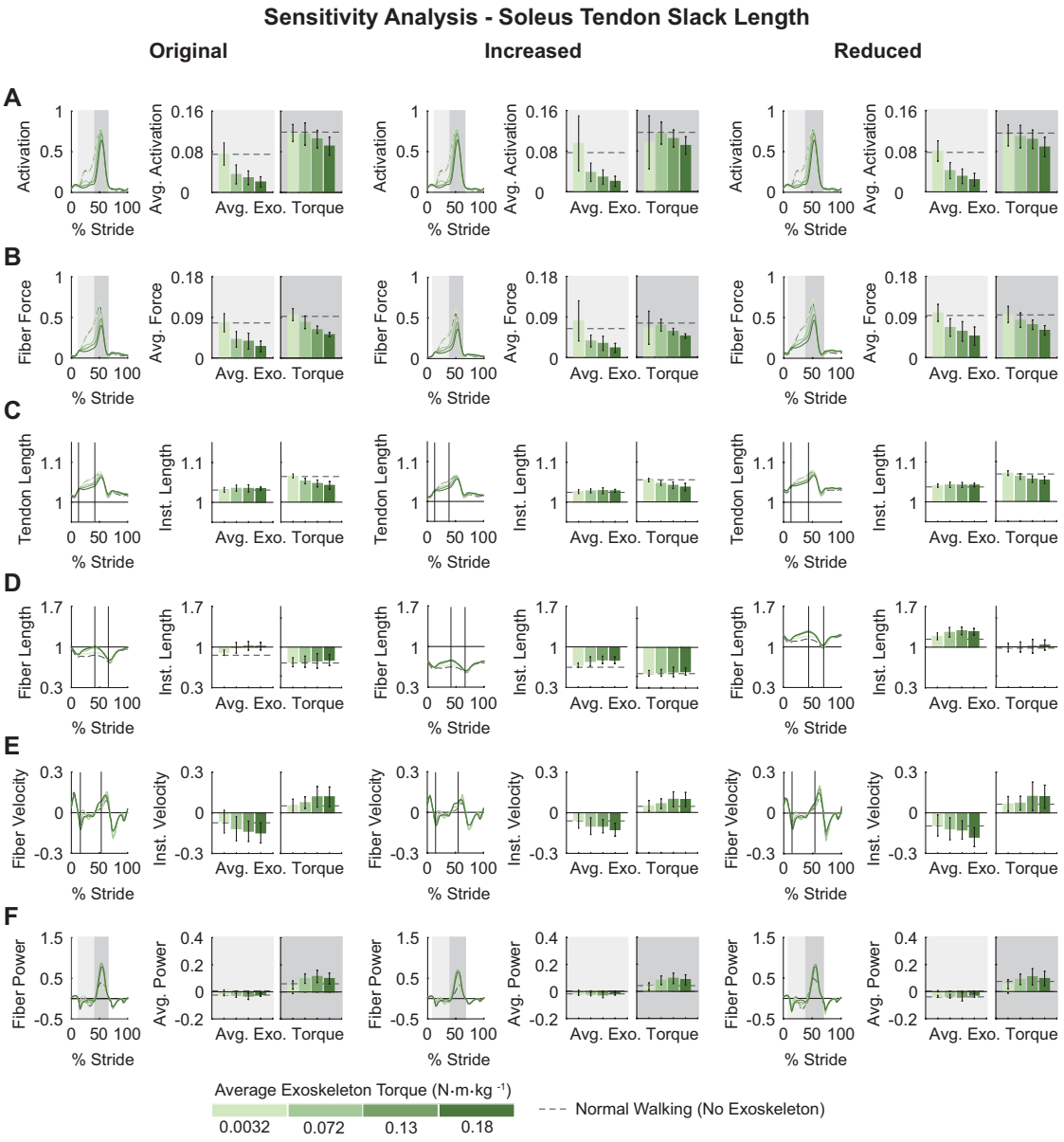

Figure 3.12: Sensitivity Analysis: Exoskeleton-side soleus muscle-tendon mechanics with varying soleus tendon slack lengths. Trends in muscle mechanics were insensitive to changes in tendon slack length. (A) Soleus activation. (B) Soleus muscle fiber force normalized to maximum isometric force. (C) Tendon length normalized to tendon slack length. (D) Soleus muscle fiber length normalized to optimal fiber length. (E) Soleus muscle fiber velocity normalized to maximum fiber shortening velocity. (F) Soleus muscle fiber power normalized to body weight. Left panel shows results with original tendon slack length, middle panel shows results with 5% increased slack length, right panel shows results with 5% reduced tendon slack length. Each curve is a subject-average ($N = 8$) trajectory. Bars and whiskers are subject means and standard deviations. Shaded bar plots represent subject-wise integration of corresponding trajectories over the shaded region. Unshaded bar plots represent subject-average instantaneous values of corresponding trajectories. Darker colors indicate higher values. Normal walking is shown by gray dashed lines.

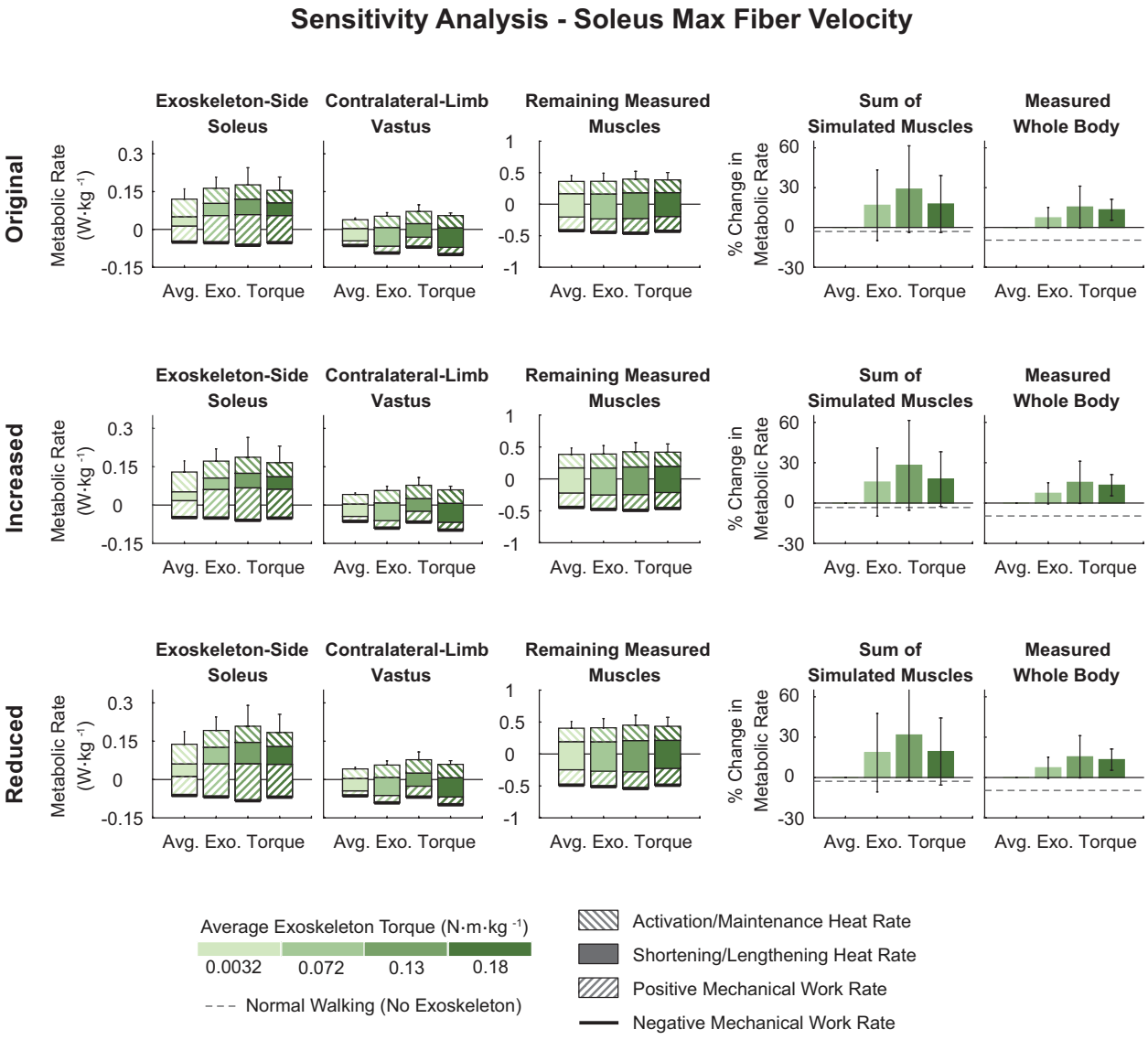

Figure 3.13: Sensitivity Analysis: Estimated individual muscle and sum of simulated muscles metabolic rate with varying soleus maximum fiber contraction velocities. Trends in muscle metabolic rate were insensitive to changes in maximum fiber contraction velocity. *From left to right:* Estimated exoskeleton-side soleus metabolic rate; estimated contralateral-limb vastus metabolic rate; estimated metabolic rate of the remaining muscles with electromyographic data; estimated percent change in the sum of the simulated muscle metabolic rates; and measured percent change in whole-body metabolic rate. The top rows show results with original tendon slack length, the middle row shows results with increased tendon slack length, and the bottom row shows results with reduced tendon slack length. Darker colors indicate higher values. Normal walking is shown by a gray dashed line. Bars and whiskers are subject means and standard deviations. Bar shadings represent different muscle heat and work rates. The solid black line at the base of each bar shows the average negative mechanical work rate. Data from $N = 8$ subjects except for plots of the contralateral-limb vastus metabolic energy consumption, for which $N = 5$.

Chapter 4

Heuristic-based online adaptation of ankle exoskeleton assistance using plantarflexor electromyography [§]

Abstract

People change their locomotor coordination patterns as they learn to walk with ankle exoskeletons, yet few locomotion assistance strategies address such adaptation. The purpose of this study was to develop a novel, heuristic-based assistance strategy that adjusts exoskeleton behavior online in response to measured changes in the user. Soleus muscle activity, measured in real time, was used to guide the discovery of a desired ankle exoskeleton torque profile with the goal of improving whole-body locomotor economy. The heuristics driving the evolution of the exoskeleton torque profile were: 1) soleus muscle activity indicates the user wants torque; 2) antagonistic muscle activity indicates the user wants less torque; and 3) torque should stop increasing if the user is not adapting. We applied our controller to bilateral ankle exoskeletons worn by participants as they walked on a treadmill at 1.25 $\mathrm{m{\cdot}s^{-1}}$ for 30 minutes. The heuristic-based adaptive controller reduced the root-mean-

[§]This work will be presented at the Dynamic Walking Conference in June 2017. A manuscript presenting this work is in preparation: Jackson, R. W. and Collins, S. H. (2017). Heuristic-Based online adaptation of ankle exoskeleton assistance using plantarflexor electromyography, *Proc. Natl. Acad. Sci. U.S.A.*, **in preparation**.

square of soleus muscle activity by 35 ± 12% and metabolic rate by 22 ± 8% compared to walking with the exoskeletons while they provided no torque. Desired exoskeleton torque stabilized quickly for most subjects, while metabolic rate stabilized over a longer time scale, suggesting that longer exposure to walking with this adaptive control strategy may provide further benefit. Our findings indicate that this form of ankle exoskeleton assistance is effective at reducing muscle activity at the assisted joint and at reducing whole-body metabolic rate. This heuristic-based adaptive approach can be applied to exoskeletons operating about the other lower-limb joints in populations with unaltered muscle activity and establishes the framework for a new class of lower-limb exoskeleton assistance strategies.

Keywords: exoskeleton, adaptation, gait, assistance, muscle activity

4.1 Introduction

Users change their locomotor coordination patterns in response to exoskeleton-applied assistance. These changes happen on multiple levels, from changes in neural coordination strategies, to changes in muscle-tendon mechanics [41, 40, 104, 62] and joint kinematics and kinetics, up to changes in whole-body metabolic rate [49, 105, 47, 66]. Additionally, these changes happen over multiple time scales, from seconds to tens of minutes [49, 47], to days and potentially even years. Such changes are specific to the user, with every individual adapting differently to a given type of exoskeleton assistance, as evidenced by the large inter-subject variability inherent in measured biomechanics outcomes [62, 66]. Given the complexity of the human musculoskeletal system and the broad range of possible locomotor strategies users can adopt, it remains a significant challenge to predict how users will respond to different assistance strategies. Subtle differences in how exoskeletons are controlled can have profound implications for the benefits users are able to derive from such devices.

Most commonly used exoskeleton control techniques do not adequately account for human locomotor adaptations and are based upon intuition-driven predictions of the human response to certain device behaviors. Time-based assistance techniques, which apply exoskeleton

torque according to a predefined trajectory in time [75, 47, 84], keep device behavior static across walking steps regardless of changes in human coordination patterns and regardless of differences across users. Yet other control techniques that incorporate changes in human coordination patterns are often too constrained to yield significant benefit to the user. Proportional myoelectric control (pEMG), which provides device torque in direct proportion to the user's muscle activity [43], requires a minimum amount of muscle activity be maintained for the exoskeleton to generate torque. This prevents exoskeleton torque from fully supplanting the user's muscle activity and limits the types of locomotor adaptations participants can adopt. Control techniques that respond to changes in the user and enable exoskeletons to completely assume the role of the muscles at the assisted joint could prove more effective.

'Human-in-the-loop' assistance strategies that adjust exoskeleton behavior in response to measured changes in the user would allow for co-adaptation of the device and the user and potentially result in improved human-robot interaction. Such control strategies do not need to know, a priori, how the user is going to react to a certain device behavior, but rather can respond directly to changes in the user, lessening the need for prediction. These adaptive techniques could loosen constraints on the set of possible assistance patterns so as to enable users to adapt in unexpected or unpredicted ways, and could result in the discovery of new, more effective, individualized assistance strategies.

The development of these control approaches is ultimately driven by the high-level goals of the intervention; decisions made regarding what objective function to use and how the controller should be formulated affect the capabilities of the approach. If the goal of an assistance strategy is to directly reduce metabolic rate, then using measured metabolic rate as the objective function is desirable. Measuring metabolic rate online, however, presents many challenges: it is noisy, takes a long time to reach steady-state, can only be sampled every breath, and does not directly translate to a joint torque profile. Muscle activity, on the other hand, is a more natural proxy for joint torque, and processed electromyography data can function as the basis of a torque assistance profile. Muscle activity is related to metabolic

rate (albeit indirectly) and can be sampled at a high frequency in order to modulate device torque on every walking step during locomotion. These features of muscle activity make it a useful objective function for a high degree-of-freedom, heuristic-based, adaptive control technique.

The goal of this project was to develop an algorithm that uses an online measurement of soleus muscle activity to update desired ankle exoskeleton torque on the subsequent walking step. We hypothesized that, over time, the exoskeleton would learn the changing pattern of soleus muscle activity and supplant the contribution of soleus muscle activity to net plantarflexion. Furthermore, we hypothesized that an exoskeleton torque profile derived from the user's own muscle activity pattern would lead to a reduction in whole-body metabolic rate. We expected this control strategy would be more effective than a static torque profile at providing locomotion assistance. We think such co-adaptive control strategies will enhance our ability to assist people with a broad range of physiological needs.

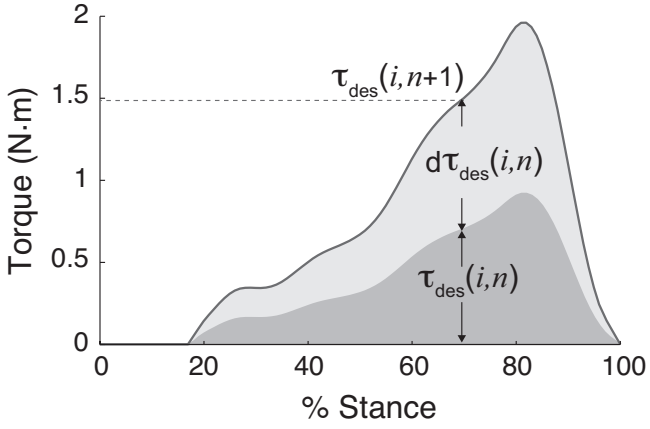

Figure 4.1: Schematic depicting the desired exoskeleton torque as defined by the proposed control scheme. Desired exoskeleton torque on the next step is dependent on the desired exoskeleton torque, processed soleus and tibialis anterior electromyography (EMG), and ankle kinematics on the current step.

4.2 Materials and Methods

We developed a novel, heuristic-based ankle exoskeleton assistance strategy that uses soleus muscle activity, measured in real time, to guide the evolution of a desired torque pattern. We

tested the effectiveness of the control approach by applying it to bilateral ankle exoskeletons worn by naïve users as they walked on a treadmill. The overarching goal of the method was to reduce whole-body metabolic rate through an intermediate goal of reducing muscle activity.

Heuristic-Based Adaptive Controller

We implemented a heuristic-based adaptive controller that uses soleus muscle activity to optimize the pattern of exoskeleton torque in real time. At a high level, the desired exoskeleton torque profile on the next walking step, $\tau_{\text{des}}(i, n+1)$, is the sum of the desired exoskeleton torque profile on the current walking step, $\tau_{\text{des}}(i, n)$, and a change in the desired torque, $d\tau_{\text{des}}(i, n)$ (Fig. 4.1). The dependence of the desired torque profile on previous walking steps prevents exoskeleton torque from decreasing in proportion to soleus muscle activity. The change in desired torque is comprised of several different contributions. Soleus muscle activity acts to increase desired exoskeleton torque. If, however, soleus muscle activity is not decreasing, the rate of growth of exoskeleton torque slows to enable the user more time to adapt. Tibialis anterior muscle activity, which acts antagonistically to the soleus muscle, drives exoskeleton torque down, as it is indicative of the user resisting or compensating for excessive plantarflexion torque. A negative force feedback term is included to naturally stabilize the controller and prevent desired torque from growing unbounded. Deviations in ankle kinematics from nominal also act to drive exoskeleton torque down, as changes in ankle angle are indicative of the user adopting coordination strategies other than reducing soleus muscle activity in response to the applied exoskeleton torque.

The control scheme is given by the following equations:

$$\tau_{\text{des}}(i, n+1) = \tau_{\text{des}}(i, n) + \text{sgn}(d\tau_{\text{des}}(i, n)) \cdot \max(|d\tau_{\text{des}}(i, n)| - d\tau_{\text{db}}, 0) \tag{4.1}$$

where

$$\begin{aligned} d\tau_{\text{des}}(i,n) =& k_1 \cdot EMG_{\text{SOL}}(i+d,n) \cdot (EMG_{\text{SOL,AVG}}(n))^{-m} \\ & - k_2 \cdot EMG_{\text{TA}}(i+d,n) - k_3 \cdot \tau_{\text{des}}(i,n) \\ & - k_4 \cdot \text{sgn}(e_{\theta_{\text{a,AVG}}}(n)) \cdot \max(|e_{\theta_{\text{a,AVG}}}(n)| - c_{\theta_{\text{a}}}, 0) \end{aligned} \tag{4.2}$$

In this formulation, i is the time index, updated every 2 ms and reset every heel strike, n is the step number, and d is a constant chosen to account for neuromechanical and mechanical delays in the system.

The fact that desired exoskeleton torque on the current walking step, $\tau_{\text{des}}(i,n)$, contributes to desired exoskeleton torque on the next walking step, $\tau_{\text{des}}(i,n+1)$, introduces history dependence. This structure prevents exoskeleton torque from decreasing when soleus muscle activity decreases, and enables the exoskeleton to fully supplant the soleus muscle's contribution to plantarflexion.

Soleus muscle activity on the current step (EMG_{SOL}) increases desired exoskeleton torque for the next step, based on the heuristic that soleus muscle activity indicates the user wants plantarflexion torque. As exoskeleton torque increases, soleus muscle activity should decrease and as soleus muscle activity decreases, the marginal contribution of soleus muscle activity to desired exoskeleton torque diminishes, thereby slowing growth of desired exoskeleton torque over time. The magnitude of the gain k_1 affects how quickly (i.e. over how many walking steps) desired torque increases. The growth rate is further adjusted on each subsequent walking step based on the ratio of soleus muscle activity at each instant in time to the average soleus muscle activity for the current step n ($EMG_{\text{SOL}}(i+d,n) \cdot EMG_{\text{SOL,AVG}}(n)^{-m}$). The value of the exponent m affects the relative contribution of average soleus muscle activity to the growth rate of desired torque. The value of m should be between 1 and 2.

Although the goal of this control scheme is to supplant soleus muscle activity with torque from the exoskeleton, users may not decrease soleus muscle activity as expected. Stabilizing features of soleus muscle activity and inherent soleus muscle reflexes may prevent soleus muscle activity from being driven to resting levels. Additionally, users can adopt coordination

strategies that do not involve reducing soleus muscle activity when responding to exoskeleton-applied torque. To account for such potential outcomes and prevent desired exoskeleton torque from growing unbounded, we added several stabilizing terms to our formulation.

Tibialis anterior muscle activity (EMG_{TA}), which acts antagonistically to the soleus muscle, decreases desired exoskeleton torque. The negative gain multiplying this term is designed to prevent co-contraction, as tibialis anterior muscle activity may increase in an attempt to resist excessive plantarflexion or to ensure certain ankle kinematics. The magnitude of gain k_2 determines the tibialis anterior muscle's contribution to the desired exoskeleton torque profile.

The forgetting term, $-k_3 \cdot \tau_{\mathrm{des}}(i,n)$, acts to stabilize the controller. As desired exoskeleton torque grows in magnitude, there is an increasingly subtractive contribution to the desired exoskeleton torque for the next step. The relative values of gains k_1 and k_3 define the desired torque that stabilizes a given reduction in soleus muscle activity.

The average deviation in ankle angle over the dorsiflexion phase of gait, $e_{\theta_{\mathrm{a,AVG}}}(n)$, negatively contributes to the desired exoskeleton torque profile. This deviation is measured relative to a user's ankle angle during walking with the exoskeleton in a zero-torque mode. This term is intended to prevent participants from changing their ankle kinematics, as opposed to reducing soleus muscle activity, when the exoskeleton applies torque. The value of gain k_4 defines the contribution of the average ankle angle deviation to the desired torque profile. Ankle angle deviations must reach a defined threshold value, $c_{\theta_{\mathrm{a}}}$, so that natural step-to-step variations in ankle kinematics do not affect the desired torque profile but large deviations induced by excessive exoskeleton torque do.

Finally, to account for the slow upward drift of desired exoskeleton torque over time caused by the existence of some non-zero amount of soleus muscle activity, we introduced a deadband on the change in desired exoskeleton torque, $\mathrm{sgn}(d\tau_{\mathrm{des}}(i,n)) \cdot \max(|d\tau_{\mathrm{des}}(i,n)| - d\tau_{\mathrm{db}}, 0)$, such that sufficiently small values of $d\tau_{\mathrm{des}}$ are set to zero.

An average stance period during normal human walking lasts about 700 ms. Given the 500 Hz sampling frequency of our data acquisition system, we can adjust approximately 350

nodes on the desired exoskeleton torque profile for the subsequent walking step. This level of resolution allows us to extract features from the desired exoskeleton torque profile that other control approaches cannot.

Soleus and tibialis anterior muscle activity were measured online, high-pass filtered with a cutoff frequency of 20 Hz, full-wave rectified, and low-pass filtered with a cut-off frequency of 6 Hz [105, 32]. Muscle activity was then normalized to peak muscle activity measured during walking with the exoskeletons in a zero-torque mode. Muscle activity measured from electrodes on both the medial and lateral aspects of the soleus was averaged to give a single soleus muscle activity signal. The gains and constants used in this experiment were determined throught extensive pilot testing of the controller. The values of the gains and constants were as follows: $k_1 = 0.0025*$body mass, $d = 42$, $m = 1.3$, $k_2 = 0.05$, $k_3 = 0.01$, $k_4 = 2$, $c_{\theta_a} = 5°$, and $d\tau_{\text{db}} = 0.01$.

Ankle Exoskeleton Emulator

External plantarflexion torque was applied to both ankles using our ankle exoskeleton emulator (Fig. 4.2), the details of which are provided in [21, 121]. The ankle exoskeleton end-effectors contacted the user at the shank below the knee via a strap worn around the calf, at the toe via a plate embedded in the front of the shoe, and at the heel via a rope embedded in the rear of the shoe. Each end-effector had a mass of 0.875 kg and was actuated by a powerful off-board motor, with forces transmitted through a flexible, unidirectional Bowden cable tether. The end-effectors had rotational joints on the medial and lateral sides of each leg, with the axis of rotation approximately aligned with the center of the user's lateral malleolus. This experimental set-up is capable of generating peak plantarflexion moments during walking of approximately 120 N·m [121].

The exoskeletons were instrumented to measure device mechanics and trigger state transitions. Four strain gages (MMF003129, Micro Measurements, Wendell, NC, USA) affixed to the frame of each exoskeleton in a Wheatstone bridge configuration measured exoskeleton plantarflexion torque with an RMS error of 0.125 N·m, or 0.25% of peak [121].

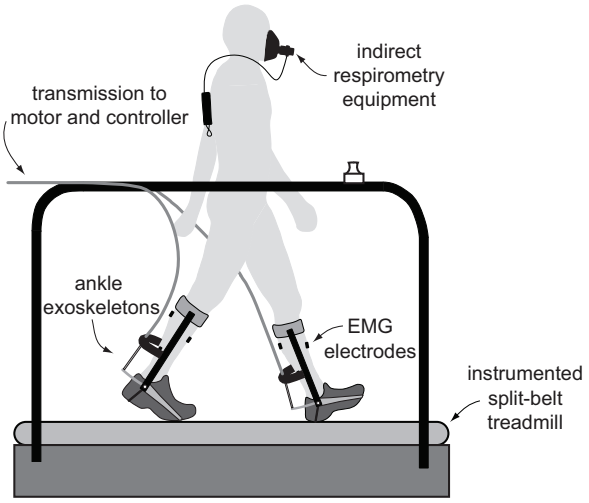

Figure 4.2: Schematic of bilateral ankle exoskeletons and experimental setup highlighting key components. Custom-built bilateral ankle exoskeletons were used to apply torque to the user. Metabolic energy consumption, muscle activity, exoskeleton mechanics, and ground reaction forces were measured.

Exoskeleton joint angle was measured using an absolute magnetic encoder (MAE3, US Digital, Vancouver, Washington, USA) mounted on the lateral side of each exoskeleton's ankle joint. A switch (McMaster-Carr, Aurora, Ohio, USA) positioned in the heel of each shoe was used to detect foot contact.

Control of the ankle exoskeletons was state-dependent, with different control methods used for the stance and swing phases of gait. During stance, we used torque control to track the time-based, desired exoskeleton torque profile. Exoskeleton torque control was achieved using a combination of proportional control, damping injection, and iterative learning compensation [128]. This method of torque control was previously shown to result in torque tracking errors as low as 1% of the peak torque during walking, which is lower than the torque tracking errors observed with other commonly used torque control methods [128]. During swing, we maintained a defined length of slack in the Bowden cable and used motor position control to track the exoskeleton ankle joint angle so as to not interfere with the natural motion of the user's ankle.

Experimental Protocol

We conducted an experiment to evaluate the effectiveness of a novel ankle exoskeleton controller at supplanting muscle activity and reducing metabolic rate in naïve exoskeleton users. We applied our assistance strategy through bilateral ankle exoskeletons worn by healthy participants as they walked on a treadmill. We computed the reductions in participants' soleus muscle activity and metabolic rate achieved with our novel heuristic-based controller below walking with the exoskeletons in a zero-torque mode and below walking with normal shoes. We compared these reductions to those observed with a static torque profile.

Participants walked on a treadmill at 1.25 $\mathrm{m{\cdot}s^{-1}}$ for 30 minutes while exoskeleton torque evolved in time using the heuristic-based adaptive algorithm described above, which we will refer to as the Adaptive condition. In order to evaluate the effectiveness of our novel controller, we compared the results from the Adaptive condition to a Static condition. In the Static condition, participants walked for 30 minutes while exoskeleton torque was held constant across walking steps. Desired exoskeleton torque was defined as the average, mass-normalized, exoskeleton torque profile found to effectively reduce metabolic rate in a previous study [130]. The presentation of the Adaptive and Static conditions was randomized to account for ordering and learning effects.

Participants also completed a six-minute walking trial in their normal shoes, referred to here as Normal Walking, and two, six-minute walking trials in which the exoskeletons were worn on both ankles while providing zero torque, referred to here as Zero Torque. The Zero Torque conditions were conducted once before and once after the Adaptive and Static conditions, and the results across the two Zero Torque conditions were averaged. These averaged results are referred to as one Zero Torque condition for the remainder of the manuscript. We measured and compared soleus muscle activity and whole-body metabolic rate across the different walking conditions. Basal metabolic rate was obtained through a Quiet Standing condition lasting four minutes.

10 able-bodied, naïve individuals (N = 10, 8 men and 2 women; age = 22.7 $\pm$ 2.0 yrs; body

mass = 68.3 ± 9.4 kg; height = 1.75 ± 0.05 m) participated in the study. No participants had worn the exoskeletons prior to participating in this study and all participants provided written informed consent before completing the protocol. The protocol was approved by the Carnegie Mellon Institutional Review Board.

Measured Outcomes

Muscle Activity

Muscle activity was measured using surface electromyography. Wired electrodes (Bagnoli Desktop System, Delsys Inc., Boston, Massachusetts, USA) were placed on the medial and lateral aspects of the soleus and on the tibialis anterior on both legs. Electromyography signals were sampled at a frequency of 500 Hz, then high-pass filtered with a cutoff frequency of 20 Hz, full-wave rectified, and low-pass filtered with a cut-off frequency of 6 Hz [105, 32] in post-processing. These signals were then normalized to average peak muscle activity observed during the Zero Torque condition. Average peak and root-mean-square (RMS) of the processed electromyography signals were calculated for the last three minutes of each walking condition and used to compare muscle activity across the different conditions.

Metabolic Rate

Metabolic rate was estimated by substituting volumetric oxygen consumption and carbon dioxide expulsion flow rates into a widely-used equation [16]. Volumetric flow rates were measured using indirect calorimetry via a portable metabolics cart (Oxycon Mobile, CareFusion, San Diego, California, USA). The average of the last three minutes of metabolics data for each condition, normalized to body mass, was used as our measure of steady-state metabolic rate. Net metabolic rate was calculated by subtracting the metabolic rate of Quiet Standing from the different walking conditions. Change in metabolic rate was calculated by subtracting the metabolic rate of each walking condition from metabolic rate of the Zero Torque condition.

Exoskeleton Mechanics

We used on-board sensors to approximate ankle exoskeleton kinematics and kinetics. Exoskeleton ankle joint angle was measured using an absolute magnetic encoder, sampled at 500 Hz and low-pass filtered with a cut-off frequency of 50 Hz. We took the discrete derivative of exoskeleton ankle joint angle to calculate ankle velocity. Exoskeleton plantarflexion torque was measured using calibrated strain gauges, sampled at 500 Hz and low-pass filtered with a cut-off frequency of 50 Hz. The desired exoskeleton torque profile was averaged over the last three minutes of the Adaptive condition. Average peak and RMS of the evolved exoskeleton torque profiles were calculated for the last three minutes of the Adaptive condition for the left and right legs independently. These measures were used to compare the evolved torque profiles across legs and subjects and to the torque profile applied in the Static condition. We multiplied exoskeleton ankle velocity and torque to calculate exoskeleton power. We calculated negative, positive, and net exoskeleton work rates by taking the integral of exoskeleton power over a stride and dividing by stride time. We averaged exoskeleton work rates over the last three minutes of the Adaptive and Static conditions. All measures of exoskeleton kinetics were normalized to body mass.

Separation into Strides

Ground reaction forces, sampled at a frequency of 500 Hz using an instrumented split-belt treadmill (Bertec, Columbus, Ohio, USA) and low-pass filtered with a cut-off frequency of 60 Hz, were used to detect the swing and stance phases of gait. A threshold of 150 N was used to trigger heel-strike and toe-off. All time-trajectories of interest were separated into strides.

Preference

Preference was measured by asking participants, after exposure to both the Adaptive and Static conditions, which condition they preferred. No comparisons were made to the Zero Torque or Normal Walking conditions.

Statistical Analysis

We compared soleus muscle activity, exoskeleton torque, metabolic rate, and preference across walking conditions. Average trajectories, normalized to percent stride, were generated for each subject. All outcomes were averaged across subjects. Standard deviations represent variations between subjects.

We performed paired t-tests to compare results across the two conditions of interest for a given outcome. We then applied the Holm-Šídák step-down correction for multiple comparisons [48] and used a significance level of $\alpha = 0.05$.

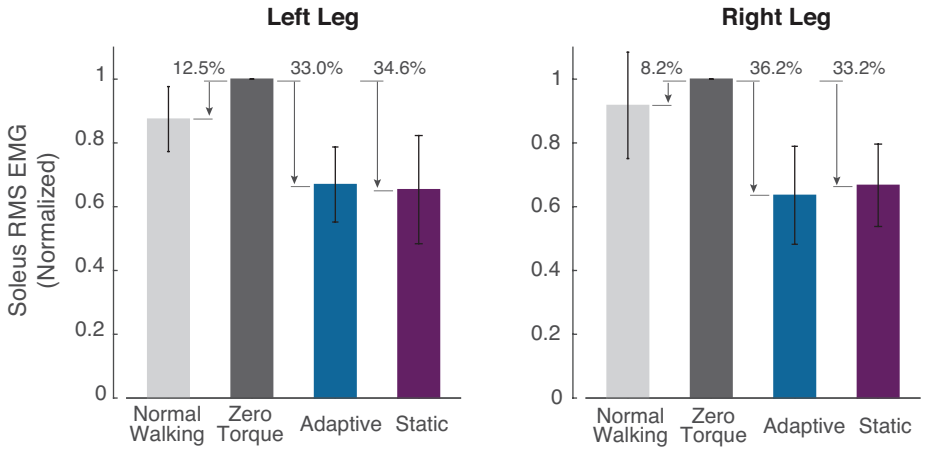

Figure 4.3: Normalized root-mean-square of soleus muscle activity for the left and right legs during walking in the different conditions. Both the Adaptive and Static conditions significantly reduced RMS of soleus muscle activity below the Zero Torque condition.

4.3 Results

The heuristic-based adaptive controller resulted in stable growth of exoskeleton torque and a significant reduction in soleus muscle activity. Although metabolic rate was not directly targeted by the adaptive control scheme, there were substantial reductions in metabolic rate below walking in the Zero Torque condition and below Normal Walking.

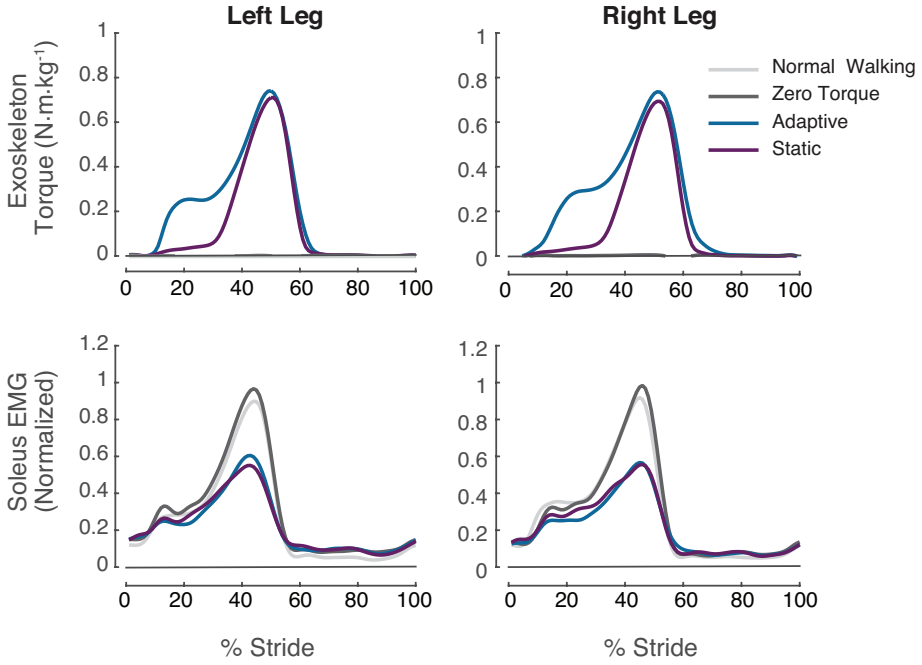

Figure 4.4: Subject-averaged measured exoskeleton torque profiles (*top*) and soleus muscle activity (*bottom*) for the right and left legs during the last three minutes of walking in each condition. Subject-averaged exoskeleton torque profiles for the Adaptive and Static conditions varied substantially during the early part of stance but converged in late stance. Average peak torque across the two conditions was not statistically different. Soleus muscle activity for the left and right legs was significantly reduced by the application of torque in the Adaptive condition, particularly around push-off. Similar reductions in soleus muscle activity were observed in the Static condition.

Soleus Muscle Activity

Soleus muscle activity, particularly during late stance, was significantly reduced when participants walked with the adaptive exoskeleton controller. RMS of soleus muscle activity was 33.0% and 36.2% lower for the left and right legs, respectively, in the Adaptive condition than in the Zero Torque condition ($p = 3 \cdot 10^{-6}$ and $p = 3 \cdot 10^{-6}$, respectively, Fig. 4.3). Peak soleus muscle activity for the left and right legs was reduced by 51% and 67%, respectively, when walking in the Adaptive condition compared to walking in the Zero Torque condition ($p = 3 \cdot 10^{-6}$ and $p = 3 \cdot 10^{-6}$, respectively, Fig. 4.4). RMS of soleus muscle activity in the Static condition was not significantly different from the Adaptive condition ($p = 0.8$ and $p = 0.5$, for the left and right legs, respectively).

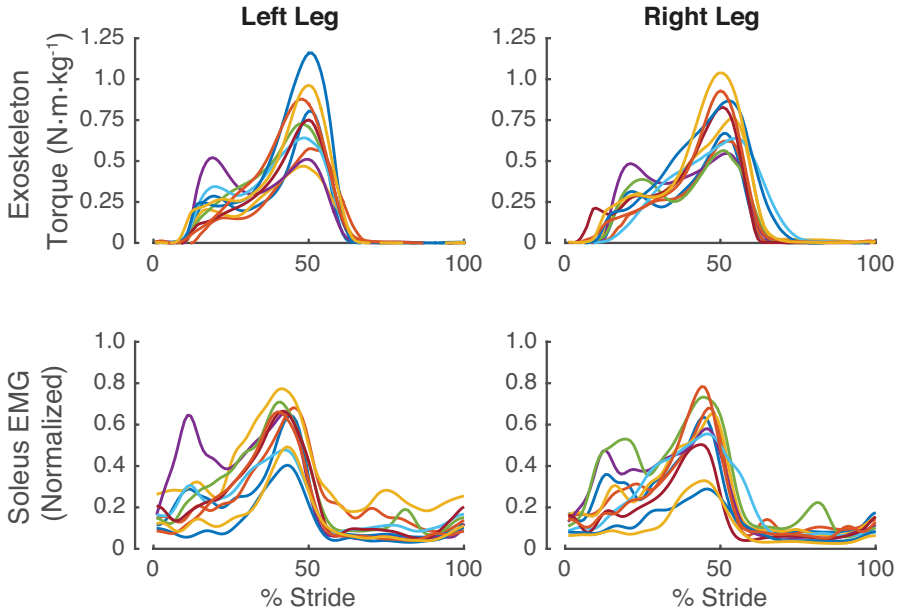

Figure 4.5: Subject-specific exoskeleton torque profiles (*top*) and soleus muscle activity profiles (*bottom*) for the right and left legs during the last three minutes of walking in the Adaptive condition. Exoskeleton torque profiles and patterns of soleus muscle activity varied substantially across participants and across legs.

Exoskeleton-Applied Torque

Exoskeleton torque evolved independently in the Adaptive condition for the left and right legs, resulting in different torque profiles for each leg (Fig. 4.4). Furthermore, exoskeleton torque evolved differently for each participant, as desired exoskeleton torque was dependent on the user's own muscle activity. These features of the control scheme led to a wide range of converged profiles across subjects and across limbs (Fig. 4.5). On average, peak exoskeleton torque was 0.75 $\pm$ 0.21 N·m·kg^{-1} and 0.75 $\pm$ 0.17 N·m·kg^{-1} for the left and right legs. Peak exoskeleton torque varied from 0.50 to 1.16 N·m·kg^{-1} for the left leg and from 0.55 to 1.04 N·m·kg^{-1} for the right leg. Average peak exoskeleton torque was not significantly different between the Static condition and Adaptive condition ($p = 0.7$ and $p = 0.5$ for the left and right legs, respectively). RMS of exoskeleton torque in the Adaptive condition was 31% and 37% higher for the left and right legs, respectively, than RMS of exoskeleton torque in the Static condition ($p = 6 \cdot 10^{-4}$ and $p = 1 \cdot 10^{-4}$, respectively).

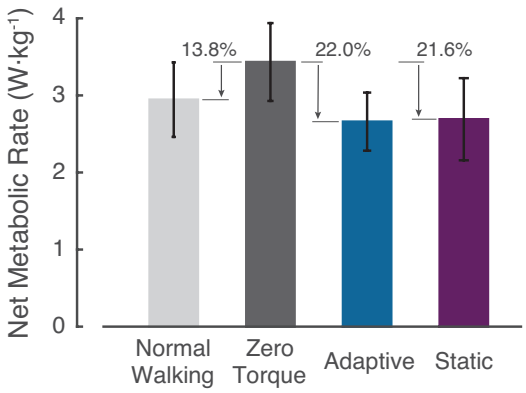

Figure 4.6: Metabolic rate of walking in the different conditions. The heuristic-based adaptive controller significantly reduced metabolic rate below walking in a zero-torque mode. The average metabolic rate of the last three minutes of walking in the Adaptive condition was 22% below that observed during walking in the Zero Torque condition. Similar reductions in metabolic rate were observed during the last three minutes of walking in the Static condition.

Metabolic Rate

The heuristic-based adaptive controller substantially reduced metabolic rate during walking (Fig. 4.6). Metabolic rate decreased from 3.43 ± 0.51 W·kg^{-1} in the Zero Torque condition to 2.66 ± 0.38 W·kg^{-1} in the Adaptive condition, a 22.0% reduction ($p = 1 \cdot 10^{-4}$). Reductions in metabolic rate below the Zero Torque condition ranged from 12.1% to 40.0% across participants. Metabolic rate in the Normal Walking condition was 2.94 ± 0.48 W·kg^{-1}, 13.8% below the Zero Torque condition. Compared to Normal Walking, the Adaptive condition reduced metabolic rate by 9.7%. Metabolic rate during the last three minutes of walking in the Static condition was not significantly different from metabolic during the last three minutes of walking in the Adaptive condition ($p = 0.8$).

Adaptation

Participants responded differently to the Adaptive condition, as demonstrated by the variation in evolved exoskeleton torque profiles, reductions in soleus muscle activity, and reductions in metabolic rate. On average, metabolic rate did not reach steady-state by the end of the 30-minute Adaptive condition, but did by the end of the 30-minute Static

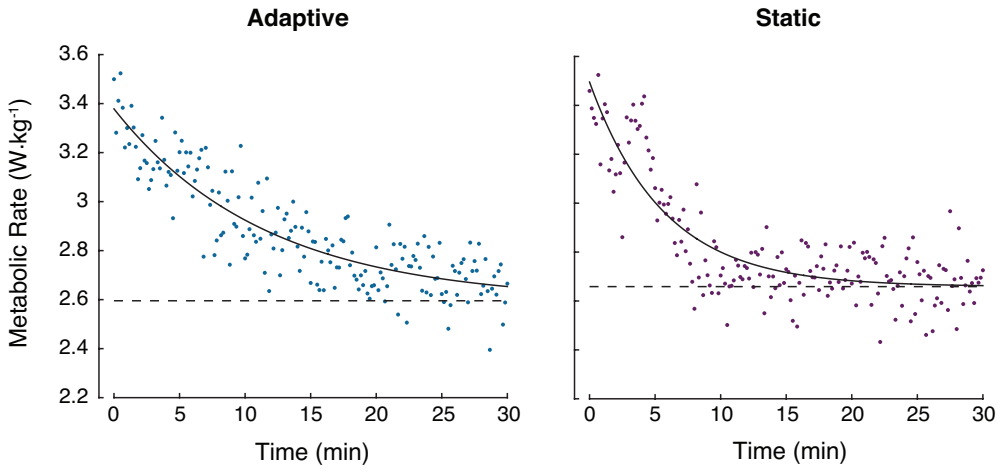

Figure 4.7: Time-series of average metabolic rate and exponential fit. Metabolic rate decreased exponentially over the 30-minute walking trial in the Adaptive condition, but did not, on average, reach steady-state by the end of the trial. In the Static condition, metabolic rate also decreased exponentially but did, on average, reach steady-state by the end of the 30-minute trial.

condition (Fig. 4.7). This, however, varied across participants (see Appendix C, Fig. 4.10).

Stability

On average, desired torque converged to within 5% of the final torque value by the end of the 30-minute Adaptive condition (Fig. 4.11). However, some subjects continued to experience large changes in desired exoskeleton torque even towards the end of the trial.

Preference

Of the 10 participants included in the study, six preferred the Adaptive condition and four preferred the Static condition. No significant correlation was found between preference and controller type, i.e. Adaptive or Static. Preference, however, negatively correlated with the reduction in metabolic rate below Zero Torque ($p = 2 \cdot 10^{-3}$), meaning participants, in general, did not prefer the controller that improved their locomotor efficiency the most.

4.4 Discussion

The novel, heuristic-based, adaptive control strategy that uses soleus muscle activity to adjust the desired exoskeleton torque profile in real time significantly reduced soleus muscle activity, as we expected. Torque from the device partially supplanted the role the soleus muscle plays in plantarflexion, thereby reducing soleus muscle activity in each participant over the 30-minute exposure to the controller. Whole-body metabolic rate was also significantly reduced below that observed during walking with the exoskeletons in a zero-torque mode, even though the controller was not designed to directly affect metabolic rate. Reductions in metabolic rate were comparable to reductions observed when participants walked with a static controller, the average trajectory of which was shown to significantly reduce metabolic rate in another study [130].

The heuristic-based, adaptive control algorithm is dependent on muscle activity measured directly from each participant's legs. Therefore, the desired exoskeleton torque profile evolved independently for the left and right legs and for each participant, resulting in converged assistance profiles that varied widely between legs and across participants. More qualitatively and quantitatively similar torque profiles across legs did not necessarily result in the largest metabolic energy reductions, suggesting that symmetry need not be optimal. Evolved torque profiles with higher peak torque seemed to lead to larger reductions in metabolic rate when compared to the reductions observed with the Static condition.

Exoskeleton torque seemed to grow quickly and reach within 90% of the maximum applied torque within minutes for most subjects (Fig. 4.11). The desired torque profile did not completely stabilize for all subjects within the 30 minutes allotted for walking in the Adaptive condition. The fact that the profiles did stabilize for a subset of participants, however, indicates that this formulation of the controller will not continue to grow unbounded. This is important because initial attempts at controller formulations resulted in unbounded growth of the desired torque profile. Longer trials should be conducted to directly measure the time required for the desired torque profile to reach steady-state for all participants. It is

important to note that small, slow adjustments on the part of the user will continue to affect and change the desired exoskeleton torque curve, if these changes are large enough such that they lie outside the defined deadband.

Metabolic rate dynamics operated on a longer time scale, often taking, on the order of, tens of minutes to stabilize. For several participants, metabolic rate was still decreasing at the end of the 30-minute Adaptive condition (Fig. 4.10). Even in the Static condition, in which the desired torque trajectory was held constant on each walking step, metabolic rate was still decreasing at the end of 30 minutes for some participants, indicating that they had not yet fully adapted to the exoskeleton assistance. This result is in conflict with prior work that suggests that metabolic rate will reach steady-state within 18 minutes of walking when exposed to exoskeletons under static control. Our results suggest that, in order for people to derive the largest benefit from the exoskeleton assistance and for metabolic rate to reach steady-state, longer, continuous exposure to walking with exoskeletons under any type of control scheme may be necessary. Perhaps differences in peak exoskeleton torque or the amount of positive or net work delivered by the exoskeleton affect how long it takes for metabolic rate to reach steady-state. For instance, higher torque and more positive or net work may require a longer adaptation period. The complexity of the controller could also influence how long it takes for participants to adapt. This experiment was not designed to study human adaptation to exoskeleton assistance in depth. How people learn to walk with exoskeletons is still not well understood, and more research is required to understand the mechanisms facilitating motor learning and adaptation.

Given more time to walk with the adaptive controller, all participants, even those whose metabolic rate had reached steady-state within 30 minutes, could potentially derive further benefit by reducing muscle activity more and consequently inducing an increase in exoskeleton torque. Participants may be trapped in a local minimum and, with more time, could discover a different, more beneficial, equilibrium point. We do not, however, know if this will happen in practice as we have not tested participants walking with this controller for longer than 30 minutes. These longer-term adaptations may not be possible with a static

controller because further reductions in muscle activity will not induce a change in the torque provided by the exoskeleton.

Other electromyography-driven approaches have not been able to achieve as substantial of reductions in soleus muscle activity and metabolic rate within 30 minutes of exposure to walking with exoskeletons. Traditional proportional myoeletric control (pEMG) found a 26% reduction in RMS of soleus muscle activity and no significant reduction in metabolic rate after one 30-minute walking session, compared to walking with the exoskeletons in a zero-torque mode [105]. After three consecutive, 30-minute sessions of walking with the exoskeletons under pEMG control, RMS of soleus muscle activity and metabolic rate were reduced by approximately 28% and 10%, respectively. An updated version of pEMG that uses an adaptive gain was able to reduce RMS of soleus muscle activity by 20.3% and metabolic rate by approximately 16% after one 30-minute walking session, compared to walking with the exoskeletons unpowered [66]. An additional 60 minutes of exposure to the adaptive, pEMG controller, over two separate 30-minute walking trials, actually resulted in less reduction of the RMS of soleus muscle activity (10.8%) compared to the zero-torque condition, and only reduced metabolic rate by another 2%.

Models of individual muscle metabolic energy consumption estimate that the ankle plantarflexor muscles consume about 27% of the metabolic energy expended during a gait cycle. Due to the fact that the RMS of soleus muscle activity was only reduced by 34.6%, on average, these reductions alone do not explain the 22.0% reduction in metabolic rate. Metabolic energy consumed by other muscles in the lower-limbs was also likely reduced and could account for the significant reductions in whole-body metabolic energy consumption we observed. Other studies have found reductions in lateral and medial gastrocnemius muscle activity, as well as knee extensor muscle activity, in participants walking with ankle exoskeleton assistance [47, 66].

Participants did not always prefer the heuristic-based adaptive controller compared to the static controller, counter to our original hypothesis. Due to the fact that the adaptive controller measures and responds to changes in the user online, we expected individuals to

overwhelmingly prefer it over the static controller, but preference was found to be evenly split between the two controller types. Preference was, however, negatively correlated with reductions in metabolic rate below the Zero Torque condition. This suggests that locomotor economy is not the only driving factor for preference, at least not on a time scale of 30 minutes. Perhaps given additional exposure to the exoskeleton assistance, preference would have positively correlated with measured reductions in metabolic rate. Preference also appeared to be negatively correlated with peak exoskeleton torque during the push-off phase of gait. This suggests that higher torque late in stance (i.e. more work) may be uncomfortable for subjects. Limits on allowable peak exoskeleton torque (or peak ankle plantarflexion angle) might help assuage this discomfort. Better contact with the user through improved mechanical design of these devices might also help resolve this issue.

The fact that the static controller was capable of achieving equivalent reductions in soleus muscle activity and whole-body metabolic rate as compared to the adaptive controller was surprising. This result suggests that static controllers with good initial guesses for torque trajectories can achieve impressive improvements in locomotor efficiency, and do so more simply. However, such controllers rely upon defining, or at least parameterizing, a "beneficial" exoskeleton torque profile, and this parameterization is not necessarily straightforward.

The heuristic-based adaptive controller has several features that make it a desirable assistance strategy. First, it is not dependent on a parameterization of the exoskeleton assistance space and is capable of generating any pattern of torque suggested by the measured muscle activity. Therefore, the algorithm can be translated easily to the other lower-limb joints without having to reparameterize the space of exoskeleton assistance. For instance, muscle activity measured from the rectus femoris (knee extensor) could be used to define the desired torque profile of an exoskeleton designed to assist with knee extension. One of the big benefits of this approach might be to discover a good pattern of assistance for new devices.

Secondly, since this algorithm makes control decisions at every time step, adding control

over exoskeleton assistance applied to a second joint is equivalent to adding one computation at every time step. Therefore, this control approach will likely scale well to multiple joints, providing the framework for the control of a full lower-limb exoskeleton during walking. The time it takes for the desired exoskeleton torque profiles to reach steady-state for each joint, may, however, increase with each added joint due to the ways in which users adapt to the intervention.

It is possible that the current formulation of the heuristic-based adaptive controller is not optimized and a slightly altered formulation could result in even better outcomes. More work could be carried out to ensure that the stabilized trajectory is comfortable for all subjects. When walking with the adaptive controller, those participants that exhibited smaller ankle angle deviations often experienced higher (mass-normalized) peak exoskeleton torque. An additional torque-stabilizing term that accounts for excessively large peak plantarflexion angles could help prevent convergence to uncomfortable exoskeleton torque profiles. Zero-phase filtering of the desired exoskeleton torque trajectory on every walking step could help smooth the profile. Averaging certain contributions to desired exoskeleton torque over multiple walking steps, such as the average of soleus muscle activity $EMG_{\mathrm{SOL,AVG}}(n)$ or the average deviation in dorsiflexion ankle angle $e_{\theta_{\mathrm{a,AVG}}}(n)$, could allow for more gradual step-to-step changes in the exoskeleton torque profile. Such changes may elicit a more beneficial interaction between the device and the user.

Although this control approach appears to work well for able-bodied individuals, it likely will not be effective for populations with altered muscle activity, such as post-stroke individuals or amputees. The elderly, who have normal patterns of muscle activity, but weakened muscular strength, could, however, greatly benefit from this form of assistance.

4.5 Conclusions

We conducted a study to test whether a novel, heuristic-based, adaptive ankle exoskeleton assistance strategy would reduce soleus muscle activity and whole-body metabolic rate during

walking in naïve exoskeleton users. Soleus muscle activity, measured online, was used to adjust the desired exoskeleton torque profile on the subsequent walking step. This assistance strategy substantially reduced soleus muscle activity and whole-body metabolic rate in all participants below that measured during walking with the exoskeletons in a zero-torque mode. The evolved exoskeleton torque profiles varied significantly between right and left legs and across participants, indicating the ability of this control approach to produce subject-specific, and even leg-specific, assistance patterns. Longer continuous exposure to this control approach could result in even greater benefits, as suggested by the fact that metabolic rate had not reached steady-state for some participants after 30 minutes of walking.

The foundation upon which this control approach is formulated makes it easily transferable to the knee and hip joints, and scalable to multiple joints, such that it could be used to provide complete lower-limb assistance during walking. We expect that 'human-in-the-loop' control techniques, such as the one presented here, will allow for the discovery of new, more beneficial assistance strategies that can be extended to a wide range of devices and populations.

Acknowledgments

This material is based upon work supported by Panasonic Corporation under Grant No. A018293. The author thanks Cecilia Morales and Thu Nguyen for help piloting and conducting experiments.

4.6 Appendix A: Subject-wise Metabolic Rate

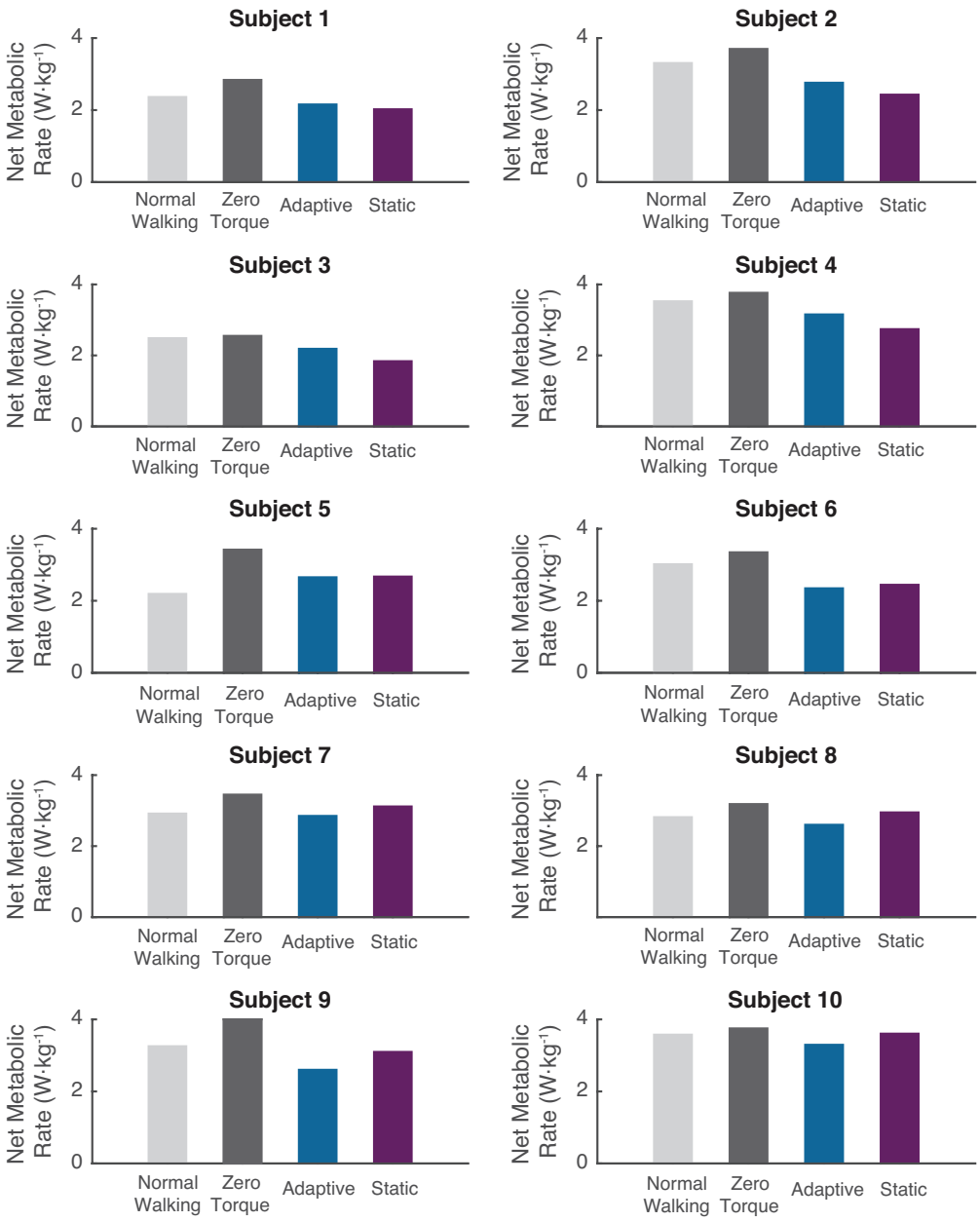

Figure 4.8: Subject-specific net metabolic rate for the different walking conditions. All participants experienced a substantial reduction in metabolic rate below the Zero Torque condition when walking with the heuristic-based adaptive controller. The Static controller was able to provide an equally good, if not better, benefit for some subjects but not all.

4.7 Appendix B: Exoskeleton Work

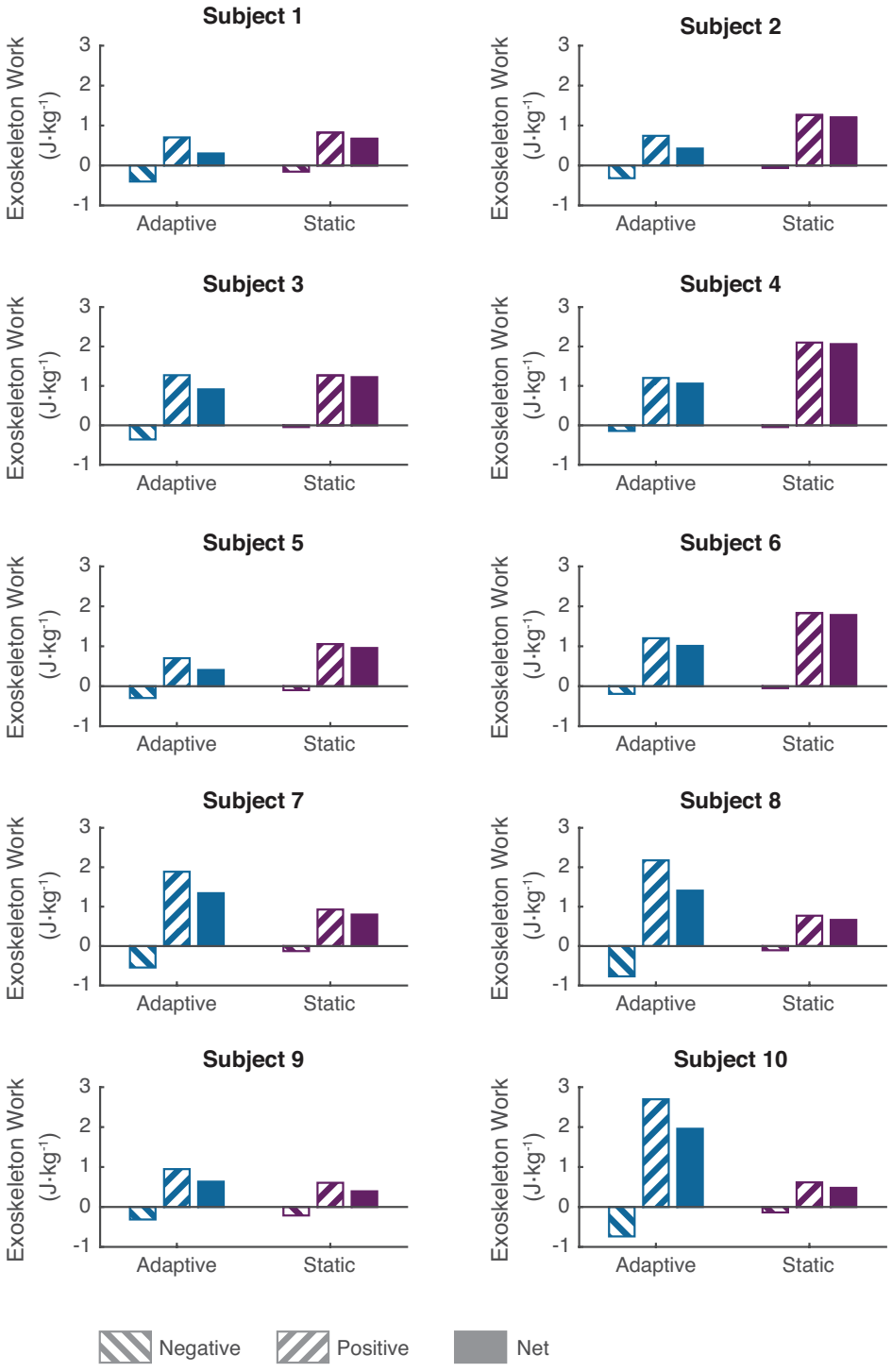

Figure 4.9: Negative, positive, and net exoskeleton work provided to each subject in the Adaptive and Static conditions. There were large variations in negative, positive, and net work delivered by the device across control strategies and across subjects.

4.8 Appendix C: Metabolic Rate Exponential Fits

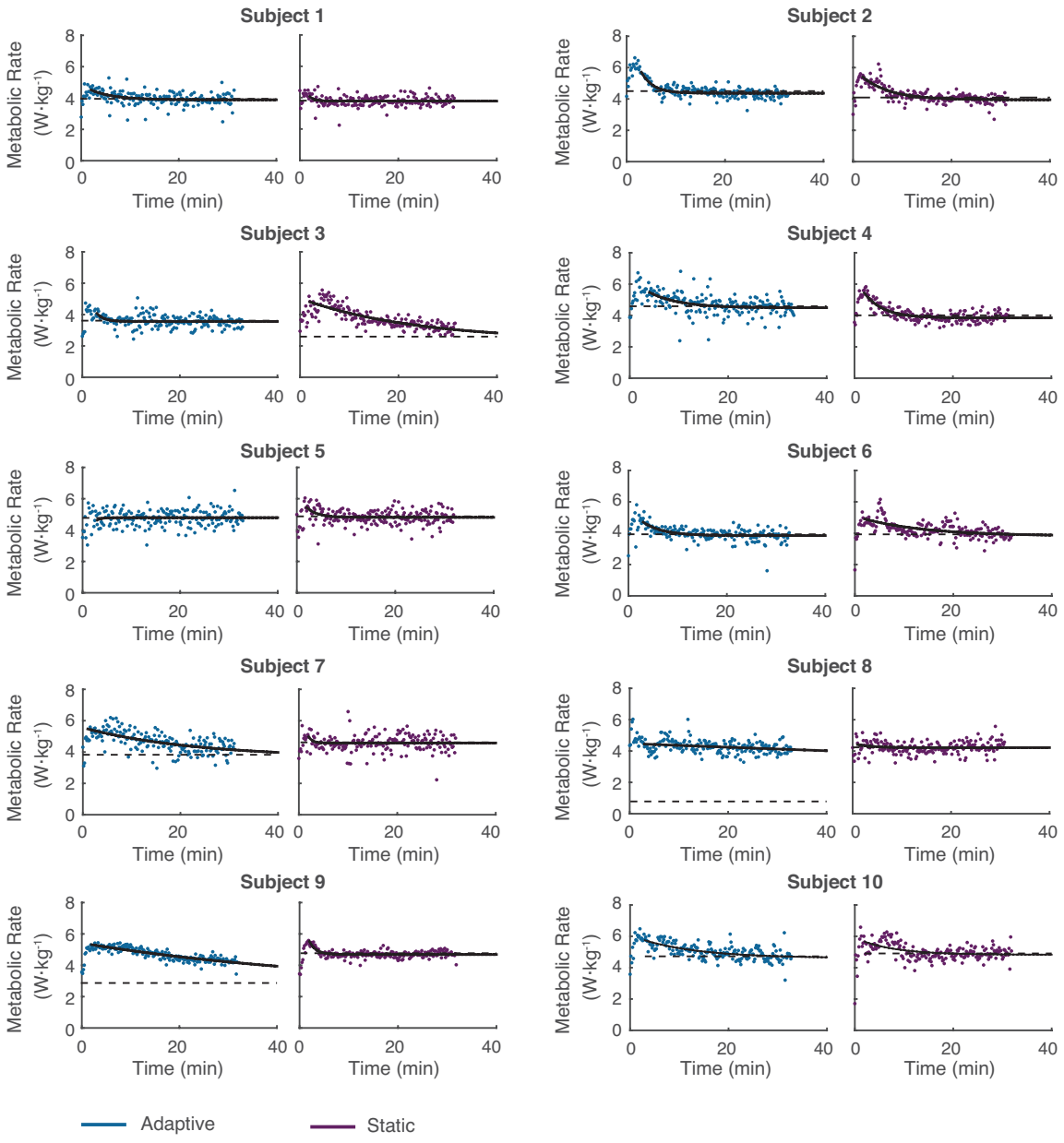

Figure 4.10: Exponential fits to time-series metabolic rate data for each subject walking in the Adaptive (blue) and Static (purple) conditions. Dots represent raw metabolic rate data. Solid lines are an exponential fit to the raw time-series data. Dashed black line is the steady-state metabolic rate approximated by the fit. Time-series metabolic data varied widely across control strategies and across subjects. Even after thirty minutes of walking, the metabolic rate for some participants had not converged to steady-state. This was true even for some participants walking in the Static condition.

4.9 Appendix D: Controller Stability

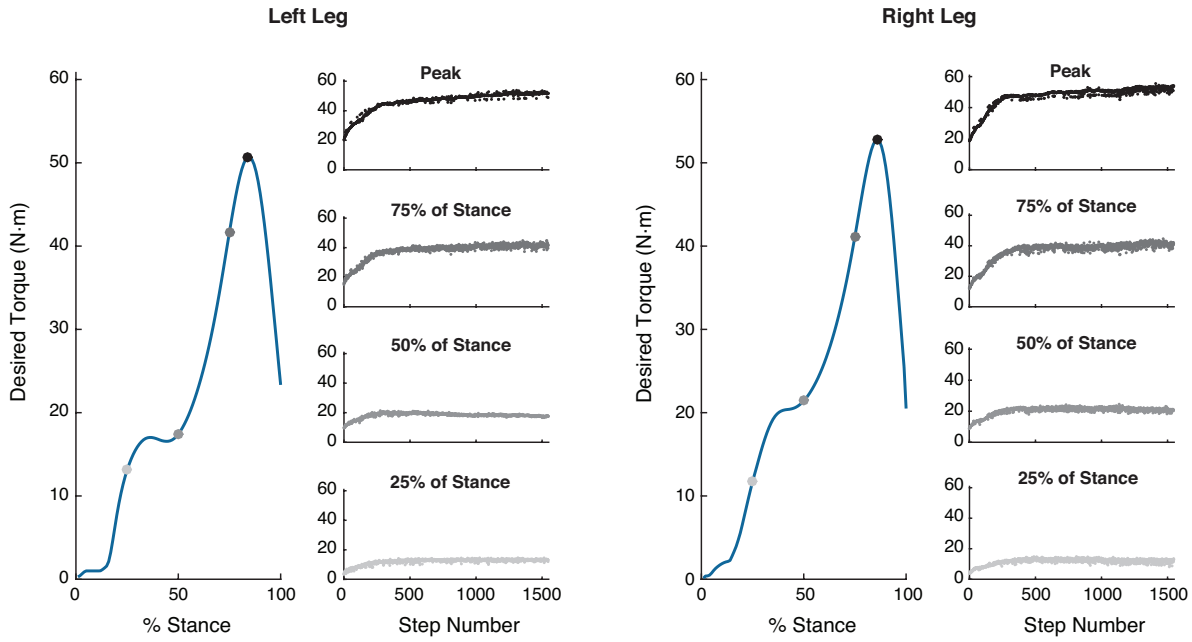

Figure 4.11: Depiction of stabilization of desired exoskeleton torque profile over time averaged across subjects for the left and right legs. The blue trajectory represents the desired exoskeleton torque, as a percent of stance, for the last walking stride of the Adaptive condition. The dots on the trajectory indicate torque at 25% of stance, 50% of stance, 75% of stance, and, lastly, peak torque. The subplots show the evolution of each of these dots over time, as a function of step number. Each portion of the desired torque profile reaches within 90% of the final value quickly, indicating a relatively fast convergence.

Chapter 5

Characterizing the relationship between step-length asymmetry and metabolic rate during locomotion in post-stroke individuals [††]

Abstract

Many stroke survivors exhibit spatial asymmetry during walking, but little work has been done to understand what mechanisms are driving this asymmetry. Research has shown that able-bodied individuals adopt gait characteristics that minimize metabolic rate– perhaps similar least-effort strategies are driving gait asymmetry in post-stroke individuals. We designed and conducted an experiment to characterize the relationship between step-length asymmetry and metabolic rate during walking in stroke survivors. Five post-stroke individuals walked on a treadmill at a subject-specific speed while targeting three different step-length asymmetries: 1) baseline asymmetry, 2) zero asymmetry, and 3) exaggerated

[††]A manuscript presenting this work is in preparation: Jackson, R. W., Nguyen, T. M., Aucie, Y., De Kam, D., Torres-Oviedo, G., and Collins, S. H. (2017). Characterizing the relationship between step-length asymmetry and metabolic rate during locomotion in post-stroke individuals, *Neurorehabil Neural Repair*, **in preparation**.

asymmetry. We used visual feedback to try to enforce each step-length asymmetry. We measured metabolic rate and step-length asymmetry in each of the three conditions. Averaging results across participants, we found no significant difference in metabolic rate between the baseline step-length asymmetry condition and the zero step-length asymmetry condition. Many potentially confounding factors, such as motivation, fatigue, and learning in the participants, make it difficult to say whether step-length asymmetry affected metabolic rate. Testing more individuals is necessary to be able to observe any statistically significant differences. We expect the results from such a study to provide clinicians with a deeper understanding of gait asymmetry in post-stroke individuals and to guide the design of robotic rehabilitation strategies.

Keywords: stroke, step-length asymmetry, least-effort strategies, gait, rehabilitation

5.1 Introduction

Every year more than 600,000 Americans experience a stroke for the first time [10]. Individuals with chronic stroke often suffer from a number of gait impairments and higher metabolic energy consumption during walking compared to their able-bodied counterparts, resulting in reduced mobility, functionality, and overall quality of life [22, 35, 65, 87, 91, 125]. One of the major gait deficits prevalent among individuals with chronic stroke is spatial gait asymmetry [88], in which there is a difference in the step lengths of the paretic and non-paretic legs. Improving symmetry in post-stroke individuals, in order to promote greater function and mobility, is a major goal of clinicians.

Recently, a significant amount of effort has been put towards developing gait rehabilitation techniques that target step-length asymmetry. Split-belt treadmill training was developed to exaggerate an individual's asymmetry by moving the two treadmill belts at different speeds, such that the nervous system might learn to correct for the error and improve gait symmetry [93, 94]. Unilateral step training, which required post-stroke individuals to repeatedly step with their unaffected limb on a treadmill while their affected limb remained stationary off

the treadmill, was designed to reduce step-length asymmetry [63]. Other researchers have tried improving step-length asymmetry by providing visual and proprioceptive feedback to post-stroke individuals [69]. Although these rehabilitation techniques have shown promise for improving step-length asymmetry, especially compared to traditional treadmill exercise [89, 92, 2], it may help to better understand the mechanisms driving step-length asymmetry before trying to correct for it.

Little work has been done to understand why post-stroke individuals choose to walk with an asymmetric gait. Many post-stroke individuals are able to modulate their step lengths with biofeedback such that they can walk with spatial symmetry [83], yet when allowed to walk freely they adopt an asymmetric gait. Without understanding the reasons for the observed coordination pattern, it is difficult to know how to best provide locomotor rehabilitation and assistance.

Perhaps post-stroke individuals adopt a spatially asymmetric gait because it requires the least amount of effort. It has been shown that able-bodied individuals choose to walk with gait parameters, including speed, step length, and step width, that minimize metabolic energy consumption [126, 36]. Since post-stroke individuals exhibit physical asymmetries, such as weakness or spasticity of the paretic-leg plantarflexor muscles and, consequently, reduced paretic-leg push-off [85, 14, 3, 99], a spatially asymmetric gait may be metabolically optimal. Underlying locomotor control observed in post-stroke individuals is, however, quantitatively and qualitatively different from that observed in able-bodied individuals and may not be driven by least-effort strategies. Other factors, such as the neurological injury caused by stroke, may contribute more significantly to adopted coordination strategies than metabolic energy economy in this population.

The purpose of this study was to characterize the relationship between step-length asymmetry and whole-body metabolic rate during walking in post-stroke individuals. We used visual feedback to enforce different step-length asymmetries and measured the resulting metabolic rate. We hypothesized that post-stroke individuals would consume the least amount of metabolic energy when walking at their self-selected step-length asymmetry and

Table 5.1: Clinical Characteristics of Post-Stroke Individuals

	Gender	Age	Paretic Limb	Step-Length Asymmetry (%)	Overground Speed ($m \cdot s^{-1}$)	Selected Treadmill Speed ($m \cdot s^{-1}$)	Fugl-Meyer
Subject 1	M	61	R	9.2	0.96	0.96	32
Subject 2	F	67	R	23.8	0.86	0.35	21
Subject 3	M	52	R	7.4	0.83	0.43	31
Subject 4	M	53	R	9.9	0.84	0.41	17
Subject 5	M	46	R	9.6	1.74	1.2	32

that metabolic energy consumption would increase when they walked with any asymmetry different than baseline, including zero asymmetry. We expect the results from this study to deepen our understanding of the mechanisms driving gait asymmetry in post-stroke individuals and to influence the development of new rehabilitation techniques.

5.2 Materials and Methods

We conducted an experiment in which we measured and compared the metabolic cost of walking with different enforced step-length asymmetries in post-stroke individuals.

Participants

Five post-stroke individuals (N = 5, 4 men and 1 woman; age = 55.8 ± 8.2 yrs; body mass = 92.5 ± 24.5 kg; height = 1.79 ± 0.15 m; Table 5.1) participated in the study. All participants were chronic stroke survivors (>6 months). To be included in the study, each participant had to meet the following set of criteria: 1) is capable of walking unassisted (excluding ankle-foot orthoses), 2) has suffered only one previous stroke, 3) has no neurological issues, 4) is able to modulate step-length asymmetry, and 5) exhibits clinically significant step-length asymmetry (>4%). All subjects provided written informed consent before completing the protocol. The experimental protocol was approved by the University of Pittsburgh Institutional Review Board.

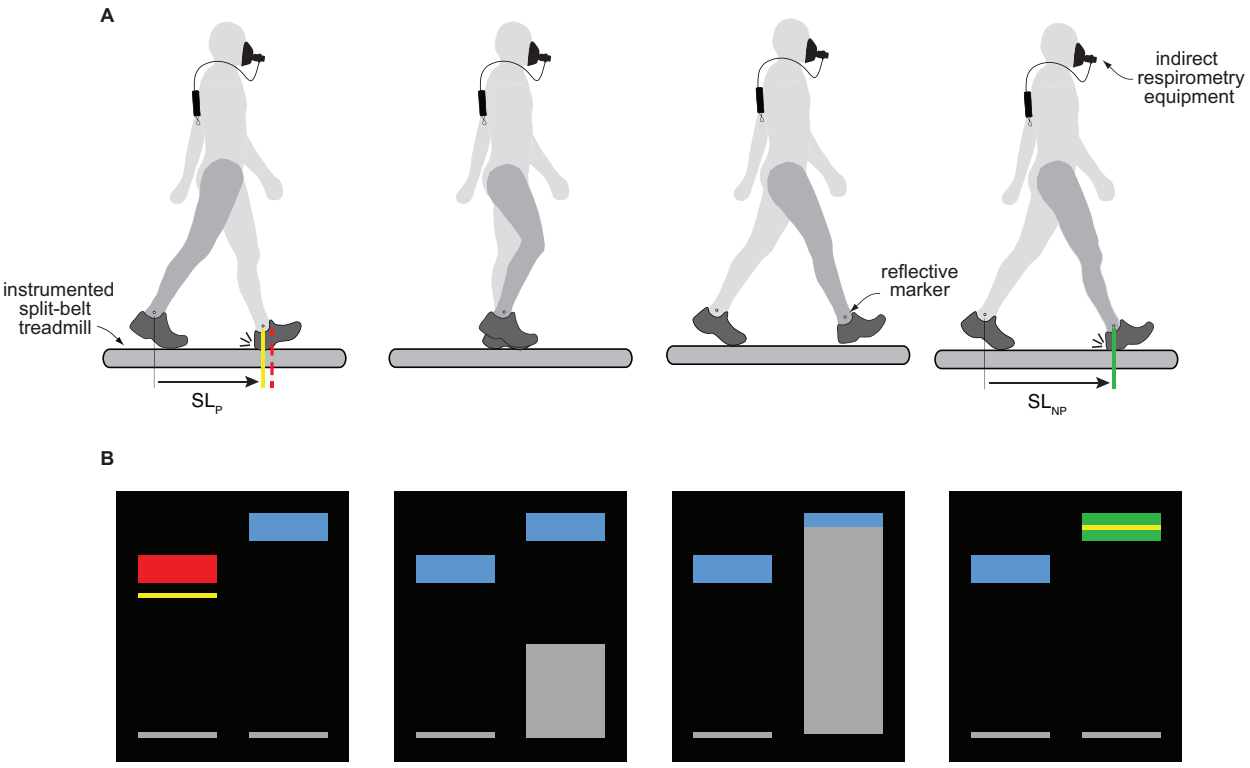

Figure 5.1: Experimental set-up and illustration of step-length asymmetry visual feedback. **A.** Schematic depicting a participant targeting different step-length asymmetries while we measured whole-body metabolic rate. **B.** Illustration of the visual feedback displayed to participants on a computer monitor at the front of the treadmill during walking under the different step-length asymmetry conditions. Blue boxes represent target step lengths of the paretic and non-paretic legs. Gray bars represent the current location of the ankle joint of one leg relative to the other. The yellow line indicates the measured location of the respective ankle joint at heel strike. If the participant overshoots or undershoots, the target turns red and the yellow line indicates the direction and magnitude of the error. If the participant hits the target, the target turns green and the yellow line indicates where within the target the participant's heel strike was.

Visual Feedback

Step-length asymmetry was enforced using visual feedback (Fig. 5.1). Step-length asymmetry was calculated in real time by measuring the relative locations of the participant's paretic and non-paretic leg ankle joints at heel strike. Ankle joint locations were measured using motion capture markers placed on the lateral malleolus of each leg and heel strike was detected by measuring ground reaction forces with an instrumented treadmill. Participants were provided with a visual representation of target step lengths and measured step lengths and were tasked with hitting the targets. The virtual targets were adjusted for each of the different step-length asymmetries tested.

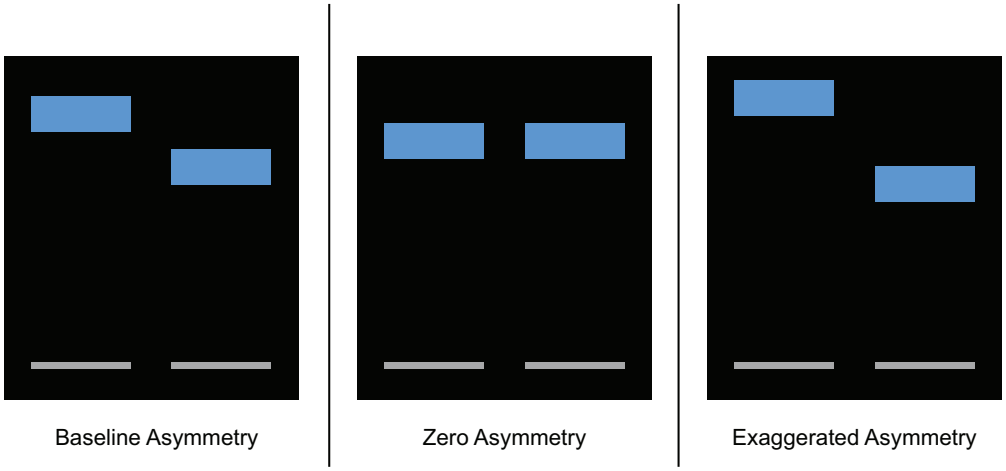

Figure 5.2: Illustration of target step lengths for the three visual feedback conditions. *From left to right:* Target paretic and non-paretic leg step lengths for the Baseline Asymmetry condition, Zero Asymmetry condition, and Exaggerated Asymmetry condition.

Experimental Protocol

We measured the metabolic rate of post-stroke individuals during walking with three different step-length asymmetries, referred to here as Baseline Asymmetry, Zero Asymmetry, and Exaggerated Asymmetry (Fig. 5.2). In the Baseline Asymmetry condition, participants targeted their baseline step-length asymmetry, measured prior to the start of the experiments. In the Zero Asymmetry condition, participants targeted zero step-length asymmetry, or, equivalently, symmetric step lengths. In the Exaggerated Asymmetry condition, participants targeted twice their baseline step-length asymmetry.

All participants were given one to two days of training before we conducted the full experiment. The full experiment consisted of the following protocol. Prior to walking in the step-length asymmetry conditions, participants first completed a quiet standing condition for four minutes to obtain basal metabolic rate. Next, participants walked on a treadmill for six minutes with no visual feedback, referred to here as Baseline No VF, to obtain baseline step-length asymmetry and metabolic rate. Participants were then exposed to walking in each of the different step-length asymmetry conditions for two minutes in order to become familiar with the task.

Participants then completed the Baseline Asymmetry, Zero Asymmetry, and Exagger-

ated Asymmetry conditions. Participants walked for six minutes in each condition and were given a rest period between each six-minute walking bout. The presentation of the step-length asymmetry conditions was randomized and the first condition was repeated at the end to mitigate learning effects. Results from only the last presentation of the repeated condition are used in our analyses and included in the main text. All walking conditions were completed at a treadmill speed selected for each individual to be able to sustain the task. A detailed description of how this speed was selected is provided in the next section.

Treadmill Speed Selection

We selected a treadmill speed that enabled participants to sustain the challenging locomotor task for six minutes while maintaining three criteria: participant must stay outside of the anaerobic regime, not exceed 90% of their maximum heart rate, and not hold on to the handrail. Treadmill speed was selected on the day each participant started the study. This speed was used across the remainder of the training and testing days. Treadmill speed was selected using the following protocol.

Participants first completed a six-minute walk test over ground to determine their averaged maximum speed. Participants were then given a brief treadmill familiarization period. The treadmill speed was initially set to 25% of their over-ground speed, then incrementally increased to 50%, 60%, 70%, 80%, 90%, and 100% of their over-ground speed. Each speed was held for about one minute. At each speed, participants were asked whether this speed was "better" or "worse" than the previous speed.

After the treadmill familiarization, participants completed a nine-minute speed selection task. Over the first three minutes, participants walked on the treadmill at 25% of their over-ground speed to obtain baseline heart rate and respiratory exchange ratio (RER) data. Over the next three minutes, the speed of the treadmill slowly increased from 25% of their over-ground speed to 100% of their over-ground speed. Over the final three minutes, the treadmill speed was held constant at 100% of their over-ground speed. If at any point during the nine-minute trial RER crossed 1.1, heart rate crossed 90% of the maximum, or

participants could not sustain walking without holding the handrail, the trial was stopped and calculations were performed up to that point.

Treadmill speed was determined using the data collected during the nine-minute trial (Fig. 5.3). Baseline metabolic rate and RER data were taken as the average from minute two to minute three of the trial. Although treadmill speed started increasing at minute three, measured metabolic rate did not change instantaneously due to delays in metabolic processes and in measurement equipment. To approximate this delay, we determined the time at which a linear regression, fit to the metabolic rate data from minute four to minute six, crossed below the baseline metabolic rate, and then subtracted three minutes from this detected time (Fig. 5.3A). Given the general behavior of RER during tasks that increase in strenuousness over time, we fit an exponential curve to the RER data from minute three to the end of the trial (Fig. 5.3B). Similarly, we fit a linear regression to heart rate data from minute three to minute six (Fig. 5.3C). We calculated the time when the exponential fit to the RER data crossed above 5% of baseline RER or an absolute value of 0.87. We also calculated when the linear fit to the heart rate data crossed 78% of maximum. We took the earlier of those two times, then subtracted the calculated time delay. We then found the treadmill speed that corresponded to this time (Fig. 5.3D), reduced the speed by 25%, and selected this as the treadmill speed for the remainder of the conditions.

Training

Participants were provided with one to two days of training, prior to the full experiment, intended to help them learn to modulate their step lengths using our visual feedback system The number of training days depended on how quickly each participant learned the task. A brief, instructional slide-show presentation was given to participants explaining the task. Participants were then given two minutes of walking while targeting their baseline asymmetry to help translate this initial instruction into the actual task. Participants then walked for six minutes while targeting each of the different step-length asymmetries. Participants were encouraged to ask questions throughout the entire training session. Verbal reinforcement

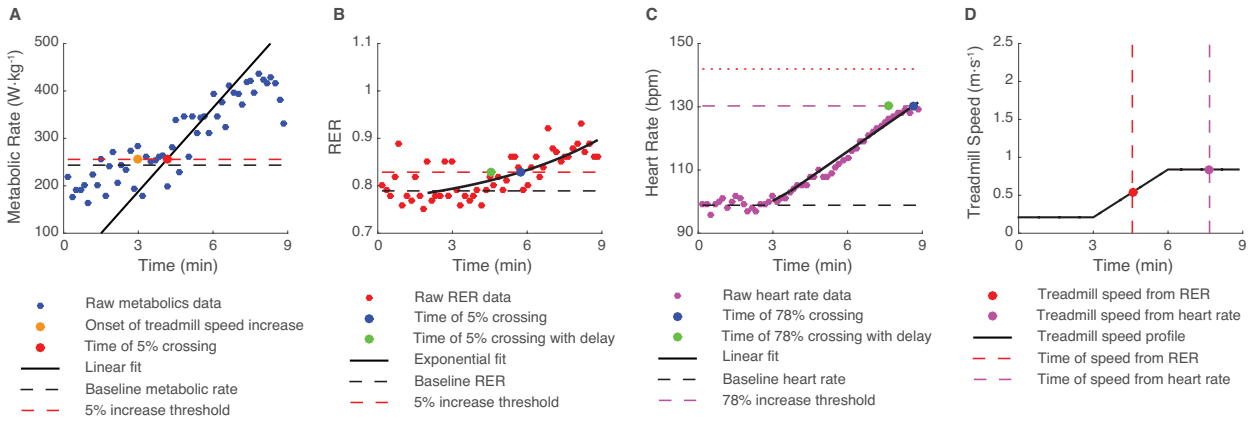

Figure 5.3: Sample data used to determine treadmill speed. **A.** Metabolic rate data over the nine-minute trial with a linear fit and 5% increase threshold used to calculate the delay. **B.** RER data over the nine-minute trial with an exponential fit and 5% increase threshold. **C.** Heart rate data over the nine-minute trial with a linear fit and a threshold at 78% of age-determined maximum heart rate. **D.** Treadmill speed profile and the speed selected based on upon both RER (red) and heart rate (pink) criteria.

and coaching were provided to the participants to help facilitate learning.

Measured Outcomes

Metabolic Rate

Metabolic rate was calculated by substituting the volumetric rates of oxygen consumption and carbon dioxide expulsion into a widely-used equation [16]. Volumetric flow rates were measured using a mobile metabolics cart (Oxycon Mobile). Measurements were acquired each breath and averaged into ten-second bins. We averaged the metabolic rate of the last three minutes of each six-minute walking condition. Net metabolic rate was calculated by subtracting the metabolic rate measured during quiet standing from each walking condition. Change in metabolic rate was calculated by subtracting the metabolic rate measured during the Baseline No VF condition from each walking condition, unless otherwise specified. Metabolic rate was normalized to body mass for each participant.

Step-Length Asymmetry

Step-length asymmetry was defined as:

$$SLA = \frac{SL_{\mathrm{P}} - SL_{\mathrm{NP}}}{SL_{\mathrm{P}} + SL_{\mathrm{NP}}} \cdot 100\% \tag{5.1}$$

where SLA is step-length asymmetry, SL_{P} is the step length of the paretic leg, and SL_{NP} is the step length of the non-paretic leg. Paretic and non-paretic leg step lengths were measured using motion capture (Vicon Motion Systems, Oxford UK). Reflective markers placed on the lateral malleolus of each ankle were sampled at 100 Hz. Step length of the leading leg was defined as the difference between the ankle markers of the leading leg and the trailing leg at the respective heel strikes. Step-length asymmetry was averaged over the last three minutes of each six-minute walking condition. Normalized step-length asymmetries were computed by dividing average step-length asymmetry in each condition by the average step-length asymmetry measured in the Baseline No VF condition, unless otherwise specified.

Accuracy

Accuracy was defined as the number of targets a participant successfully hit divided by the maximum number of targets that could have been hit for a given condition. Accuracy was calculated for the last three minutes of walking in the different step-length asymmetry conditions for each leg, then averaged across legs.

Statistical Analysis

We compared metabolic rate, step-length asymmetry, and accuracy across all walking conditions with visual feedback. All outcomes were averaged across subjects. Standard deviations represent variations between subjects.

We performed paired t-tests to compare results across the two conditions of interest for a given outcome. We used a significance level of $\alpha = 0.05$.

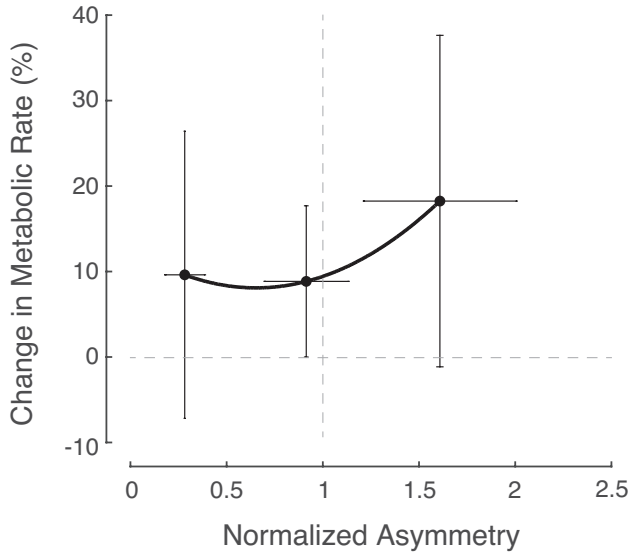

Figure 5.4: Percent change in metabolic rate versus step-length asymmetry relative to baseline. Circles represent subject-average change in metabolic rate across different measured step-length asymmetries. Vertical and horizontal solid black lines represent standard deviations in metabolic rate and step-length asymmetry, respectively, across subjects. Solid blue line represents a quadratic fit to the cost landscape.

5.3 Results

No statistically significant relationship was found between metabolic rate and step-length asymmetry in the five post-stroke individuals that completed the protocol. Participants were, however, able to significantly modulate their step-length asymmetries across the different conditions.

Metabolic Rate vs. Step-Length Asymmetry

On average, there was no statistically significant variation in metabolic rate across the different asymmetry conditions (Fig. 5.7). Metabolic rate was 2.53 ± 0.77 W·kg^{-1} in the Baseline Asymmetry condition and 2.56 ± 0.86 W·kg^{-1} in the Zero Asymmetry condition, which was equivalent to a 0.3% difference ($p = 0.8$). Metabolic rate was higher in the Exaggerated Asymmetry condition than in the Baseline Asymmetry condition for four out of five participants. Metabolic rate was 2.76 ± 0.96 W·kg^{-1} in the Exaggerated Asymmetry condition, 8.2% higher than in the Baseline Asymmetry condition, though this result was not statistically significant ($p = 0.2$).

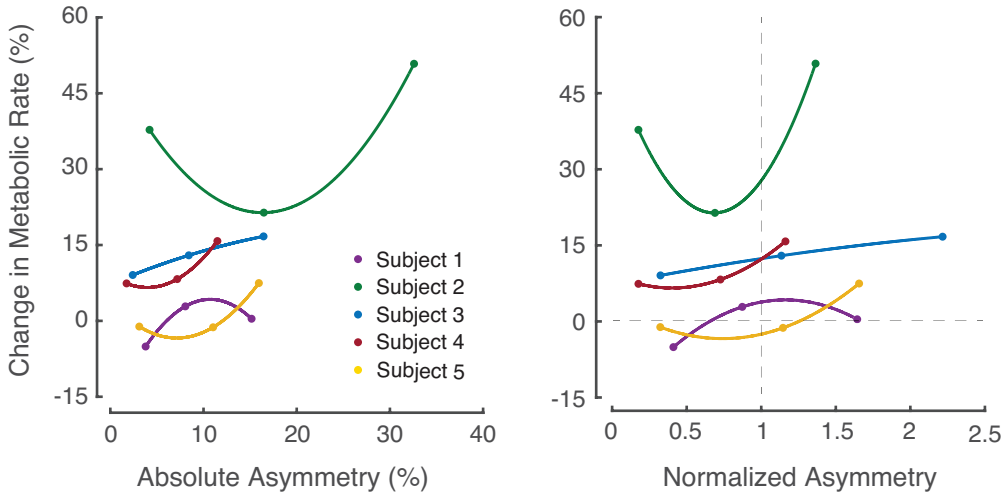

Figure 5.5: Percent change in metabolic rate versus step-length asymmetry for individual participants. *Left:* Percent change in metabolic rate versus absolute asymmetry (%). *Right:* Percent change in metabolic rate versus asymmetry normalized to Baseline No VF. Each color represents a different participant. Each dot represent a measured point in metabolic rate versus asymmetry space. Lines are quadratric fits to the three measured points for each participant.

The relationship between metabolic rate and step-length asymmetry varied widely across participants (Fig. 5.5). Subject 1 exhibited a cost landscape with the minimum occurring at the baseline asymmetry value and increasing as asymmetry moved away from baseline in either direction. Subjects 2, 3, and 5 showed no significant variation in metabolic rate across any of the three conditions. The profile of Subject 4 showed the opposite trend from the proposed hypothesis, with metabolic rate at a maximum in the Baseline Asymmetry condition, and decreasing as asymmetry moved away from baseline. Differences in metabolic rate across conditions for this subject were not outside the range of noise in metabolic measurements and, therefore, may not be indicative of any real interaction between step-length asymmetry and metabolic rate.

Step-Length Asymmetry

Baseline step-length asymmetry, measured during walking with no visual feedback, varied across the five post-stroke individuals (Table 5.1). Baseline step-length asymmetry ranged from 7.4% to 23.8%, with an average of 12.0 $\pm$ 6.7%.

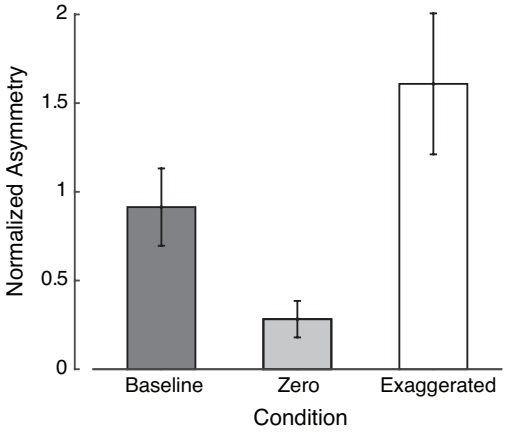

Figure 5.6: Average step-length asymmetry across conditions. Bars represent subject-averaged means and whiskers represent standard deviations.

Step Length Modulation

The five post-stroke individuals included in the study were capable of modulating their step lengths such that there was a significant difference in step-length asymmetry across the three conditions. On average, participants walked with 10.2 ± 3.8% step-length asymmetry in the Baseline Asymmetry condition, 3.0 ± 1.0% step-length asymmetry in the Zero Asymmetry condition, and 18.3 ± 8.2% asymmetry in the Exaggerated Asymmetry condition. Measured step-length asymmetry in the Zero Asymmetry condition and Exaggerated Asymmetry condition was significantly different from measured step-length asymmetry in the Baseline Asymmetry condition ($p = 7{\cdot}10^{-3}$ and $p = 0.02$, respectively, Fig. 5.6).

Accuracy

Accuracy in hitting the targets varied significantly across conditions and across participants. On average, participants hit the targets in the Baseline Asymmetry condition with 74.7 ± 10.1% accuracy, in the Zero Asymmetry condition with 61.6 ± 12.3% accuracy, and in the Exaggerated Asymmetry condition with 53.7 ± 16.0% accuracy. Target accuracy was significantly lower in the Exaggerated Asymmetry condition than in the Baseline Asymmetry condition ($p = 0.03$). Four out of five subjects showed reduced accuracy in the the Zero Asymmetry condition compared to the Baseline Asymmetry condition, but the trend was

not significant ($p = 0.1$). Accuracy, averaged across both legs, ranged from 35.4% to 88.3% when including all conditions and participants.

For four out of the five participants, accuracy decreased from the first instance of the repeated condition to the second instance of the repeated condition. On average, accuracy decreased by $3.8 \pm 6.2\%$ from the first instance of the repeated condition to the second instance of the repeated condition, although this difference was not statistically significant ($p = 0.2$).

5.4 Discussion

We designed and conducted an experiment to study the relationship between metabolic rate and step-length asymmetry in post-stroke individuals. Although participants were able to modulate their step lengths using visual feedback, as has been shown previously [83], we did not find a significant trend between metabolic rate and step-length asymmetry. For most participants, it seemed that walking with an exaggerated step-length asymmetry resulted in the highest metabolic energy consumption, but differences in metabolic rate across conditions were often not outside the range of noise inherent in metabolic measurements.

Accuracy in hitting the step-length targets appeared to vary across conditions, with accuracy being, on average, highest in the Baseline Asymmetry condition and lowest in the Exaggerated Asymmetry condition. This seems to suggest that the task of presented in the Zero Asymmetry condition and in the Exaggerated Asymmetry condition was more challenging than the task presented in the Baseline Asymmetry condition. Accuracy in the Zero Asymmetry condition was not significantly lower than accuracy in the Baseline Asymmetry condition, but we expect that, with a larger sample size, we would find this difference to be significant.

Qualitative observations of the post-stroke individuals walking with different step-length asymmetries suggest that there were inherent differences in locomotor coordination strategies adopted across conditions. Participants seemed to struggle to discover coordination

strategies that enabled consistent, repeatable modulation of paretic and non-paretic leg step lengths throughout the entire six-minute trial in the Zero Asymmetry and Exaggerated Asymmetry conditions. Often, some form of instruction or verbal feedback was needed to help participants complete the task. Different coaching strategies worked for different participants. Certain participants found temporal feedback, provided orally, to be most helpful. Others responded well to more mechanical descriptions of the task such as "reach your left leg forward," or "place you right leg farther in front of your left leg," or "keep your leg in the air for a longer period of time." We found that providing additional encouragement throughout the six-minute trial was important towards helping to maintain participants' motivation. Occasionally, participants preferred not to be spoken to during the task so their focus would not be disrupted.

Although we did not observe a significant relationship between metabolic rate and step-length asymmetry during walking in the post-stroke individuals we tested, it is difficult to know whether the metabolic rate measured in each condition was strictly a result of step-length asymmetry. Factors including fatigue, learning, motivation, and others, could have impacted the metabolic rate measured in a given condition. To be able to better measure the effect that our controlled independent variable, step-length asymmetry, had on our chosen dependent variable, metabolic rate, we need to conduct this experiment with more participants.

Study limitations

There were a number of limitations to this study which make it difficult to state stronger claims about the metabolic rate of walking as a function of step-length asymmetry in post-stroke individuals. Although we tried to account for confounding factors, such as fatigue, learning, and motivation, we were not able to adequately remove them. We included one repeated step-length asymmetry condition (randomly selected) for every participant, presented once at the beginning of the visual feedback walking trials and once at the end of the visual feedback walking trials, to try to account for learning and fatigue. Additionally,

we scheduled participants for multiple days of training to try to remove any further effects of learning. We added animations and a scoring system, in which participants got a point every time they accurately hit a step-length target, to try to improve engagement and motivation. We found, however, that despite these implementations, measurements of metabolic rate across the different conditions were still subject to these other influencing factors. In several participants, we observed a substantial difference in metabolic rate (up to 20%) between the first and second instances of the repeated condition even though the average measured step-length asymmetry was similar across both instances. As mentioned in the results, accuracy in the second instance of the repeated condition was often lower than in the first instance, which might be the result of fatigue or reduced motivation, and could explain part of the observed difference in metabolic rate.

Accuracy and motivation seem to be associated with each other and have potentially interesting implications for measured metabolic rate. Achieving high accuracy may have motivated participants to try harder, so they would continue to hit the targets and attain a high score. Therefore, participants may have exerted more effort trying to do the task extremely well in those conditions which were actually easier for them to coordinate. Achieving low accuracy may have demotivated participants, such that they felt incapable of completing the task and reduced the amount of effort they put towards trying to hit the targets. This highlights the importance of presenting a task that contains the appropriate level of challenge for the participants, such that they maintain an adequate level of motivation throughout each condition and the entire experiment.

It is possible that changes to the experimental protocol or to our implementation of the visual feedback could better mitigate effects related to motivation. For instance, the location of the step-length targets could have been iteratively adjusted on each step, or every couple of steps, to make them more attainable for each individual while still enforcing a step-length asymmetry that was significantly different from the other two conditions. Changing how scores were computed and when or how scores were shown to participants (e.g. during the condition or at the end of the condition), could improve motivation and accuracy.

Variation among individuals, however, makes it difficult to know how to equally motivate all participants.

Due to the fact that metabolic rate data are noisy, it is difficult to measure changes in metabolic rate that are smaller than 5% with fewer than ten subjects. Thus, 5 to 10% changes in metabolic rate measured in a single post-stroke individual could be the result of noise and do not have statistical power. It is possible that the mechanisms driving step-length asymmetry differ across individuals, but this is difficult to prove when metabolic rate differences across conditions for a given individual lie within the noise of the data. Therefore, this study does not enable us to make claims about subject-specific locomotor coordination strategies related to metabolic rate.

Challenges in recruiting and testing post-stroke individuals

Working with post-stroke individuals presents a number of challenges not inherent in studies involving able-bodied individuals. Although we present results from five participants, we have brought in a total of 21 post-stroke individuals. Multiple factors affected whether participants were able to be included in our study. Of the 21 stroke survivors, eight did not exhibit a statistically significant step-length asymmetry and three could not voluntarily modulate their step-length asymmetry using our visual feedback protocol. Another two could not walk on the treadmill without using the handrails and another two did not complete the study. Thus, finding participants that are willing and able to complete the protocol has been difficult and has prevented us from providing results from a larger number of post-stroke individuals.

Locomotor capabilities of post-stroke individuals are substantially different from their able-bodied counterparts. Furthermore, the variability within the population of stroke survivors is much greater than the variability within a non-patient population. Developing a protocol that adequately accommodates the large variability inherent in this population has proven challenging. For instance, selecting a speed that post-stroke individuals can sustain walking at for six minutes while trying to perform a new locomotor task, i.e. modulating step

lengths, greatly depends on each participant's capabilities and such decisions can impact a participant's ability to perform the task. Substantial piloting and testing of different protocols designed to answer our specific research question was necessary and additional work is currently being put forth to further improve the design of the experiment.

5.5 Conclusions

Many post-stroke individuals walk with step-length asymmetry, but the mechanisms driving this asymmetry are not well understood. We conducted a study to see if step-length asymmetry in post-stroke individuals is the result of an attempt to minimize metabolic energy consumption, similar to coordination patterns observed in able-bodied individuals. Walking with different step-length asymmetries did not significantly affect metabolic rate in five post-stroke individuals. Due to our small sample size, and potential influencing factors such as fatigue, motivation, and learning, it is difficult to say definitively that metabolic rate is or is not affected by step-length asymmetry. These results indicate the need for a larger number of participants. The results from this study could have important implications for our understanding of locomotion in post-stroke individuals and for the development of rehabilitation strategies.

Acknowledgments

This material is based upon work supported by the University of Pittsburgh under Grant No. CRDF 4.30541. The authors thank Kirby Ann Witte, Carly Sombric, Bailey Peterson, and Will Anderton for their intellectual contributions to the project and for their help piloting and conducting experiments.

5.6 Appendix A: Step-Length Asymmetry Plots

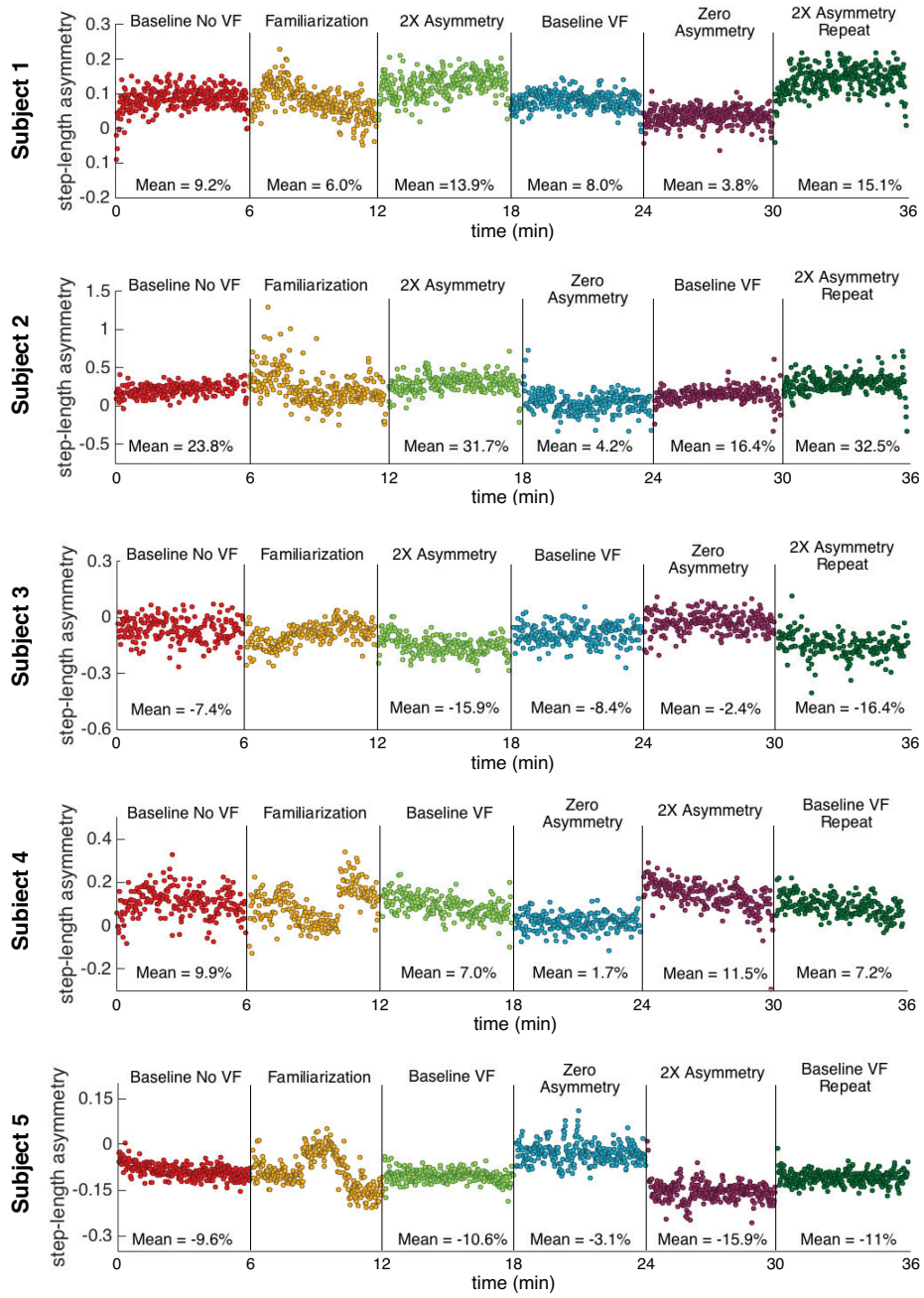

Figure 5.7: Step-length asymmetry time-trajectories for each participant across the different conditions. Absolute step-length asymmetry varied among participants. Furthermore, ability to sustain a specific step-length asymmetry for the entire six-minute trial depended on each post-stroke individual. There were, however, significant differences in step-length asymmetry across the three visual feedback conditions for the five post-stroke individuals tested.

Chapter 6

Conclusions

Lower-limb exoskeletons have the potential to improve locomotor performance, and overall quality of life, for a wide range of individuals, but developing effective exoskeleton assistance strategies remains a significant challenge. In order to deliver the intended benefit, such devices must interact well with the highly complex and redundant human musculoskeletal system. To avoid the limitations inherent in traditional, intuition-driven development approaches, we used an iterative approach for the development of exoskeleton assistance strategies involving experimentation, simulation, and application. We observed the human response to a variety of exoskeleton behaviors by conducting biomechanics experiments, we explained the observed responses by simulating changes in muscle-level mechanics and energetics using a musculoskeletal model, and we used our findings to guide the development of a novel, adaptive exoskeleton assistance strategy. The findings presented in this thesis have important implications for the field of assistive lower-limb exoskeletons.

6.1 Summary of Findings

The type of assistance provided by an exoskeleton can have profound implications for the benefits a user can derive. Through controlled experimentation using our exoskeleton emulator, we found that work input from an exoskeleton can improve the efficiency of human locomotion while torque support provided by an exoskeleton may not be an effective way

of assisting locomotion. These findings exemplify our lack of understanding of how humans respond to different assistance strategies and support the case for experimental approaches designed to measure the complicated human-device interaction during locomotion.

The effectiveness of different exoskeleton assistance strategies partially depends on how they impact muscle-tendon mechanics at the assisted joint. We performed electromyography-driven simulations of a musculoskeletal model to estimate how muscle-level mechanics and energetics change with different types of exoskeleton assistance. Our results suggest that the plantarflexor muscle-tendon units are sensitive to interactions from external devices and can change in unpredictable and undesirable ways. These findings highlight the complexity of the muscle-tendon interactions at the assisted joint and the difficulty in predicting the human response to novel exoskeleton behaviors. Furthermore, they stress the importance of considering how muscle-tendon mechanics might change in response to device interactions when developing new assistance strategies.

'Human-in-the-loop' control approaches, which respond to measured changes in human coordination patterns and lessen the need for prediction, show promise as effective exoskeleton assistance strategies. Our novel, heuristic-based control technique, that adjusts exoskeleton behavior online in response to measured changes in the user, resulted in substantial reductions in soleus muscle activity and whole-body metabolic rate when applied to bilateral ankle exoskeletons. These findings stress the importance of including measurements of human locomotor adaptations in the discovery of new assistance techniques.

Extension of such findings to the development of robotic rehabilitation techniques remains a challenge due to a lack of understanding of the mechanisms driving gait impairments in, e.g., stroke survivors. We sought to better understand gait asymmetry in post-stroke individuals by designing and conducting an experiment to test whether an individual's self-selected step-length asymmetry minimizes metabolic rate during locomotion. Results from five post-stroke individuals suggest that metabolic rate is not affected by step-length asymmetry, but the small sample size and potential confounding factors make it difficult to state any findings with certainty. Findings from this study, when run on at least 10 stroke

survivors, could have large implications for how gait rehabilitation techniques should be designed.

6.2 Implications

The ideas and results presented in this thesis have broad implications for the next steps towards the discovery and development of lower-limb assistance strategies.

Improved Predictive Models

We expect the empirical data we collected through extensive experimentation of the human response to various exoskeleton assistance strategies will help improve predictive models of human locomotor coordination. With better predictive models, the field can begin to design and test novel assistance strategies using simulations rather than through building physical hardware and conducting time-intensive biomechanics experiments. Such models may even be able to provide insight into the mechanisms driving human locomotion.

Individualized Assistance

'Human-in-the-loop' assistance strategies, such as the heuristic-based adaptive control technique discussed in this thesis, provide a framework for a class of control techniques that discover exoskeleton behaviors customized to each user. Such individualized assistance strategies could potentially help people adapt more quickly to exoskeleton assistance and converge to a more beneficial, co-adapted state.

Scalability

Due to the fact that our heuristic-based adaptive control approach uses measured muscle activity patterns to generate exoskeleton torque profiles, we expect it will be naturally transferable to the knee and hip joints. Application of this control strategy to multiple joints would enable full lower-limb assistance during locomotion.

Autonomous Devices

As we continue to deepen our understanding of how devices should behave to provide the intended benefit to the user, we can start to design autonomous devices that incorporate those capabilities found to be most important.

Assisting those with Walking Disabilities

As we learn more about the mechanisms driving gait impairments in patient populations, we can begin to adapt our assistance approaches to serve as locomotor rehabilitation tools.

Open Areas

Although we have made significant strides in the field of assistive lower-limb exoskeletons in the last several years, there is still a lot left to learn. How do humans adapt to exoskeleton assistance and what features facilitate the learning process? How large of metabolic reductions are we capable of achieving with exoskeleton assistance and what factors will ultimately limit further gains? How do we translate what we have learned through lab-based experimentation to real-world applications? Finally, how can we harness the capabilities of these devices to improve the health and well-being of all different types of individuals? As we continue to seek the answers to such questions, we will find new and better ways of providing all types of individuals with new locomotor capabilities and we will continue pushing the limits of what is possible with lower-limb exoskeleton assistance.

Bibliography

[1] M. Ackermann and A. J. van den Bogert. Optimality principles for model-based prediction of human gait. *J. Biomech.*, 43:1055–1060, 2010.

[2] L. Ada, C. M. Dean, J. M. Hall, J. Bampton, and S. Crompton. A treadmill and overground walking program improves walking in persons residing in the community after stroke: A placebo-controlled, randomized trial. *Arch. Phys. Med. Rehab.*, 84:1486–1491, 2003.

[3] J. L. Allen, S. A. Kautz, and R. R. Neptune. Step length asymmetry is representative of compensatory mechanisms used in post-stroke hemiparetic walking. *Gait Post.*, 33:538–543, 2012.

[4] F. C. Anderson and M. G. Pandy. Dynamic optimization of human walking. *J. Biomech. Eng.*, 123:381–390, 2001.

[5] D. Aoyagi, W. E. Ichinose, S. J. Harkema, D. J. Reinkensmeyer, and J. E. Bobrow. A robot and control algorithm that can synchronously assist in naturalistic motion during body-weight-supported gait training following neurologic injury. *Trans. Neural Syst. Rehabil. Eng.*, 15(3):387–400, 2007.

[6] A. S. Arnold, D. J. Asakawa, and S. L. Delp. Do the hamstrings and adductors contribute to excessive internal rotation of the hip in persons with cerebral palsy? *Gait Post.*, 11:181–190, 2000.

[7] E. M. Arnold and S. L. Delp. Fibre operating lengths of human lower limb muscles during walking. *Phil. Trans. R. Soc. B*, 366:1530–1539, 2011.

[8] E. M. Arnold, S. R. Hamner, A. Seth, M. Millard, and S. L. Delp. How muscle fiber lengths and velocities affect muscle force generation as humans walk and run at different speeds. *J. Exp. Biol.*, 216:2150–2160, 2013.

[9] E. M. Arnold, S. R. Ward, R. L. Lieber, and S. L. Delp. A model of the lower limb for analysis of human movement. *J. Biomed. Eng.*, 38:269–279, 2010.

[10] E. J. Benjamin, M. J. Blaha, and S. E. C. et. al. Heart disease and stroke statistics – 2017 update. *Circulation*, 135:e1–e458, 2017.

[11] L. J. Bhargava, M. G. Pandy, and F. C. Anderson. A phenomenological model for estimating metabolic energy consumption in muscle contraction. *J. Biomech.*, 37:81–88, 2004.

[12] A. A. Biewener. Muscle function *in vivo*: A comparison of muscles used for elastic energy savings *versus* muscles used to generate mechanical power. *Amer. Zool.*, 38:703–717, 1998.

[13] A. A. Biewener and T. J. Roberts. Muscle and tendon contributions to force, work, and elastic energy savings: A comparative perspective. *Exerc. Sport Sci. Rev.*, 28:99–107, 2000.

[14] M. G. Bowden, C. K. Balasubramanian, R. R. Neptune, and S. A. Kautz. Anterior-posterior ground reaction forces as a measure of paretic leg contribution in hemiparetic walking. *Stroke*, 37:872–876, 2006.

[15] D. J. J. Bregman, J. Harlaar, C. G. M. Meskers, and V. de Groot. Spring-like ankle foot orthoses reduce the energy cost of walking by taking over ankle work. *Gait Post.*, 35:148–153, 2012.

[16] J. M. Brockway. Derivation of formulae used to calculate energy expenditure in man. *Hum. Nutr. Clin. Nutr.*, 41C:463–471, 1987.

[17] R. C. Browning, J. R. Modica, R. Kram, and A. Goswami. The effects of adding mass to the legs on the energetics and biomechanics of walking. *Med. Sci. Sports Exer.*, 39:515–525, 2007.

[18] T. S. Buchanan, D. G. Lloyd, K. Manal, and T. F. Besier. Estimation of muscle forces and joint moments using a forward-inverse dynamics model. *Med. Sci. Sports Exer.*, pages 1911–1916, 2005.

[19] J. M. Caputo and S. H. Collins. An experimental robotic testbed for accelerated development of ankle prostheses. In *Proc. Int. Conf. Rob. Autom.*, pages 2630–2635, 2013.

[20] J. M. Caputo and S. H. Collins. Prosthetic ankle push-off work reduces metabolic rate but not collision work in non-amputee walking. *Sci. Rep.*, 4:7213, 2014.

[21] J. M. Caputo and S. H. Collins. A universal ankle-foot prosthesis emulator for experiments during human locomotion. *J. Biomech. Eng.*, 136:035002, 2014.

[22] G. Chen, C. Patten, D. H. Kothari, and F. E. Zajac. Gait differences between individuals with post-stroke hemiparesis and non-disabled controls at matched speeds. *Gait Post.*, page ??, 2004.

[23] S. H. Collins. What do walking humans want from mechatronics? (invited presentation). In *Int. Conf. Mech.*, pages 24–27, 2013.

[24] S. H. Collins and R. W. Jackson. A method for harnessing least-effort drives in robotic locomotion training. In *Proc. Int. Conf. Rehab. Rob.*, pages 1–6, 2013.

[25] S. H. Collins and A. D. Kuo. Recycling energy to restore impaired ankle function during human walking. *PLoS: ONE*, 5:e9307, 2010.

[26] S. H. Collins, M. B. Wiggin, and G. S. Sawicki. Reducing the energy cost of human walking using an unpowered exoskeleton. *Nature*, 522:212–215, 2015.

[27] E. C. Conchola, B. J. Thompson, and D. B. Smith. Effects of neuromuscular fatigue on the electromechanical delay of the leg extensors and flexors in young and old men. *Eur. J. Appl. Physiol.*, 113:2391–2399, 2013.

[28] D. M. Corcos, G. L. Gottlieb, M. L. Latash, G. L. Almeida, and G. C. Agarwal. Electromechanical delay: An experimental artifact. *J. Electromyogr. Kinesiol.*, 2:59–68, 1992.

[29] N. J. Cronin, J. Avela, T. Finni, and J. Peltonen. Differences in contractile behavior between the soleus and medial gastrocnemius muscles during human walking. *J. Exp. Biol.*, 216:909–914, 2013.

[30] N. J. Cronin, J. Peltonen, M. Ishikawa, P. V. Komi, J. Avela, T. Sinkjaer, and M. Voigt. Achilles tendon length changes during walking in long-term diabetes patients. 25:476–482, 2010.

[31] P. de Leva. Adjustments to zatsiorsky-seluyanov's segment inertia parameters. *J. Biomech.*, 29:1223–1230, 1996.

[32] C. J. De Luca, L. D. Gilmore, M. Kuznetsov, and S. H. Roy. Filtering the surface emg signal: Movement artifact and baseline noise contamination. *J. Biomech.*, 43:1573–1579, 2010.

[33] S. L. Delp, F. C. Anderson, A. S. Arnold, P. Loan, A. Habib, C. T. John, E. Guendelman, and D. G. Thelen. Opensim: open-source software to create and analyze dynamic simulations of movement. *Trans. Biomed. Eng.*, 54:1940–1950, 2007.

[34] S. L. Delp, J. P. Loan, M. G. Hoy, F. E. Zajac, E. L. Topp, and J. M. Rosen. An interactive graphics-based model of the lower extremity to study orthopaedic surgical procedures. *Trans. Biomed. Eng.*, 37:757–767, 1990.

[35] C. Detrembleur, F. Dierick, G. Stoquart, F. Chantraine, and T. Lejune. Energy cost, mechanical work, and efficiency of hemiparetic walking. *Gait Post.*, 18:47–55, 2003.

[36] J. M. Donelan, R. Kram, and A. D. Kuo. Mechanical and metabolic determinants of the preferred step width in human walking. *Proc. Roy. Soc. Lon. B*, 268:1985–1992, 2001.

[37] J. M. Donelan, R. Kram, and A. D. Kuo. Mechanical work for step-to-step transitions is a major determinant of the metabolic cost of human walking. *J. Exp. Biol.*, 205:3717–3727, 2002.

[38] J. M. Donelan, R. Kram, and A. D. Kuo. Simultaneous positive and negative external mechanical work in human walking. *J. Biomech.*, 35:117–124, 2002.

[39] R. Drillis, R. Contini, and M. Bluestein. Body segment parameters: A survey of measurement techniques. *Artificial Limbs*, 25:44–66, 1964.

[40] D. J. Farris, J. L. Hicks, S. L. Delp, and G. S. Sawicki. Musculoskeletal modelling deconstructs the paradoxical effects of elastic ankle exoskeletons on plantar-flexor mechanics and energetics during hopping. *J. Exp. Biol.*, 217:4018–4028, 2014.

[41] D. J. Farris, B. D. Robertson, and G. S. Sawicki. Elastic ankle exoskeletons reduce soleus muscle force but not work in human hopping. *J. Appl. Physiol.*, 115:579–585, 2013.

[42] D. J. Farris and G. S. Sawicki. Linking the mechanics and energetics of hopping with elastic ankle exoskeletons. *J. Appl. Physiol.*, 113:1862–1872, 2012.

[43] D. P. Ferris, K. E. Gordon, and G. S. Sawicki. An improved powered ankle-foot orthosis using proportional myoelectric control. *Gait Post.*, 23:425–428, 2006.

[44] D. P. Ferris, G. S. Sawicki, and A. R. Domingo. Powered lower limb orthoses for gait rehabilitation. *Top. Spinal Cord Inj. Rehab.*, 11:34–49, 2005.

[45] B. J. Fregly, T. F. Besier, D. G. Lloyd, S. L. Delp, S. A. Banks, M. G. Pandy, and D. D. D'Lima. Grand challenge competition to predict in vivo knee loads. *J. Orthop. Res.*, 30:503–513, 2012.

[46] T. Fukunaga, K. Kubo, Y. Kawakami, S. Fukashiro, H. Kanehisa, and C. N. Maganaris. *In vivo* behavior of human muscle tendon during walking. *Proc. Roy. Soc. Lon. B*, 268:229–233, 2001.

[47] S. Galle, P. Malcolm, W. Derave, and D. D. Clercq. Adaptation to walking with an exoskeleton that assists ankle extension. *Gait Post.*, 12:97, 2013.

[48] S. A. Glantz. *Primer of Biostatistics, Seventh Edition*. The McGraw-Hill Companies, Inc., 2012. 65.

[49] K. E. Gordon and D. P. Ferris. Learning to walk with a robotic ankle exoskeleton. *J. Biomech.*, 40:2636–2644, 2007.

[50] K. E. Gordon, D. P. Ferris, and A. D. Kuo. Metabolic and mechanical energy costs of reducing vertical center of mass movement during gait. *Arch. Phys. Med. Rehab.*, 90:136–144, 2009.

[51] K. E. Gordon, G. S. Sawicki, and D. P. Ferris. Mechanical performance of artificial pneumatic muscles to power an ankle-foot orthosis. *J. Biomech.*, 39:1832–1841, 2006.

[52] A. Grabowski, C. Farley, and R. Kram. Independent metabolic costs of supporting body weight and accelerating body mass during walking. *J. Appl. Physiol.*, 98:579–583, 2005.

[53] T. M. Griffin, T. J. Roberts, and R. Kram. Metabolic cost of generating muscular force in human walking: insights from load-carrying and speed experiments. *J. Appl. Physiol.*, 95:172–183, 2003.

[54] E. Guizzo and T. Deyle. Robotics trends for 2012. *Rob. Autom. Mag.*, pages 119–123, 2012.

[55] H. B. Hayes, Y.-H. Chang, and S. Hochman. Stance-phase force on the opposite limb dictates swing-phase afferent presynaptic inhibition during locomotion. *J. Neurophys.*, 107:3168–3180, 2012.

[56] H. M. Herr and A. M. Grabowski. Bionic ankle-foot prosthesis normalizes walking gait for persons with leg amputation. *Proc. Roy. Soc. Lon. B*, 279:457–464, 2012.

[57] J. L. Hicks, T. K. Uchida, A. Seth, A. Rajagopal, and S. L. Delp. Is my model good enough? best practices for verification and validation of musculoskeletal models and simulations of movement. *J. Biomech. Eng.*, 137:020905, 2015.

[58] A. V. Hill. The heat of shortening and the dynamic constants of muscle. *Proc. Roy. Soc. Lon. B*, 126:136–195, 1938.

[59] J. Hitt, A. M. Oymagil, T. Sugar, K. Hollander, A. Boehler, and J. Fleeger. Dynamically controlled ankle-foot orthosis (DCO) with regenerative kinetics: incrementally attaining user portability. In *Proc. Int. Conf. Rob. Autom.*, pages 1541–1546, 2007.

[60] F. Hug, L. Lacourpaille, and A. Nordez. Electromechanical delay measured during a voluntary contraction should be interpreted with caution. *Muscle Nerve*, 44:838–839, 2011.

[61] M. Ishikawa, P. V. Komi, M. J. Grey, V. Leopla, and G. Bruggemann. Muscle-tendon interaction and elastic energy usage in human walking. *J. Appl. Physiol.*, 99:603–608, 2005.

[62] R. W. Jackson and S. H. Collins. An experimental comparison of the relative benefits of work and torque assistance in ankle exoskeletons. *J. Appl. Physiol.*, 119:541–557, 2015.

[63] J. H. Kahn and T. G. Hornby. Rapid and long-term adaptations in gait symmetry following unilateral step training in people with hemiparesis. *Phys. Ther.*, 89:474–483, 2009.

[64] P. Kao, C. L. Lewis, and D. P. Ferris. Invariant ankle moment patterns when walking with and without a robotic ankle exoskeleton. *J. Biomech.*, 43:203–209, 2010.

[65] J. O. Kelly, S. L. Kilbreath, G. M. Davis, B. Zeman, and J. Raymond. Cardiorespiratory fitness and walking ability in subacute stroke patients. *Arch. Phys. Med. Rehab.*, 84:1780–1785, 2003.

[66] J. R. Koller, D. A. Jacobs, D. P. Ferris, and C. D. Remy. Learning to walk with an adaptive gain proportional myoelectric controller for a robotic ankle exoskeleton. 12:97, 2015.

[67] A. D. Kuo. A simple model predicts the step length-speed relationship in human walking. *J. Biomech. Eng.*, 123:264–269, 2001.

[68] A. D. Kuo, J. M. Donelan, and A. Ruina. Energetic consequences of walking like an inverted pendulum: step-to-step transitions. *Exerc. Sport Sci. Rev.*, 33:88–97, 2005.

[69] M. D. Lewek, J. Feasel, E. Wentz, F. P. B. Jr., and M. C. Whitton. Use of visual and proprioceptive feedback to improve gait speed and spatiotemporal symmetry following chronic stroke: A case series. *Phys. Ther.*, 92:748, 2012.

[70] G. A. Lichtwark and C. J. Barclay. The influence of tendon compliance on muscle power output and efficiency during cyclic contractions. *J. Exp. Biol.*, 213:707–714, 2009.

[71] G. A. Lichtwark and A. M. Wilson. Interactions between the human gastrocnemius and the achilles tendon during incline, level and decline locomotion. *J. Exp. Biol.*, 209:4379–4388, 2006.

[72] G. A. Lichtwark and A. M. Wilson. Is achilles tendon compliance optimised for maximum muscle efficiency during locomotion? *J. Biomech.*, 40:1768–1775, 2007.

[73] G. A. Lichtwark and A. M. Wilson. Optimal muscle fascicle length and tendon stiffness for maximising gastrocnemius efficiency during human walking and running. *J. Theor. Biol.*, 252:662–673, 2008.

[74] D. G. Lloyd and T. F. Besier. An emg-driven musculoskeletal model to estimate muscle forces and knee joint moments in vivo. *J. Biomech.*, 36:765–776, 2003.

[75] P. Malcolm, W. Derave, S. Galle, and D. De Clercq. A simple exoskeleton that assists plantarflexion can reduce the metabolic cost of human walking. *PLoS: ONE*, 8:e56137, 2013.

[76] K. Manal, K. Gravare-Silbernagel, and T. S. Buchanan. A real-time emg-driven musculoskeletal model of the ankle. *Multibody Syst. Dyn.*, 28:169–180, 2012.

[77] J. Markowitz and H. Herr. Human leg model predicts muscles forces, states, and energetics during walking. *PLoS Comput. Biol.*, 12:e1004912, 2016.

[78] A. P. Marsh and P. E. Martin. Effect of cycling experience, aerobic power, and power output on preferred and most economical cycling cadences. *Med. Sci. Sports Exer.*, 29:1225–1232, 1997.

[79] T. A. McMahon. *Muscles, Reflexes, and Locomotion.* Princeton, NJ, Princeton University Press., 1984. 34-35.

[80] M. Meinders, A. Gitter, and J. M. Czernieckie. The role of ankle plantar flexor muscle work during walking. *Scand. J. Rehab. Med.*, 30:39–46, 1998.

[81] R. H. Miller. A comparison of muscle energy models for simulating human walking in three dimensions. *J. Biomech.*, 47(6):1373–81, may 2014.

[82] W. F. H. M. Mommaerts. Energetics of muscular contraction. *Physiol. Rev.*, 49:427–508, 1969.

[83] R. Montoya, P. Dupui, B. Pagés, and P. Bessou. Step-length biofeedback device for walk rehabilitation. *Med. Biol. Eng. Comput.*, 32:416–420, 1994.

[84] L. M. Mooney, E. J. Rouse, and H. M. Herr. Autonomous exoskeleton reduces metabolic cost of human walking during load carriage. *J. Neuroeng. Rehabil.*, 11:80, 2014.

[85] S. Nadeau, D. Gravel, A. B. Arsenault, and D. Bourbonnais. Plantarflexor weakness as a limiting factor of gait speed in stroke subjects and the compensating role of hip flexors. *Clin. Biomech.*, 14:125–135, 1999.

[86] R. R. Neptune, S. A. Kautz, and F. E. Zajac. Contributions of the individual ankle plantar flexors to support, forward progression and swing initiation during walking. *J. Biomech.*, 34:1387–1398, 2001.

[87] S. J. Olney and C. L. Richards. Hemiparetic gait following stroke. part i: Characteristics. *Gait Post.*, 4:136–148, 1996.

[88] K. K. Patterson, I. Parafianowicz, C. J. Danells, V. Closson, M. C. Verrier, W. R. Staines, S. E. Black, and W. E. McIlroy. Gait asymmetry in community-ambulating stroke survivors. *Arch. Phys. Med. Rehab.*, 89:304–310, 2008.

[89] S. L. Patterson, M. M. Rodgers, R. F. Macko, and L. W. Forrester. Effect of treadmill exercise training on spatial and temporal gait parameters in subjects with chronic stroke: A preliminary report. *J. Rehabil. Res. Dev.*, 45:221–228, 2008.

[90] J. Perry and J. M. Burnfield. *Gait Analysis: Normal and Pathological Function, Second Edition.* Thorofare, NJ, SLACK Inc, 2010. 53-82.

[91] M. M. Platts, D. Rafferty, and L. Paul. Metabolic cost of overground gait in younger stroke patients and healthy controls. *Med. Sci. Sports Exer.*, 84:1041–1046, 2006.

[92] P. Plummer, A. L. Behrman, P. W. Duncan, P. Spigel, D. Saracino, J. Martin, E. Fox, M. Thigpen, and S. A. Kautz. Effects of stroke severity and training duration on locomotor recovery after stroke: A pilot study. *Neurorehab. Neur. Rep.*, 21:137–151, 2007.

[93] D. S. Reisman, H. McLean, and A. J. Bastian. Split-belt treadmill training post-stroke: A case study. *J. Neurol. Phys. Ther.*, 34(4):202–207, 2010.

[94] D. S. Reisman, H. McLean, J. Keller, K. A. Danks, and A. J. Bastian. Repeated split-belt treadmill training improves poststroke step length asymmetry. *Neurorehab. Neur. Rep.*, 27:460–468, 2013.

[95] T. J. Roberts. The integrated function of muscles and tendons during locomotion. *Comp. Biochem. Physiol. A*, 133:1087–1099, 2002.

[96] T. J. Roberts, R. L. Marsh, P. G. Weyand, and C. R. Taylor. Muscular force in running turkeys: The economy of minimizing work. *Science*, 257:1113–1115, 1997.

[97] T. J. Roberts, R. L. Marsh, P. G. Weyand, and C. R. Taylor. Muscular force in running turkeys: The economy of minimizing work. *Science*, 275:1113–1115, 1997.

[98] B. D. Robertson, D. J. Farris, and G. S. Sawicki. More is not always better: modeling the effects of elastic exoskeleton compliance on underlying ankle muscle-tendon dynamics. *Bioinspir. Biomim.*, 9:046018, 2014.

[99] M. Roerdink and P. J. Beek. Understanding inconsistent step-length asymmetries across hemiplegic stroke patients: Impairments and compensatory gait. *Neurorehab. Neur. Rep.*, 25:253–258, 2011.

[100] J. Rubenson, N. J. Pires, H. O. Loi, G. J. Pinniger, and D. G. Shannon. On the ascent: the soleus operating length is conserved to the ascending limb of the force-length curve across gait mechanics in humans. *J. Exp. Biol.*, 215:3539–3551, 2012.

[101] A. Ruina, J. E. A. Bertram, and M. Srinivasan. A collision model of the energetic cost of support work qualitatively explains leg sequencing in walking and galloping, pseudo-elastic leg behavior in running and the walk-to-run transition. *J. Theor. Biol.*, 237:170–192, 2005.

[102] S. A. Safavynia, G. Torres-Oviedo, and L. H. Ting. Muscle synergies: implications for clinical evaluation and rehabilitation of movement. *Top. Spinal Cord Inj. Rehab.*, 17:16–24, 2011.

[103] M. Sartori, M. Reggiani, D. Farina, and D. G. Lloyd. Emg-driven forward-dynamic estimation of muscle force and joint moment about multiple degrees of freedom in the human lower extremity. *PLoS: ONE*, 7:1–11, 2012a.

[104] G. Sawicki and N. Khan. A simple model to estimate plantarflexor muscle-tendon mechanics and energetics during walking with elastic ankle exoskeletons. *Trans. Biomed. Eng.*, 63:914–923, 2016.

[105] G. S. Sawicki and D. P. Ferris. Mechanics and energetics of level walking with powered ankle exoskeletons. *J. Exp. Biol.*, 211:1402–1413, 2008.

[106] A. Silder, T. Besier, and S. L. Delp. Predicting the metabolic cost of incline walking from muscle activity and walking mechanics. *J. Biomech.*, 45:1842–1849, 2012.

[107] S. Song and H. Geyer. Generalization of a muscle-reflex control model to 3d walking. In *Proc. Int. Conf. Eng. Med. Biol. Soc.*, pages 7463–7466, 2013.

[108] S. Srinivasan, E. R. Westervelt, and A. H. Hansen. A low-dimensional sagittal-plane forward-dynamic model for asymmetric gait and its application to study the gait of transtibial prosthesis users. *J. Biomech. Eng.*, 131:031003, 2009.

[109] K. M. Steele, M. C. Tresch, and E. J. Perreault. The number and choice of muscles impact the results of muscle synergy analyses. *Frontiers Comp. Neurosci.*, 7:105, 2013.

[110] C. R. Taylor. Force development during sustained locomotion: a determinant of gait, speed and metabolic power. *J. Biomech.*, 40:1768–1775, 2007.

[111] D. G. Thelen and F. C. Anderson. Using computed muscle control to generate forward dynamic simulations of human walking from experimental data. *J. Biomech.*, 39:1107–1115, 2006.

[112] T. K. Uchida, J. L. Hicks, C. L. Dembia, and S. L. Delp. Stretching your energetic budget: How tendon compliance affects the metabolic cost of running. *PLoS: ONE*, 11:e0150378, 2016.

[113] B. R. Umberger. Stance and swing phase costs in human walking. *J. Roy. Soc. Int.*, 7:1329–1340, 2010.

[114] B. R. Umberger, K. G. M. Gerritsent, and P. E. Martin. A model of human muscle energy expenditure. *Comput. Methods Biomech. Biomed. Eng.*, 6:99–111, 2003.

[115] B. R. Umberger and J. Rubenson. Understanding muscle energetics in locomotion: New modeling and experimental approaches. *Exerc. Sport Sci. Rev.*, 39:59–67, 2011.

[116] A. J. van den Bogert. Exotendons for assistance of human locomotion. *BioMed. Eng. OnLine*, 2:17, 2003.

[117] W. van Dijk, H. van der Kooij, and E. Hekman. A passive exoskeleton with artificial tendons: Design and experimental evaluation. In *Proc. Int. Conf. Rehab. Rob.*, pages 1–6, 2011.

[118] S. R. Ward, C. M. Eng, L. H. Smallwood, and R. L. Lieber. Are current measurements of lower extremity muscle architecture accurate? *Cllin. Orthop. Relat. Res.*, 467:1074–1082, 2009.

[119] M. B. Wiggin, G. S. Sawicki, and S. H. Collins. Apparatus and clutch for using controlled storage and release of mechanical energy to aid locomotion. Provisional patent, Unites States Patent Office, 2012. 13/586,528.

[120] D. A. Winter. *Biomechanics and Motor Control of Human Movement*. John Wiley & Sons, Inc., Toronto, Canada, 2nd edition, 1990. 107-138.

[121] K. A. Witte, J. Zhang, R. W. Jackson, and S. H. Collins. Design of two lightweight, high-bandwidth torque-controlled ankle exoskeletons. In *Proc. Int. Conf. Rob. Autom.*, 2015. pages 1223-1228.

[122] C. J. Wutzke, G. S. Sawicki, and M. D. Lewek. The influence of a unilateral fixed ankle on metabolic and mechanical demands. *J. Biomech.*, 45:2405–2410, 2012.

[123] J. T. Yen, A. G. Auyang, and Y.-H. Chang. Joint-level kinetic redundancy is exploited to control limb-level forces during human hopping. *Exp. Brain Res.*, 196:439–451, 2009.

[124] F. E. Zajac, R. R. Neptune, and S. A. Kautz. Biomechanics and muscle coordination of human walking; part ii: Lessons from dynamical simulations and clinical implications. *Gait Post.*, 17:1–17, 2003.

[125] P. Zamparo, G. D. Luca, L. Lovati, and P. E. di Prampero. The energy cost of level walking in patients with hemiplegia. *Scand. J. Med. Sci. Sports*, 5:348–352, 1995.

[126] M. Y. Zarrugh, F. N. Todd, and H. J. Ralston. Optimization of energy expenditure during level walking. *Eur. J. Appl. Physiol.*, 33:293–306, 1974.

[127] K. E. Zelik, V. La Scaleia, Y. P. Ivanenko, and F. Lacquaniti. Can modular strategies simplify neural control of multidirectional human locomotion? *J. Neurophys.*, 111:1686–1702, 2014.

[128] J. Zhang, C. C. Cheah, and S. H. Collins. Experimental comparison of torque control methods on an ankle exoskeleton during human walking. In *Proc. Int. Conf. Rob. Autom.*, pages 5584–5589, 2015.

[129] J. Zhang, C. C. Cheah, and S. H. Collins. Torque control in legged locomotion. in *Bio-Inspired Legged Locomotion: Concepts, Control and Implementation*. eds. Sharbafi, M., Seyfarth, A., Elsevier, in press, 2017.

[130] J. Zhang, P. Fiers, K. A. Witte, R. W. Jackson, K. L. Poggensee, C. G. Atkeson, and S. H. Collins. Human-in-the-loop optimization of exoskeleton assistance during walking. ***In review***.